Feasibility Study of a Novel Electrospinning System with Uniform & Non-Uniform Electric Fields

Yasir Al-Hilali

Supervised by:

Associate Professor Andrew Lowe

Associate Professor Frances Joseph

Professor Tek-Tjing Lie

A thesis submitted to Auckland University of Technology in fulfillment of the requirements for the degree of Master of Engineering.

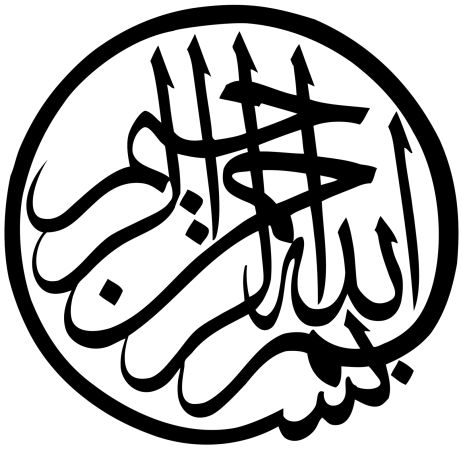
بسم الله الرحمن الرحيم

For Akram Al-Hilali

1939 - 2015

Attestation of Authorship

I hereby declare that this submission is my own work and that, to the best of my knowledge and belief, it contains no material previously published or written by another person (except where explicitly defined in the acknowledgments), nor material which to a substantial extent has been submitted for the award of any other degree or diploma of a university or other institution of higher learning.

Yasir Al-Hilali

Blank Page

Abstract

Nanofibres are fibres that are 1000 times thinner than a human hair, they are a versatile form of material made from various polymers. They inherit the properties of the base material while also yielding the properties resulting from being a nanofibre and having a very high surface area to volume ratio.

Producing nanofibre yarn is a complex electro-chemical process that requires field manipulation to allow bundles of fibres to form and align in a manner to be gathered into a yarn. In order to achieve this, a setup is required to allow an investigation into the relationship between electric field shape and behavior of electrospinning solution is conducted. The feasibility of the setup testing the effects of changing polarity of the electrodes and electrode geometry is investigated as well.

This thesis investigates and explores experimental methodology, modeling electrostatic fields for electrospinning, design and build of an experimental setup which will be used to acquire electrospinning data to assess the feasibility of a novel method of electrospinning for future design optimization on existing methods of electrospinning.

Simulating electrostatic fields of different electrode geometries with ANSYS Maxwell is used to plot the fields for various of electrodes and the influence of non-conductive enclosures and nearby objects on the static electrospinning field. The plots are then gathered and processed to calculate the differences in electric field strength of two fields to evaluate the significance of changes in geometry.

Results from the simulations indicate the effect of having a non-conductive enclosure around the electrodes have an effect that is negligible. Nearby earthed objects require shielding by means of using high impedance film with an applied voltage gradient, to minise the effects of the earthed object.

Two experimental configurations were used to investigate the feasibility of electrospinning in uniform and non-uniform electric fields using needle and needle-less methods. No electrospinning was observed in a uniform field prior to the breakdown of air. However, solution convection was observed when the fluid container is placed near edge of the electrode. Non-uniform field electrospinning was tested with a needle-plate setup using two different diameter drill bits pointing through a petridish submerged in mineral oil. This test led to the conclusion that electrospinning with the designed modular setup was feasible.

Glossary

CNT	*Carbon nanotube* - large molecules of pure carbon
DMA	*Dimethylacetamide* - an organic solvent
DMF	*Dimethylformamide* - an organic solvent
DSLR	Digital Single Lens Reflex camera
FEA	Finite Element Analysis
FEM	Finite Element Modeling
GSM	Grams per Square Meter
HVDC	High Voltage Direct Current
HVAC	Heating, Ventilation and Air Conditioning
NN-PP	Negative Needle - Positive Plate
PAN	*Polyacrylonitrile* - chemical precursor to Carbon Fibre
Perspex	Solid transparent plastic made of *polymethyl methacrylate*
PMMA	*polymethyl methacrylate* - same material as Perspex
PN-NP	Positive Needle - Negative Plate
PSU	Voltage power supply
PVDF	*polyvinylidene difluoride* - a piezoelectric thermoplastic
SEM	Scanning Electron Microscope
Streamer	Highly conducting luminous filamentary discharge

Contents

List of Figures

List of Tables

Chapter 1

Background

1.1 Nanofibre Industry

Fine fibrous meshes of polymer based fibres have been shown to be very useful and practical in modern material applications. Their benefits are widely appreciated in the industries of composite reinforcement, air filtration and more recently in the biomedical field of surgical sutures and wound dressings. From carbon fibre composite reinforcement to effective air filtration for HVAC systems and from improved lithium battery performance to biodegradable slow drug delivering sutures, nanofibres have found a home in almost all industries.

Electrospinning is one effective method to produce nanofibers with diameter ranging from several nanometers to hundreds of nanometers. However, this method has its issues in particular in designing to cope with the electrostatic high voltage nature of the process. This led many current manufacturers to attempt to develop their own methods of production with designs that have an inadequate grasp of understanding the process itself.

The traditional electrospinning device includes a micro-injection pump, a high voltage electrostatic generator, a spinning needle, and a collecting plate. Connecting the anode of the high voltage electrostatic generator with the spinning needle, results in a high voltage electric field between spinning needle and collecting plate. The polymer solution is supplied by the microinjection pump, which can form a "Taylor cone" at the tip of a spinning needle due to the high voltage electric field. When the applied voltage exceeds the surface tension of the polymer solution, a charged micro jet is ejected from the tip of the spinning needle. With solvent evaporation, nanofibers are deposited on the collection plate. There has been some commercial success producing nanofibres using traditional electrospinning methods. A New Zealand based company Revolution Fibres was able to develop an industrial scale nanofibre production machine called 'The Komodo' shown in Figure 1.1. It is a machine that is capable of producing up to 1000 m^2 per hour (at 0.05 gsm). It utilizes a proprietary needle-less method of electrospinning that was successfully up scaled. Few others have been as successful as The Komodo where most production methods have been limited in their up scaling capabilities due to the limitations associated with needle based electrospinning. The next section highlights the issues that are faced when attempting to upscale conventional electrospinning processes.

Figure 1.1: Revolution Fibres production scale adaptable nanofibre manufacturing machine named 'The Komodo' – Image courtesy of Revolution Fibres

1.2 Scalability of Nanofibre Production

Nanofibre production via electrospinning requires the polymer to be dissolved in an acid or solvent that is quick to evaporate. This solvent property can be an issue to deal with when moving the fluid through pipes in the system. These solvents can break through piping material over time, therefore selecting the right material for those pipes can be expensive and not necessarily compatible with other solvents.

Needle electrospinning systems have an issue of clogging the needle that is caused by the increased viscosity of the solution due to evaporation and can lead to polymer hardening at the tips if left unattended. This requires constant maintenance to the system where the process has to be stopped in order to remove unwanted electrospinning solution. This stoppage increases production costs due to the required manual labour to maintain and service the system during that time. This can also affect the consistency of the produced fibre.

Attempts at manipulating the electric fields to improve on manufacturing is covered in the Literature Review in Chapter 2. Most of these setups produce nanofibre yarn, which requires multiple electrodes of opposite polarities. This research is aimed to be a contributing component to the Nanofibre Yarn Project that is a conjoint project with Revolution Fibres and Auckland University of Technology. The next sections feature an overview of nanofibre yarn and the Nanofibre Yarn Project and the significance of both.

1.3 Nanofibre Yarn Project

Nanofibre in the form of yarn is a rising field of interest in fields such as medicine being used as sutures, reinforcing composite materials and in the world of textiles and wearables as sensors. These applications are only a few of many recent advances using nanofibre yarn. However, the production rate of nanofibre yarn is still slow and expensive using existing methods of production. When comparing nanofibre yarn production methods to the conventional non-aligned nanofibre production methods, nanofibre yarn production is not scalable to commercial scale production.

Yarn is a material structure of long interlocked fibres that can consist of various materials. In its long and pliable form, yarn is a versatile material that can be integrated into what is worn near to the human body. Changing the material of the yarn can possess properties of that material while being just as wearable. Integrating yarns with materials that hold other non-mechanical properties, such as high conductivity or piezoelectricity, into existing garments is an interesting field of research with commercialization potential.

Recent work that has been done with Revolution Fibres and AUT has shown that there is potential to adapt their existing electrospinning technology in Sonic Electrospinning to be used to produce nanofibre yarn. Sonic Electrospinning is a proprietary "needle-less" electrospinning technology developed and currently used at Revolution Fibres. Results showed that the technology was capable of producing yarn with higher throughput than other lab scale setups were able to achieve. This setup is referred to as the Aardvark.

However it required refinement and had issues around spinning efficiency. To take those next steps in optimizing the setup, an investigation was conducted into developing a testing setup that is modular and can test different electrospinning methods. The results of these methods were observed and implemented onto the Aardvark setup.

1.3.1 The Aardvark

Nanofibre yarn was produced at AUT successfully using the Aardvark. It showed that there was much to improve on in terms of spinning consistency and fibre collection efficiency. Figure 1.3 shows an SEM of one of the nanofibre yarn samples collected from the Aardvark spinning setup. The SEM image shows that there is good alignment in the fibres and consistency in fibre diameter. Fibre alignment is an indicator of good axial yarn strength. Fibre alignment is achieved by manipulating the electric field to have them align right before attaching to the nanofibre bundle that forms the yarn.

The Aardvark setup will be continously developed to produce a more refined nanofibre yarn electrospinning machine after this research is completed. The designs, models and builds of the Aardvark can be seen in Appendix D.

1.4 The Two Prong Approach

The work done in this research is part of a larger project that contains a Nanofibre yarn development project and an experimental setup that tests different electrospinning configurations. The experimental setup is to be used to test the feasibility

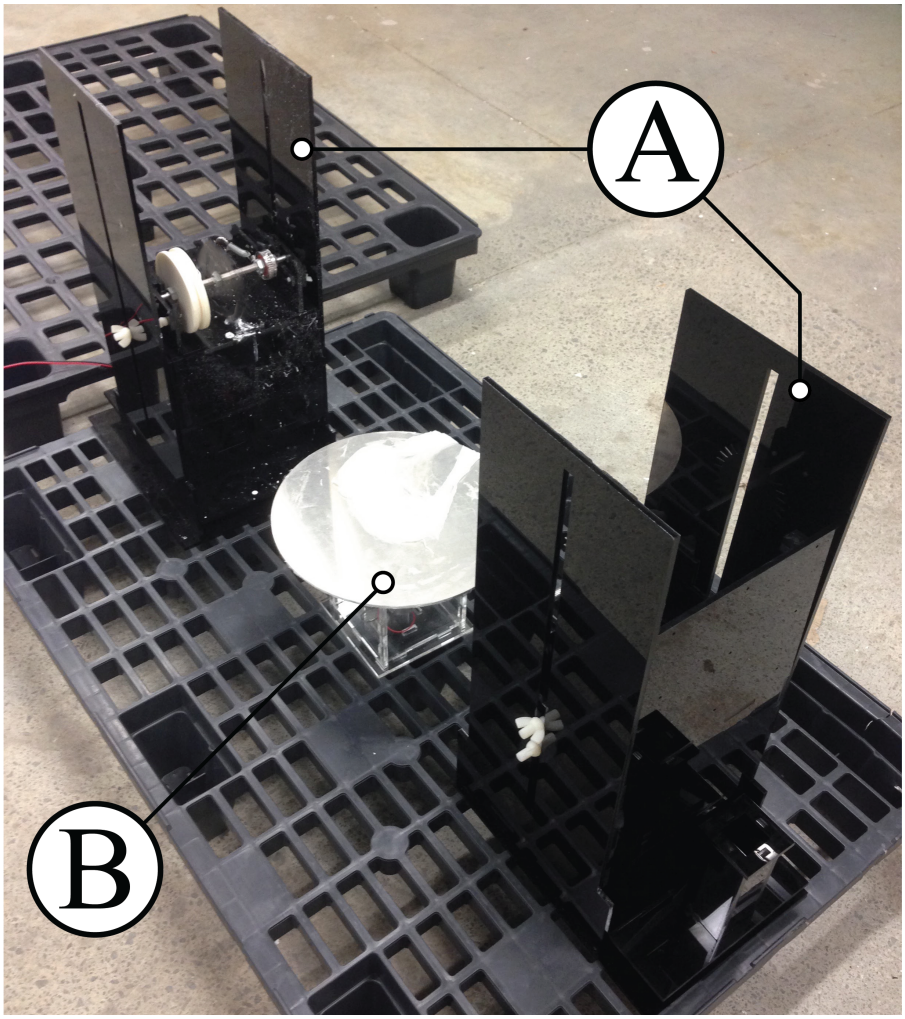

Figure 1.2: Aardvark - a nanofibre yarn production rig. (A) Fibre spinning towers (B) Rotating fibre bundle collection unit

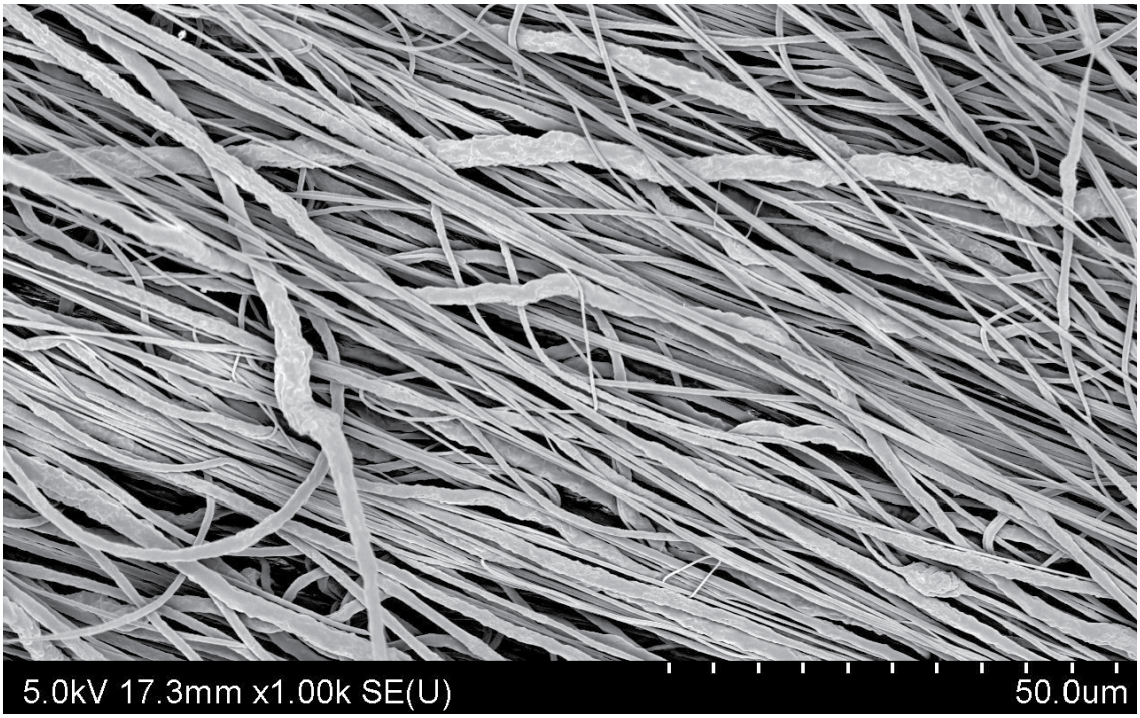

Figure 1.3: SEM image of nanofibre yarn fabricated with the Aardvark

of different electrospinnning methods that can potentially be implemented on the Aardvark setup. This approach is used to allow experimental work on electrospinning to be done in an isolated setup that could lessen the number of variables that affect the system. This is a more effective method of testing that can help improve design considerations for the Aardvark.

1.5 Research Aim & Objectives

This body of research aims to investigate the feasibility of other electrospinning mechanisms that can potentially be implemented to better understand electrospinning and its mechanisms. This feasibility study will:

- Simulate the effects that geometry and materials have on the electric field shape
- Develop, design and build an electrospinning setup that will test electrospinning in uniform and non-uniform electric fields
- Investigate the feasibility of using the mentioned setup for electrospinning.
- Investigate the feasibility of electrospinning using a submerged needle to manipulate the spinning direction.

Chapter 2

Literature Review

This chapter reports on the literature surveyed, which assisted in putting together the research methodology for this thesis. It starts by covering the fundamentals of nanofibres and the basis of their production via a method termed electrospinning. This chapter then presents issues relating to electrospinning and identifies a potential change in production methods. The chapter then concludes with the research question.

2.1 Introduction to Nanofibres

A nanofibre, is a fine fibre with that ranges in diameter from several nanometers to hundreds of nanometers[17]. These nanofibres hold characteristics of the material they are made from while also possessing the properties that come with being very thin in diameter. Properties such as a high surface area to volume ratio significantly increases the van der Waals forces between the fibres and between other objects that come in near contact attracting the particles towards the fibres [18]. These properties make nanofibres advantageous as they deliver superior mechanical and electrochemical properties [19].

Commonly used polymers to produce nanofibres are PA6 /PA66 Nylon [20][21], chitosan in the form of a carbohydrate polymer [22], poly methyl methacrylate (PMMA) and polyacrylonitrile (PAN) which is used to produce carbon nano- tubes (CNT's) [23, 24, 25], and polyvinylidene fluoride (PVDF) [26, 27] which is a polymer with piezoelectric properties that is of interest in the world of textiles and wearable sensing [28].

Polymer nanofibers are being used in filtration, protective clothing, biomedical applications including wound dressings, drug delivery systems, the design of solar sails, light sails, and mirrors for use in space, the application of pesticides to plants, as structural elements in artificial organs, and in reinforced composites [29, 30, 31, 32].

The research initiated by Sir Geoffrey Taylor in 1969 and his findings laid the foundation for research in the field and termed the Taylor cone, a phenomena found in electrospinning, after his name. His findings were around using conducting viscous fluids that become conical in form when in the presence of a high voltage static electric field [2]. His work showed that the stability of the jets depend on the geometry of the electrodes because their shapes would determine the direction of the electric field and the gradient if present. Taylor's work would reignite interest in

the field. His findings in electrospinning would be replicated and advanced by other researchers[5, 33].

2.2 Electrospinning

Electrospinning involves using a solution consisting of a polymer that is dissolved in a strong acid or solvent [20]. Fibers are formed by fast evaporation of solvent from a polymer solution jet that spin off a nozzle that is charged [34].

The process uses two oppositely charged electrodes with a high DC voltage and introduces an electrospinning solution into the static field produced by the electrodes. This initiates a process of extruding a jet from the solution which starts off as a uniform jet and then starts to whip in an erratic manner which then leaves behind an extremely fine jet of solution which dries up and lands as a fibre on the electrode that is oppositely charged.

Theoretical and experimental activities in this area in the last 30 years were revitalized by several important contributions by Taylor in 1969 as shown in the plot in Figure 2.1 which shows an increase in the use of his findings to date. He produced noticeable experimental evidence that relates strength of an electrostatic field to the magnitude of the deformations that appear on the surface of a droplet of liquid placed in that electric field. He first found that fine jets of slightly conducting viscous fluids and thicker jets or drops of less viscous ones fluids can be drawn from conducting tubes by electric forces. As the electrical potential of the tube relative to a neighboring plate increases, viscous fluids become nearly conical and fine jets come from the vertices. The potentials at which these jets or drops first appear was measured and compared with calculations.

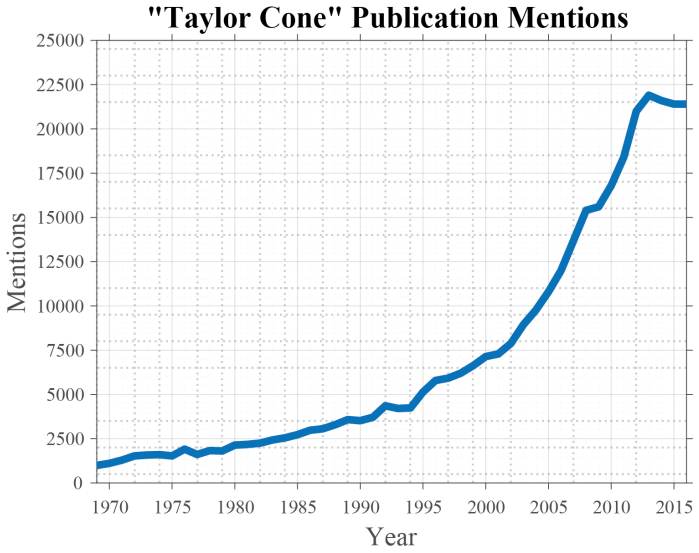

Figure 2.1: Number of mentions of the term 'Taylor Cone' in the public domain. Data acquired using python script that extracts the historic word occurrence of a search term in academic papers (from Google Scholar) [1]

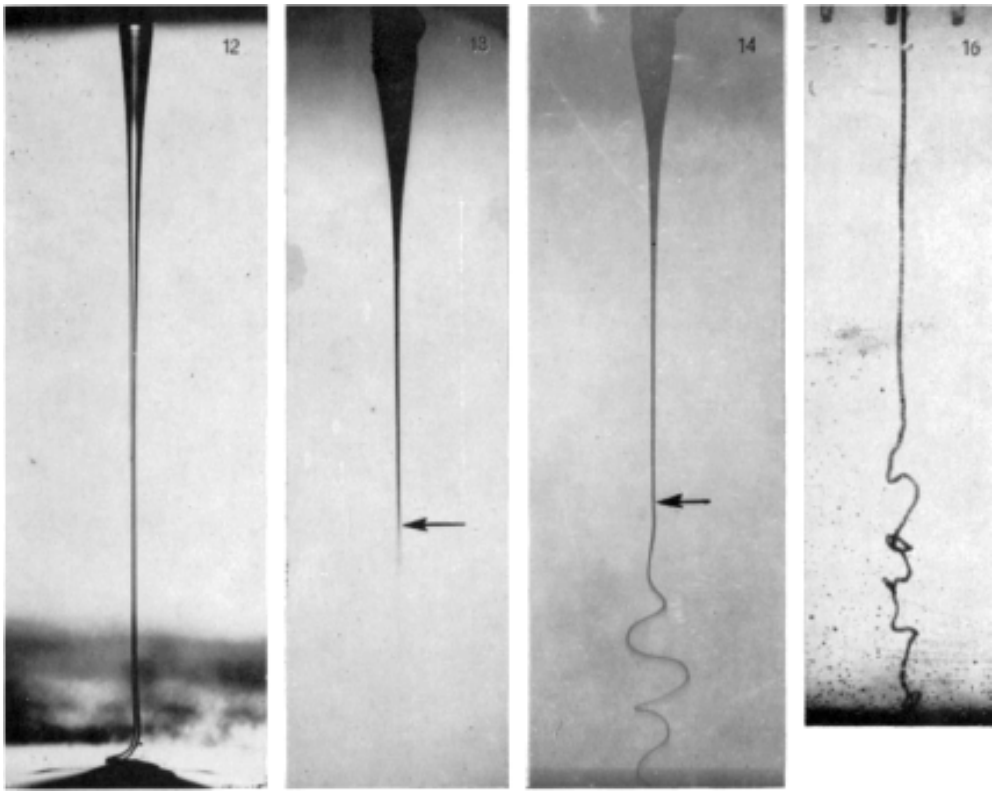

Figure 2.2: Samples of Taylor's experimental data [2]

Taylor [2] had tested various solutions under similar conditions and used photography to capture the jets and analyze his experimental data as shown in Figure 2.2. He had used various solutions to test his model which is based around their viscosity. His findings show that in some circumstances a jet was observed which appeared to rise steadily for a short distance and then to disappear suddenly. This finding led to the possibility of nanofibre formation using this phenomena. In an attempt to explain the unstable behaviour of the jet, he stated that the viscous stresses play a role to show it being stretched like a string while it is extending. Also in a setup where the jet is going against or tangential to gravity, the formation of the jet stream would contract longitudinally and then becomes unstable with an instability analogous to that of Euler when an elastic column is under end compression.

Taylor's work was limited to only anecdotally mention that the tail end of the jet that is formed becomes invisible. He stated that the electrically charged jet traveled for a few centimeters in a straight line. At the end of this straight segment, a diaphanous shape, also conical, with its vertex at the end of the straight segment, was seen when proper illumination was provided, and then disappears. What happens to the jet after it disappears is where Peter k. Baumgarten did the bulk of his work in 1971, however this time using a solution mixture of a polymer-solvent mix.

Baumgarten's research worked with one of the two setups that Taylor had performed and that was a needle with plate setup where a single fiber was drawn out from the electrically charged drop which was suspended from the needle or capillary tube [3]. He setup his experimental work to show that various polymers could be spun using the same methods that the patents from the 1930's and 1940's were using to produce fine meshes of polymer fibres [35, 36]. The experimental data gathered uses similar imaging methodology as that used with Taylor's work which is shown in Figure 2.3a.

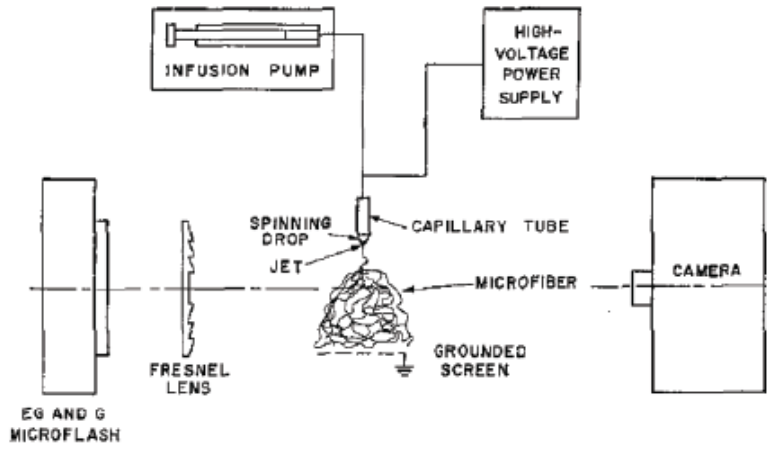

(a) Overview of Baumgarten's Experiemntal setup with camera position relative to the electrospinning setup

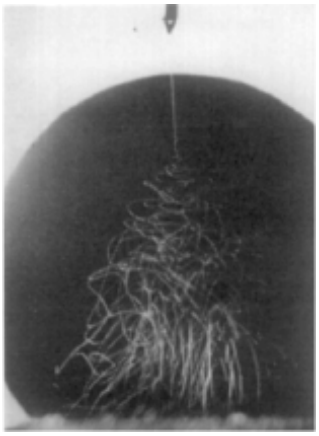

(b) Sample of Baumgarten's electrospun jet experiment

Figure 2.3: Overview of Baumgarten's Experiemntal work [3]

His images were one of the first to clearly show the chaotic nature of the electrospun jet shown in Figure 2.3b . These results depict the random motion of the electrospun jet as it travels towards the target. However, because Baumgarten had the intentions of producing fibres from the solution mixture like those in the previous patents, the variables added were considerably more than in Taylor's experiments. The addition of a volatile organic solvent like dimethylformamide (DMF) meant that the variables such as viscosity and polymer concentration were dynamic and changed rapidly in different stages of the experiment. This added another layer of complexity to the mathematical model, meaning it would only be valid during a short stage of the electrospinning process because the nature of the solution changed. In spite of that issue, Baumgarten's methodology proved to be more appealing to the research masses which was evident in the publications that ensued in the years to come [24, 27, 37]. This redirected research output away from the fundamentals of electrospinning that Taylor had begun exploring such as the two plate experiment.

The next significant achievement in electrospinning research in the years that followed Baumgarten's work came at the turn of the century with the studies that Darrell Hyson Reneker carried out on electrospinning. Reneker published work on electrospinning nanofibre, however Reneker mostly validated what Baumgarten had already pointed out in terms of electrospinning. Reneker's setup in 1993 and in 1996 were only slightly modified versions of what Baumgarten had where the needle and metal screen would be positioned in parallel to the ground rather than the needle being above the plate and gravity working with the spinning direction [20, 33].

In 2000 Reneker and Yarin would revisit the investigation of electrospinning fundamentals using methodology and setup similar to that which Taylor had worked with and then attempt to build a more refined mathematical model that would better explain the bending instability of the jet [4]. This involved a needle-based electrospinning setup where the needle is placed directly above an earthed plate and the spinning direction in-line with gravity. Reneker would analyse the spinning using a camera coupled with a fresnel lens to aid in magnification, as shown in Figure 2.4. Reneker would go on to investigate the ion mobility inside the fluid and compare it to the relative speed of the fluid flow in the jet. He found that the ions in the jet would move at an estimated rate of 0.1 m/s whereas the jet as a whole would travel

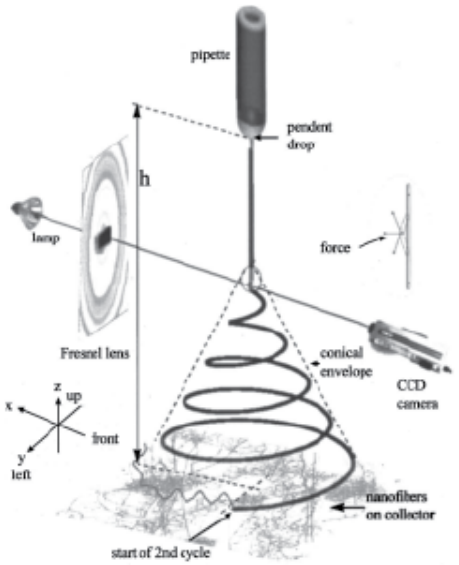

Figure 2.4: Reneker's experimental setup portraying camera's position in reference to the electrospun jet [4]

at about 1 m/s. In other literature reviewed it was observed that the jets would be moving at a speed of up to 5 m/s [38].

Reneker's experiment uses the 'typical' electrospinning setup as portrayed in Figure 2.4. The testing conditions noted are environment temperature, polymer molecular weight and solvent mixture. However little is mentioned on the electrical parameters and the effects the direction and shape of the electric field would have on the spinning. This is where the addition of FEM modeling on the experimental setup would be beneficial and that is what Deitzel supplemented his body of work with in his research on the controlled deposition of nanofibres.

Deitzel's work discusses how the electrostatic forces acting on the charged elements making up the jet and the visco-elastic responses of the polymer based solution react to these forces. The instabilities are caused by variables that include viscosity, surface tension, electrostatic forces, air friction, and gravity. These are the variables that Reneker's mathematical model of the jet motion took into account, however Deitzel goes on to mention that Reneker's efforts were met with little success because other variables played a significant role in the process and the complexity of the model would increase. He would go on to mention that the detailed understanding of the jet motion would remain elusive and decided to focus on the electrostatic forces acting on the charged elements making up the jet and the viscoelastic response of the polymer solution to these electrostatic forces [5].

His work continues to delve into methods of controlling the electrospinning jet and the deposition process using mechanical and electrostatic means to shape the electric field. His idea was by controlling the shape and strength of the macroscopic electric field between the electrodes (i.e. syringe and collection target), it should be possible to dampen jet instability and to control the deposition of the electrospun fibres on a target.

The objective was to dampen the bending instability inherent in the process and that it would be done by using conductive electrode rings that would be charged to a potential near the potential of the needle that initiates the spinning process, as

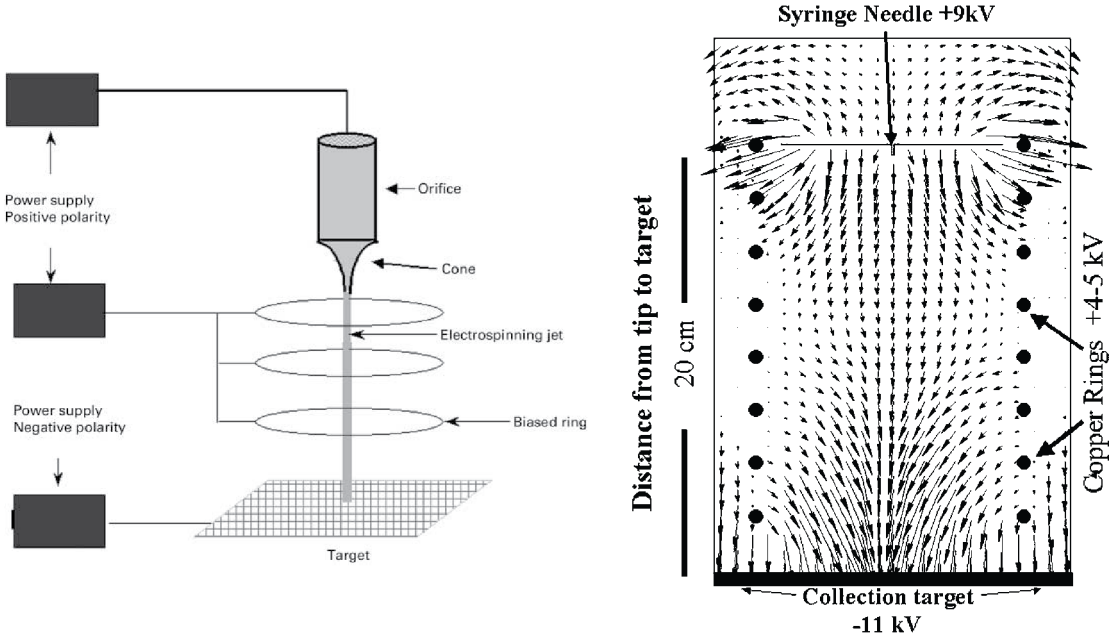

(a) Electrode geometry and potentials used in Deitzel's experiment

(b) Result of FEM analysis showing the direction and magnitude of the electric field on a plane

Figure 2.5: Illustrations of Deitzel's multiple electrode setup to dampen the instability inherent in the jet [5]

demonstrated in the illustration shown in Figure 2.5a. The dampening is achieved by designing a setup based on knowing how the electrostatic interaction between individual charge elements in the jet and the charged elements in the macroscopic electric field. The design of the electrospinning apparatus would in turn eliminate the bending instabilities through controlling of the shape, direction, and strength of the electric field. The field exists as a result of the potential difference between the point of jet initiation and collection targets highlighted in both the illustrations in Figure 2.5.

With Deitzel's experimental setup designed, he was one of the early few to add an FEM component (Figure 2.5b) to supplement his findings and to prove his idea that the superposition would be applied to calculate the strength of an electric field. FEM or Finite Element Modeling is a powerful tool that can help visualize aspects of electrostatics. His diagram in Figure 2.5b shows how the effects of making the rings at the same polarity as the initiating needle electrode would strengthen the field lines through the centre and weaken those that are pointing in different directions. Using FEM would become a staple in portraying the shape of the electrostatic fields in research publications that followed Deitzel's work.

The end result was that he achieved a setup that forced the jet to the centre of the setup in a manner that is analogous to a stream of water that is poured into a funnel. A comparison was done showing the significant decrease in the diameter of the nanofibre deposition area on the collector in the case of using the multiple field electrospinning apparatus. Deitzel states that this reduction in the area of coverage is the result of dampening the bending instability. The collection time for each strip was at 1.5 hours.

Interest in Deitzel's findings around controlling the deposition of fibres would then

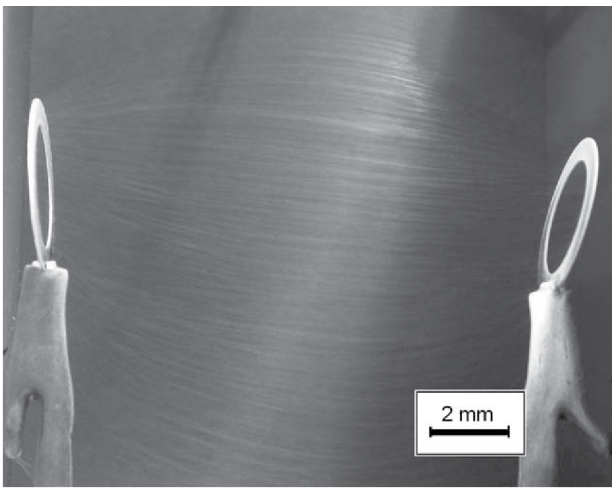

(a) Spun nanofibre bridging between the rings

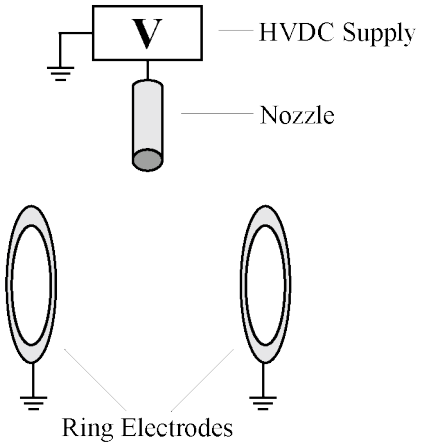

(b) Dalton's configuration

Figure 2.6: Dalton's two ring electrospinning setup [6]

influence further research to look at methods of controlling fibre alignment. Fibre alignment is important to the structural integrity of a nanofibre scaffold. Having the fibres in line would help distribute an axial load on all the fibres evenly and hence strengthen the structure. Most electrospun fibre collections systems result in a thin sheets of non-aligned fibre forming on the collector. They use a single collection plate that is earthed or oppositely charged to collect the fibres. The work of Dalton would show a method of aligning the deposition of the nanofibres in a suspended form with considerable volume of fibres [6].

Dalton's electrospinning setup consisted of three electrodes highlighted in Figure 2.6. The first being the hollow needle that initiates the electrospinning and two rings which are equidistant from the needle. Unlike Deitzel's setup, Dalton arranged the rings in a format where the direction of spinning is tangential to the perimeter of the two rings as opposed to spinning through them. The result of that is having fibres line up between the two conductors and 'bridge' between the two electrodes and can be seen as the fine lines between the two rings in Figure 2.6.

Unlike Deitzel's experiment which concludes with looking at the diameter of the deposition area, Dalton collects the aligned fibres and applies a certain level of twist to those fibres and then analyses the bundle as a yarn. This provides a means of producing yarn with a high level of alignment. This procedure however produces yarn in a manner that is discontinuous, meaning that a finite length of yarn can only be collected which in this case was between 40 and 100 mm in length. This advent though provided insight to an interesting behavior of electrospinning that Dalton noted. He says that there was poor formation of the electrospun fibre array. He continues to state that the fibres were situated at the lower part of the collection system and that work would have to be done to better direct the fibre deposition.

It seems that providing a research goal directed towards a more intricate and complex problem, like producing yarn via field manipulation, forces research to address what is unknown with the knowledge. The next section looks at setups that attempt to shape fields to address gaps in the electrospinning knowledge.

2.3 Electrospinning Yarn

Nanofibre when produced in an aligned format then collected and twisted would give a length of yarn that has the properties of being very thin and the inherited properties of the material. Hao summarised the benefits of yarn by stating that single nanofibers cannot be used directly due to their thin nature [39]. One way to overcome this obstacle is to spin nanofibers into yarns. Yarns hold more lateral interaction and friction between nanofibers. The twist is one of the most important reasons that keep their self-lock structure stable according to Hao. However, for yarn to be produced, fibres would have to be aligned and for that to happen it would have to done during the electrospinning process [40]. Dalton managed to produce a length of yarn but it was very limited in length. From a practical standpoint, yarn must be produced in a process allowing it to vary in length while maintaining its consistency. A continuously electrospun yarn is the only true way to produce yarn. For that reason, continuous nanofiber bundles with an interlocked fibrous structure offer a promising solution to drawing nanofibers effectively and continuously [34]. In recent years, various ordered nanofibrous structures with aligned bundled fibres have been achieved by means of field manipulation and moving or rotating mechanical parts. This section explores the different methods used to shape electric fields by means of electrode geometry that produce continuously electrospun nanofibre yarn.

2.3.1 Yarn Electrospinning Arrangements

In the research literature covered, it is clear that there is no one method of producing nanofibre yarn. Some have manipulated the electric field to have the bundling of fibres occur in an area suspended between the initiating electrodes [14, 39, 41]. Other research has found using a ring setup similar to that of Dalton's [42, 43, 15]. Another common method was using rotating collectors, whether it be in a drum form where fibre bundles are spun onto the surface of the rotating drum and 'pulled' out the electric field and wound up on the drum [9] and other methods by means of spinning on top of a spinning conductive plate that distributes the spun fibres onto a cone scaffold that winds into a yarn at the peak of the cone [7, 10]. That same concept of winding up fibres into a cone was implemented by spinning on to static curved surfaces such as cylinders and hemispherical conductors [11, 44]. However more recently there has been more success in terms of yarn throughput by spinning onto a funnel shaped collector that is static and surrounded by spinning nozzles that spin onto the nanofibre scaffold that converges into a yarn [45, 46, 47, 16, 12].

Drawing from the aforementioned publications with varying setups, there are two key elements that are important to achieving a yarn structure. Firstly, in all the setups, voltages of opposite polarities are used meaning that there would be an element that is positively charged and other elements in the setup that would be negatively charged, as opposed to having a single polarity and an earth. The second element is that the fibres are spun in a manner where they would bundle and align to one another and would help build the scaffold that starts the yarn drawing process. These two elements are not mutually exclusive, when spinning with a single polarity the bundling phenomenon does not appear to be achievable and in turn acquiring yarn becomes unfeasible.

When these fibres are spun into bundles, nanofibre yarns can be produced by aligning the bundles in a collinear manner. If the yarn is extracted at a sufficient rate from the field, newer fibre bundles would restore what is being extruded assuming the bundles are produced in a manner where they would replace the bundles that are being removed from the field which is a process that would be considered producing continuous yarn. The yarn is subsequently wound on a rotating drum collector as a twisted yarn [45]. The research on electrospun yarn is apparent in its systematic methodology that succeeded the work of Dabirian who spun nanofibre yarn using a modified conventional electrospinning setup [13].

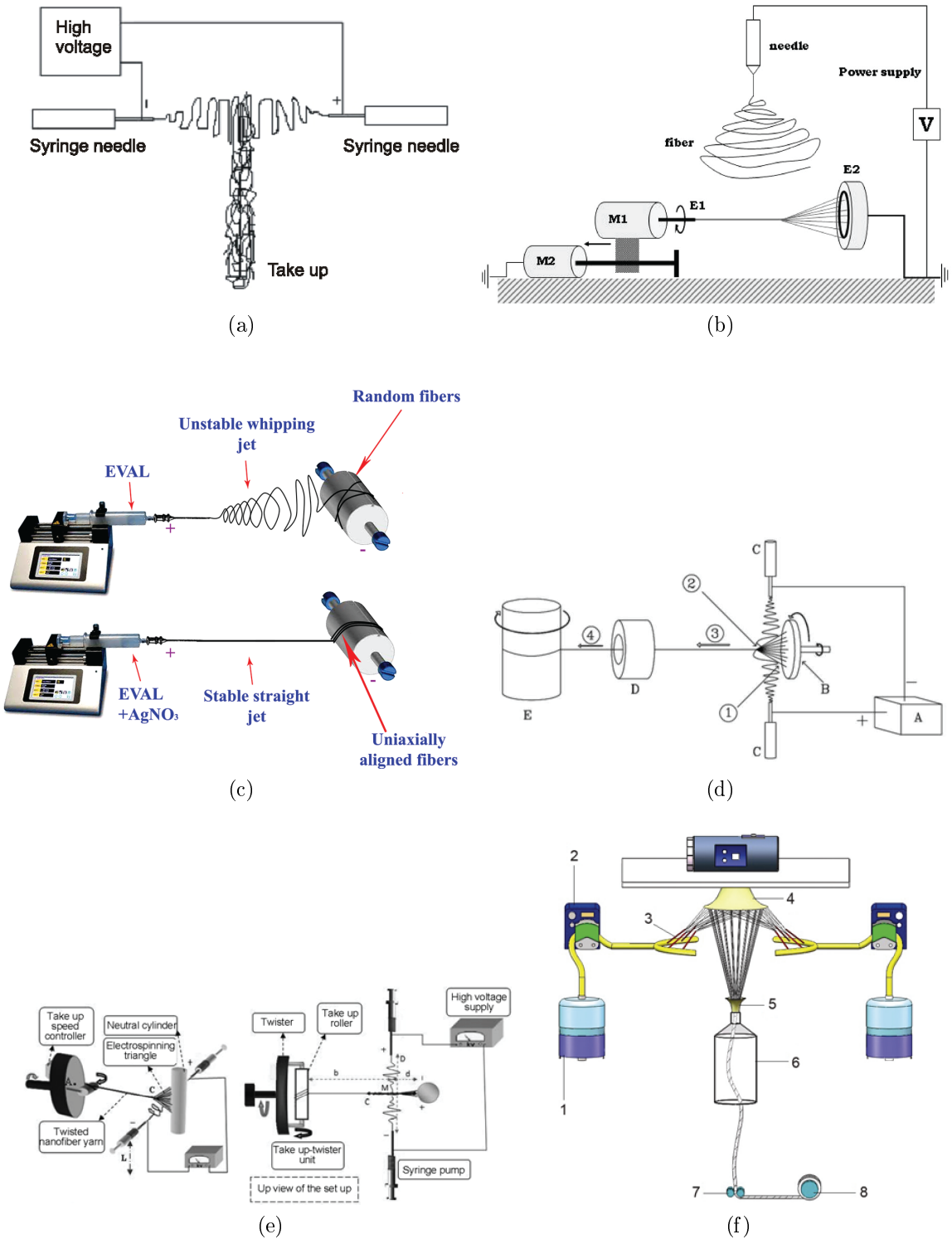

Figure 2.7: Various methods of electrospinning yarn by manipulating the electric field using varying collector geometry. 2.7a Spinning into space between nozzles [7]. 2.7b Yarn collected off ring electrode [8]. 2.7c Spun fibre wound onto drum as yarn [9]. 2.7d Yarn drawn from fibre scaffold from plate [10]. 2.7e Yarn collection from scaffold forming on spherical surfaces [11]. 2.7f Yarn drawn from scaffold on funnel [12].

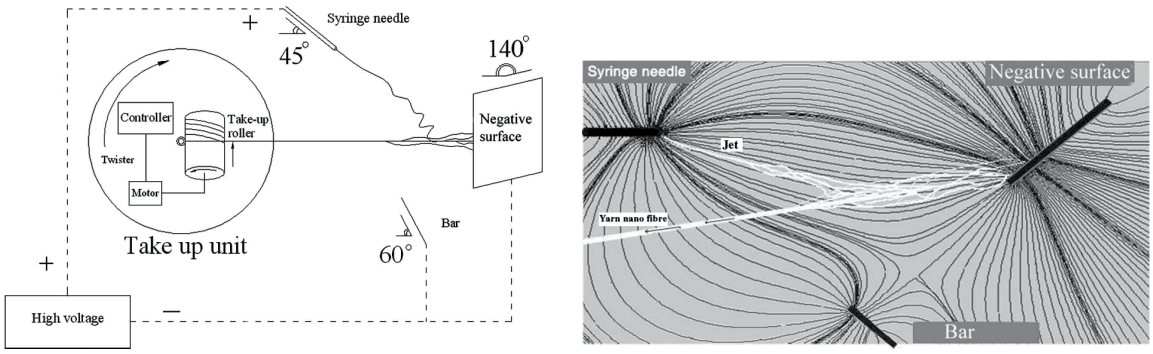

(a) Overview of the setup

(b) FEM analysis of Electric field lines

Figure 2.8: Dabirian's yarn spinning setup [13]

2.3.2 The Two Polarity Setups

Dabirian was one of the first to implement the use of an opposite polarity voltage to electrospin. His work in 2007 provided a foundation for research in electrospun yarn by showing how the manipulation of the electric field by using a different voltage polarity would initiate the bundling of fibres and collect them from within the field [6]. The aim of his work is manipulating the electric field of the electrospinning system to produce and collect continuous uniaxial electrospun bundled fibres into yarn. He is to achieve it while using a continuous yarn production method since many others have only been able to produce a very small finite length of yarn like Dalton's. The amount of fibres produced is controlled by conductive elements placed around the charged needle to shape the field using a negatively charged plate and a floating rod. The yarn is extruded from the collection of fibres in the field tangent to the field lines shown in Figure 2.8.

The basic operation is discharging fibers between the syringe needle and negative surface by concentrating negative charges at the apex bar located in the front of the syringe needle between the negative surface and the take up unit, seen in Figure 2.8. He claims that the amount of discharged fibres can be controlled by changing the distances between these parts. Dabirian also applied the use of an FEM tool to draw the electrostatic field and claimed the direction that nanofibers move inside the field is in an arc shape and the yarn is taken up at a direction tangent to that arc. Dabirian went on to post-process the yarns by passing them through boiling water and leaving to dry in hot chambers and compared them to those that were not left to dry. Having the fibre morphology analysed as the objective and comparing it to the changes in the electrospinning geometry would become a common method used to characterize the performance of the system in the literature that followed Dabirian's work. Some examples that demonstrate this trend are covered in the following section.

2.3.3 Collector Geometry

Electrospinning is initiated by a nozzle that is charged and jets are spun onto a surface or region termed the collector. Collector shapes and sizes have been varied through the research as displayed earlier in this section in Figure 2.7. In some cases though, the substrate used as the collector would be a region or a space between the two conductors, such that the yarn is collected in-between the two nozzles. The work of Fuqian Sun demonstrates this phenomena [14]. He produced PVDF-HFP nanofiber yarns which are prepared by conjugate electrospinning in order to extend the applications of nanofibers in the fabric industry and protective clothing fields. He claims that thicker yarns can be achieved by using several pairs of fibre spinning spinnerets. PVDF is used as the base polymer because of its micro filtration membranes and protective coatings. The setup used is a two needle setup facing each other at equally opposite polarities shown in Figure 2.9a.

Yarn is extracted from the space in-between the two needles that has fibres seemingly crashing into each other and in a fibre orientation which is not discussed. The term charged nanofibres is used by Sun claiming that the fibres attract to each other because they hold a charge. The method is seemingly promising however the fibres produced are poorly aligned and have a poor structural integrity as shown in the SEM images in Figure 2.9b. This could be because the fibres had poor direction the further they got from the initiating needle. Having that collector can help in strengthening the field at points further out from the needles edge which is something Dabirian explored in 2011 by using a round plate collector and auxiliary electrodes [10].

Dabirian's subsequent work involved two charged metallic spinnerets which were placed opposite each other, as seen in Figure 2.7d. He demonstrates that using a plate collector has the potential to produce quality yarns with improved consistency. SEM images of those yarns can be seen in Figure 2.10. His addition using a heating ring that post-treats the yarn strengthens the yarn itself. This paper follows the method mentioned earlier where the yarn produced is compared with the change in electrospinning geometry in play. There is little to no electrical analysis of the setup and no basis to work from as to why the rotating plate would work better than the other methods.

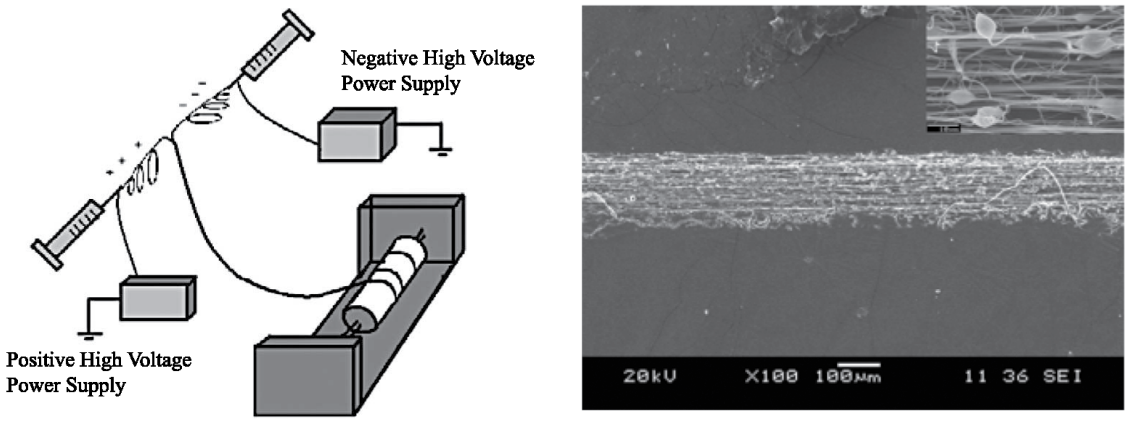

(a) Sun's electrospinning configuration (b) SEM of Sun's yarn

Figure 2.9: Sun's collector-less electrospinning yarn setup [14]

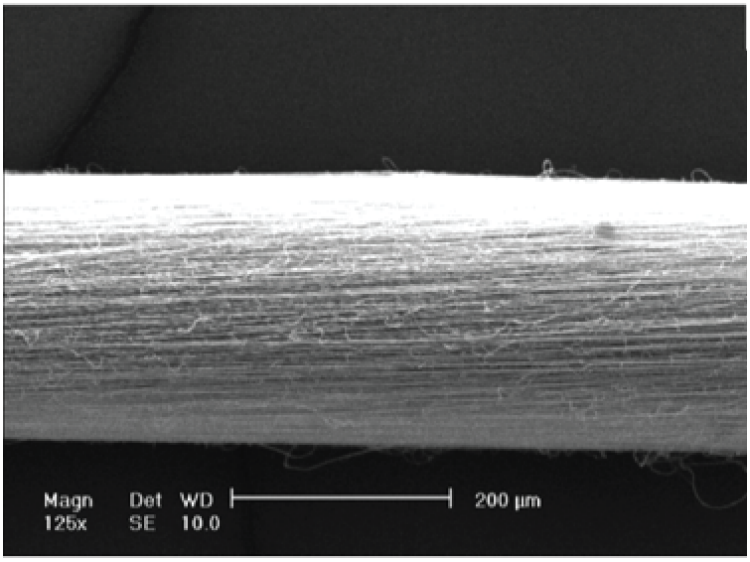

Figure 2.10: SEM image of Dabirian's electrospun yarn from the plate spinning setup [10]

The examples continue with recent research that tries inadequately to justify the use of different geometry that works with producing yarn, such as the recent ring electrospinning setups from Deakin University with research from Muhammad Nadeem Shuakat [15]. His work utlises a disc-based fibre spinner, which is a needleless electrospinning method shown in Figure 2.11, and claims to have used it because it is easy to operate at a relatively low applied voltage. There was no FEM analysis or a stated motive behind this selection other than it seemed to work better by a visual inspection.

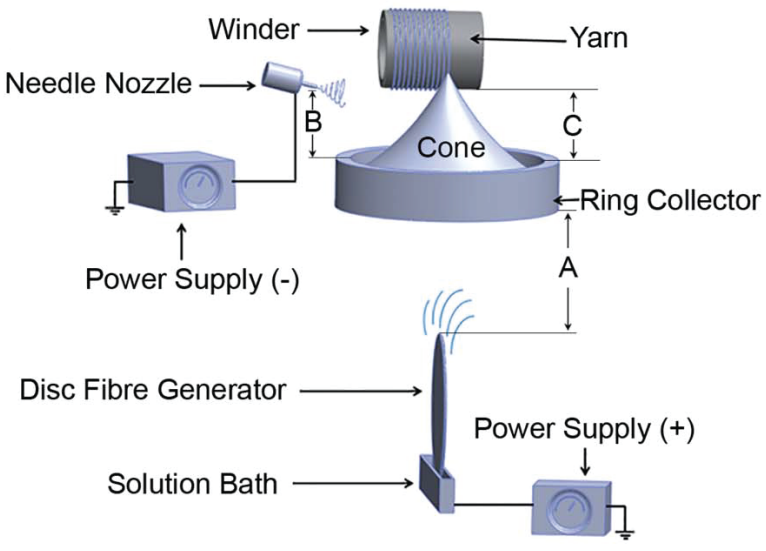

Figure 2.11: Shuakat's Needleless electrospinning yarn diagram [15]

2.3.4 Recent Use of FEM in Electrospinning

From the publications covered so far, the use of FEM as a tool to pre-analyse and investigate geometry selection for electrospinning is used sporadically. However, there has been a resurgence of FEM use that is evident within the latest series of publications from the Zhongyuan University of Technology in China. Two principle investigators, Jian-Xin He and Tong Lin, have had some involvement in all the research involving electrospun yarn. They had used FEM to analyze the effects of having a funnel shaped collector surrounded by two sets of nozzles oppositely charged to one another with the funnel left with a floating voltage. Starting from 2013 [16], He and Tong had incrementally improved the design of the setup year after year up until 2016 where Jianxin He worked on a multiple polymer electrospinning setup [48].

The use of FEM in the research from Zhongyuan University of Technology shows signs of promise of guaranteed incremental improvements in each iteration over the short period from 2010 to 2016 which is leading to the much anticipated success in commercially scaling electrospun nanofibre yarn for purposes such as wearable applications. The Figures in 2.12 show the progress in chronological order based on the publication dating.

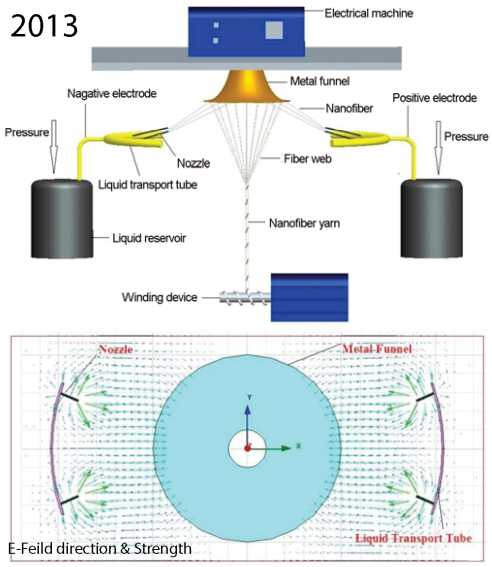

(a)

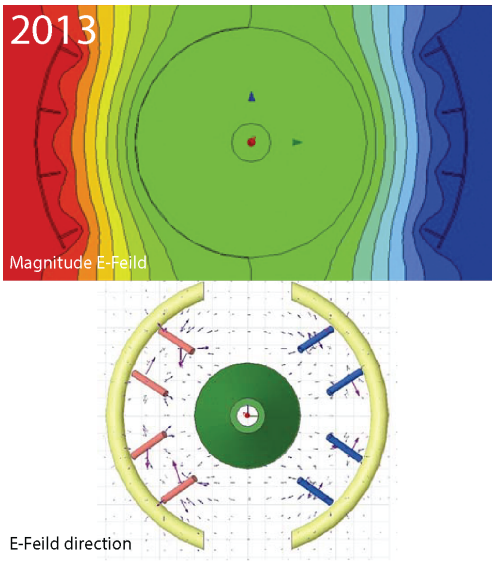

(b)

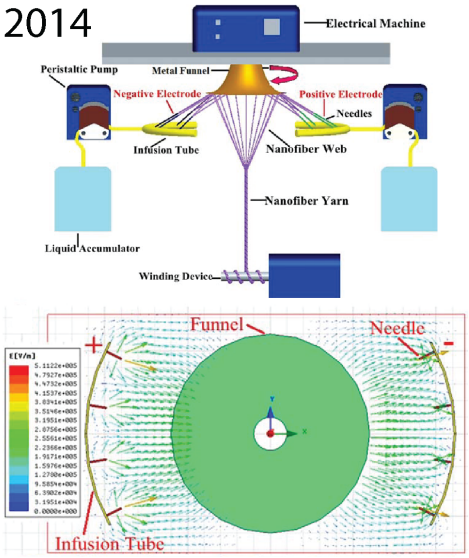

(c)

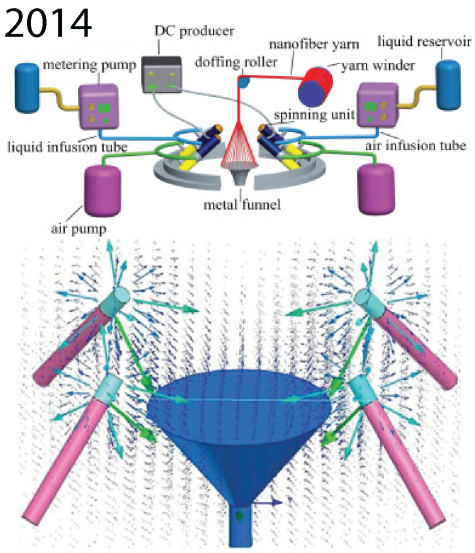

(d)

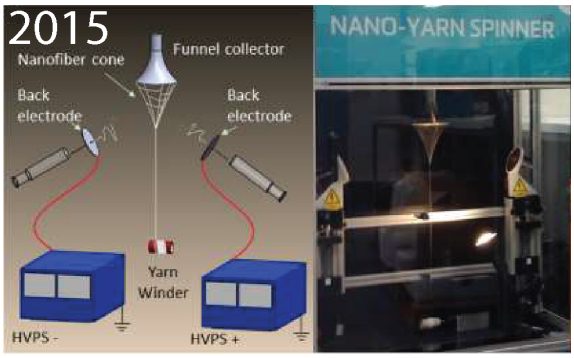

(e)

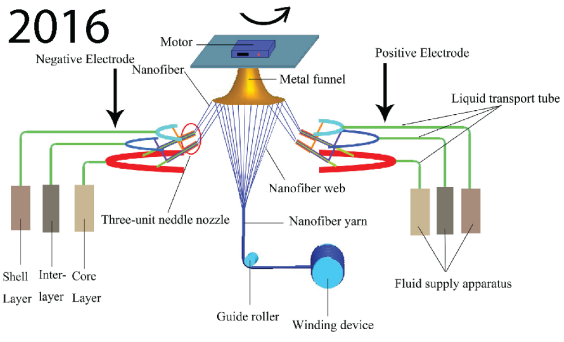

(f)

Figure 2.12: The progression of electrospinning yarn from Zhongyuan University of Technology. 2.12a First design using FEM to validate field direction and material dielectric properties [16]. 2.12b Second iteration analyses the effect of adding twice the number of nozzles.

2.4 Current State of Electrospinning

The addition of a second polarity in electrospinning evidently changes the way that the fibres behave in the electric field. However little is explained or referenced to explain why having different polarity plays a significant role, and why wouldn't having the same potential difference but using a single polarity achieve the same results. This and other issues are expanded upon in this following section.

Throughout the research there were many claims as to what 'works' and how that could be described by one variable without evaluating others. It seems to be a recurring theme with the more recent publications which are highlighted in this section.

Dietzel would talk about how electrospinning would occur once a critical voltage is exceeded and mentions a typical voltage [5], which in his case was 5 kV for the solutions mentioned in his paper. Yet he does not discuss how distance between the two electrodes plays a role where field strength is measured in V/m and 5 kV is a figure that is relative to the distance that is used. Another example that he claimed is that a jet of solution would erupt from the apex of the cone and is accelerated towards the electrically grounded collection target by the macroscopic electric field. There is no mention on whether the power supply is referenced to the same earth. He also continues to use analogies with little description of the basis on whether the claim is true where he says that it seemed the electrospinning jet can be thought of as a string of charged elements connected by a viscoelastic medium, with one end fixed at the point of origin and the other end free.

As briefly covered from Reneker's research on bending instability [4], he would mention the experimenting conditions such as temperature and solution concentration etc in detail, which is a recurring theme in most of the literature covered [24, 47, 27]. Yet another recurring theme is the fact that most, if not all, fail to get into detail around selecting certain geometric sets and mention whether or not the objects are earthed or left floating and whether or not the potentials of the power supplies are referenced to each other.

An example of this is in Deitzel's [5] work where he mentions the details relating to the electrodes and the spacing between them and then would go on to mention the three 'typical' electric potentials applied to the electrodes. It is not clear why this would be the typical situation because the electrospinning process is not digital and has its stages and varies in jet diameter with the changing electric field strength. Was it inspected visually and what seemed to 'work' remained constant through the testing procedure? Would having different voltages significantly change the outcome of the experiment? Further investigation can be done by implementing an experiment that would vary the voltages between the electrodes beyond what would seem to work well visually.

2.4.1 Geometric Selection

Dalton's setup which produced aligned nanofibre which was twisted into short yarn had little to say regarding the reason behind choosing the geometry of the electrodes and just had placed the two rings equidistant from the spinning nozzle and recorded his results [6]. Most of the work researched lacked a methodological approach of modeling multiple geometries and comparing the results in order to make an analytical decision to what works better for the application.

2.4.2 Charged Fibres

In Sun's research, he claims that at a certain distance the fibres would not attract anymore but does not explain why that occurs [14]. Would it be because the fibres lose their charge as they travel farther? Or would it be related to the influence the field would have on the dipoles in the fibres? The study then continues to detail the relationship between the yarn formed and the distance between the two spinnerets. The study states that beyond a certain distance of 50 cm, the fibres spun are too far apart to attract to each other to form a yarn. The study does not clarify this finding any further. His claim earlier that the yarn collection is made possible because the fibres attract to each other because they hold a charge seems unsupported.

2.5 Literature Review Summary

In conclusion, Taylor's research [2] provided an intriguing methodology for electrospinning that if repeated with present day methods of imaging and modeling can provide better insights into the fundamentals of electrospinning. This can be valuable when making decisions around electrode geometry and the relationship between the shape, strength and polarity of the electric field with the electrospinning process. He lacked a conclusion that would directly benefit the purpose of electrospinning nanofibre and that would be because there was very little work done at the time in that field. Taylor's expirements are used as the platform for the experimentation in this thesis. FEM analysis is also adopted as a principal component of this investigation to help optimize the experimental setup similarly to the research from Zhongyuan University of Technology [16]. The results from the experimental setup will be captured by photography similar to that of Baumgarten which provided a useful means of analyzing the behavior of the jet.

Concluding from all the aforementioned issues with electrospinning, Deitzel summarized it when trying to explain the behaviors of the excess charge and the motion of charge in the electrospun jet and that is that

> "The details of charge motion in the electrospinning jet are not well understood" — [5]

2.6 Objectives

The main objective of this research is to test the feasibility of a novel experimental electrospinning setup that could alleviate some of the issues faced in existing needle based electrospinning methods such as poor throughput rates and production efficiency. The feasibility will be assessed by observing the formation of an electrospinning jet with the setup.

A novel setup that can electrospin with needle-less configurations is investigated. Specifically, this work will focus on

1. Developing a computational model to help guide the design of the experimental set up, including physical dimensions. This part of the work is described in Chapter 3.
2. Developing and building the experimental setup for electrospinning. Chapter 4 describes this body of work.
3. Conducting experimental investigation to determine the feasibility of the novel configuration and the effect of various parameters on the performance. The results are presented and discussed in Chapter 5.

Chapter 3

Simulation - FEM and Data Analysis

3.1 Introduction

FEM analysis is an important aspect of the research. The literature review found that studies that have implemented this component found success in better shaping and designing the electrospinning field. For this research, FEM was used to answer questions about how changes in the shape of the electrode or test setup would affect the electric field.

The electric fields were simulated using software that calculates the electric field in terms of vector fields. Multiple experimental setups were modeled and compared in terms of field strength. The results were imported into MATLAB from the simulation tool for a more elaborate analysis.

3.2 Finite Element Modeling Procedure

Finite Element Modeling (FEM), sometimes denoted as Finite Element Analysis (FEA), is a computerized method for predicting how a product reacts to real-world forces, vibration, heat, fluid flow, and other physical effects. For this research, FEM was used to analyse the shape of the electric field around materials of varying dielectric strengths and shape. FEM works by breaking down a real object into a large number (thousands to hundreds of thousands) of finite elements, such as little cubes. Mathematical equations help predict the behavior of each element. A computer then adds up all the individual behaviors to predict the behavior of the actual object.

There are many software applications that are able to run FEM for electrostatics. For this research Maxwell 3D is used as the FEM modeler which is part of the ANSYS® Workbench software package (ANSYS, Inc. USA). Analysis was run using the steps outlined in Table 3.1.

The following sections will expand on each of the steps mentioned in Table 3.1. Each section will elaborate on the settings set for the model and the reason why it is considered valuable for this research. Also noted are calculations about issues that could affect the results and the action taken to work around the raised issue.

Table 3.1: Maxwell 3D's solution prerequisites

Procedure of Modeling with Maxwell	
1.	Select FEM solver
2.	Draw and extrude entities
3.	Set region size/boundary conditions
4.	Assign materials
5.	Assign excitation/voltages
6.	Define mesh
7.	Select solution interpretation(s)
8.	Define solution settings
9.	Start solver
10.	Modify data representation

3.2.1 Solver Selection

The Solver is software that solves mathematical problems. In this case, a solver is used to solve for all the voltages in the electric field. Different solvers require different parameters. With Maxwell 3D there are 5 different solvers: Magnetostatic, Eddy Current, Transient, DC Conduction, Electric Transient and an electrostatic solver. For this set of simulations, the electrostatic solver is used as the electrospinning process requires the analysis of static DC electric fields.

When selecting the electrostatic solver, all the frequency dependent parameters disappear because they are not required for the electrostatic solution. DC or static fields are used for electrospinning to move charges to the surface of the solution. Having an AC or changing electric field would move the charges back and forth which can make it more difficult to initiate an electrospinning jet.

3.2.2 Geometric Selection

The standard Maxwell drawing tools were used to draw up and extrude the models. Following the findings of the literature review and out of all the setups discussed, Sir Geoffrey Taylor's experimental setups were used as a starting point to further investigate electrospinning behavior [2].

Taylor's two setups consisted of a two plate setup and a needle-plate setup. Those configurations are drawn up in Maxwell and are modified slightly to accommodate the structure that would hold the two configurations together in a frame. The resultant electric fields are acquired from the configurations. Then, the geometry is changed presenting different electrode shapes and combinations that result in different electric fields. The list of geometric models are given in Figure 3.2.

3.2.2.1 The Two Plate Model

The two plate setup is a set of two parallel plates a fixed distance apart. The enclosure that surrounds the two plates was varied to observe how this changes the shape of the electric field. The model was based on the prototypical capacitor model which produces a uniform electric field between the two parallel plates. The vector field is calculated along the y-z plane as seen in figures that show before and after the vector field overlay in Figure 3.1.

Two different parallel plate geometries were analyzed, square and circular plates with equal side and diameter lengths. The effects of having a non-conductive enclosure to hold the plates apart was analyzed as well. The incorporation of high impedance conductive film was modeled to show the effects a gradient induced field would have on the plate setup in the enclosure. Finally, the placement of earthed conductors and non-conductors near the geometry was modeled to simulate the effects of having the experimental setup near features of a building.

1- **Two Square Plates** Two square 500x500mm plates, that are 2 mm in thickness, are placed parallel to each other as shown in Figure 3.2a. The distance between the inner surfaces of the two plates is 500mm. The plates are placed equidistant from the origin of the 3D drawing environment which helps scripting the data gathering algorithm for the electric field data later on. This configuration is the benchmark and will be used to compare against the other arrangements.

2- **Boxed plates** The actual build of the two plate setup is to be held up by a frame or an enclosure that replicates the effects of having an enclosed environment for electrospinning. The two square plate configuration is supported with a non-conductive box-like enclosure of Plexiglas or Perspex portrayed as the semi-transparent sheets of the model in Figure 3.2b. This is done to assess the effects of having those materials present near the charged plates and how significant are the effects of the enclosure on the uniformity of the electric field. Results from this model are directly contrasted with the results of two plates without an enclosure to better interpret the effects of the enclosure.

3- **Circular plates** Having square plates can have adverse effects on the electric field in particular in the corners of the plate. These sharp edges of the square have a significant effect on the shape of the electric field. One way to mitigate the effects of those corners is not to have them to at all and that can be done by using a circular plate. A circle with the diameter of 500 mm is drawn up, as shown in Figure 3.2c, with the same thickness of 2 mm and is distanced equally from the origin at 500 mm apart between the two inner surfaces. There is, however, a compromise in the surface areas of the two plates but for the purposes of this test the areas concerned are more towards the center of the two plates.

4- **Voltage gradient film** A thin sheet or film is drawn and placed near the edges of the two plates. This arrangement is to examine the effects of a high impedance material that is applied with a high voltage gradient that would be inducing the direction of the electric field to be in the same direction that is between the two plates. The purpose of this model is to show whether applying such an arrangement would mitigate the effects of any structural infrastructure nearby the arrangement would have on the uniformity of the electric field.

5- Earthed conductive rod This configuration is the same as the two square plate setup with the addition of a cylindrical structure offset by a distance from the center of the plate couple placing it outside of the two plates. This configuration simulates the effects of having the two plates near a structural body of the built environment that the experiment is run in. From this arrangement, it can be deduced if having nearby conductive objects to the experimental setup at that distance would possess a significant risk of affecting the uniformity of the field. Figure 3.2d shows that configuration.

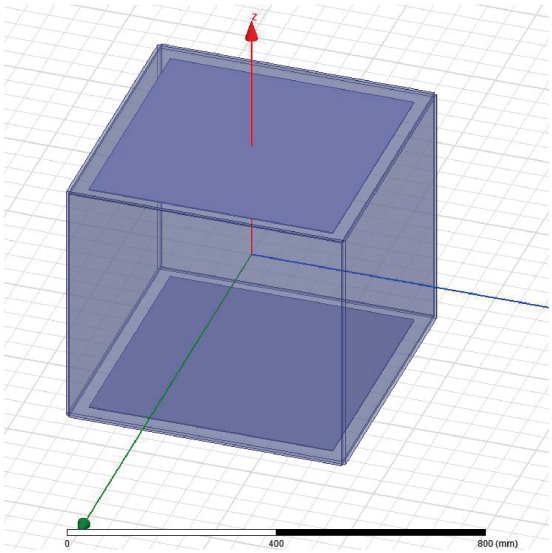

(a) Boxed two square plate setup

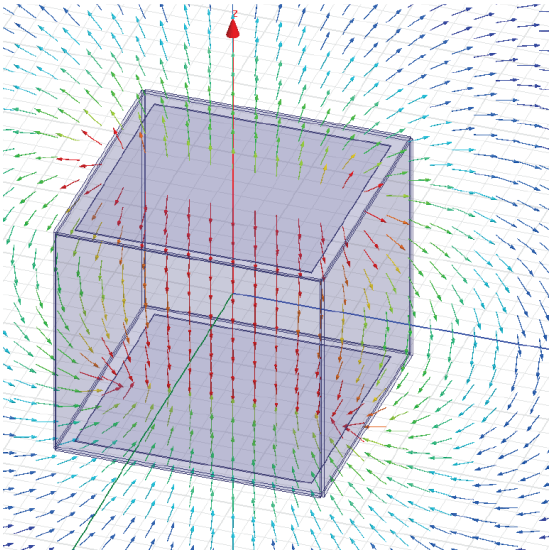

(b) Solved vector fields with acrylic material

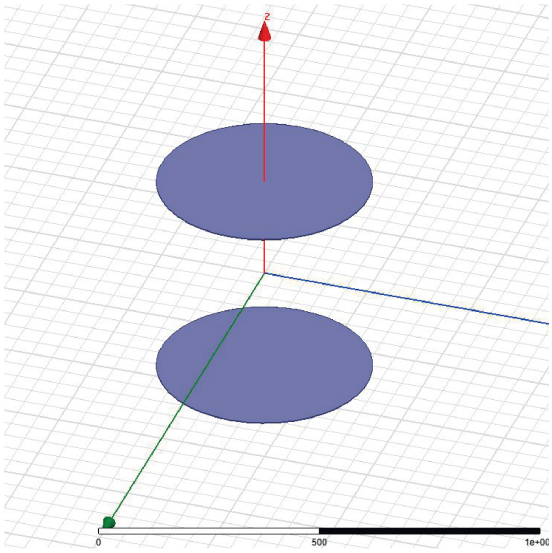

(c) Circular plate geometry

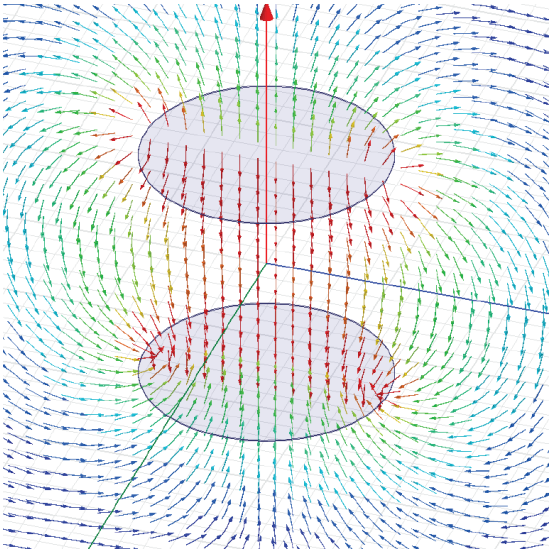

(d) Solved electric vector fields

Figure 3.1: Two Maxwell solved vector fields with and without solved vector field overlay

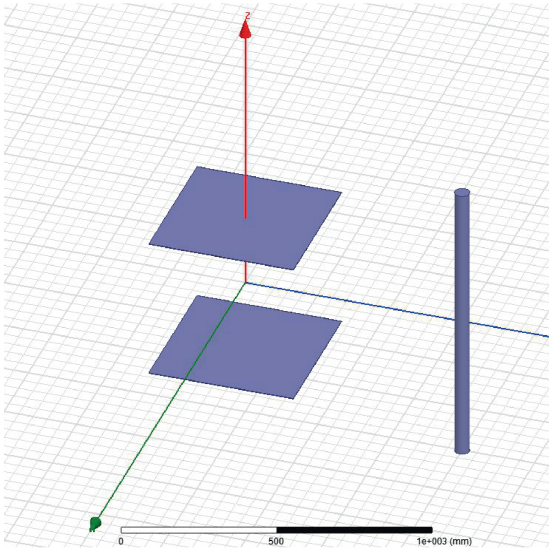

(a) Two Square Plate Model (Side = 500 mm)

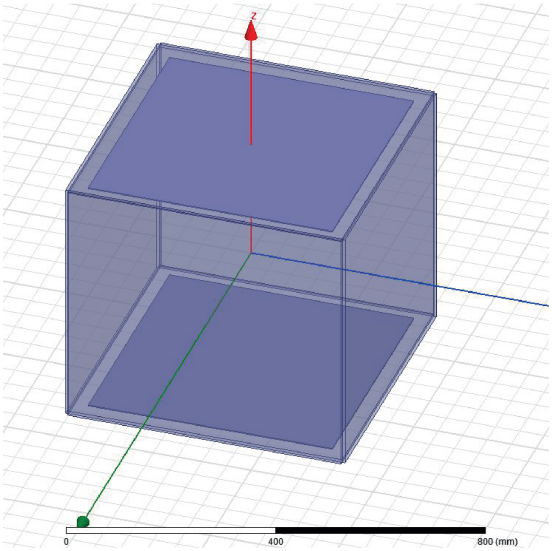

(b) Two Plate setup boxed in Perspex

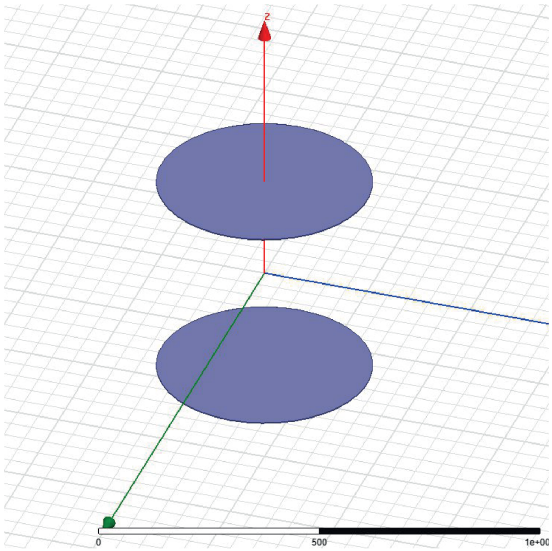

(c) Two circular plates (Diameter = 500 mm)

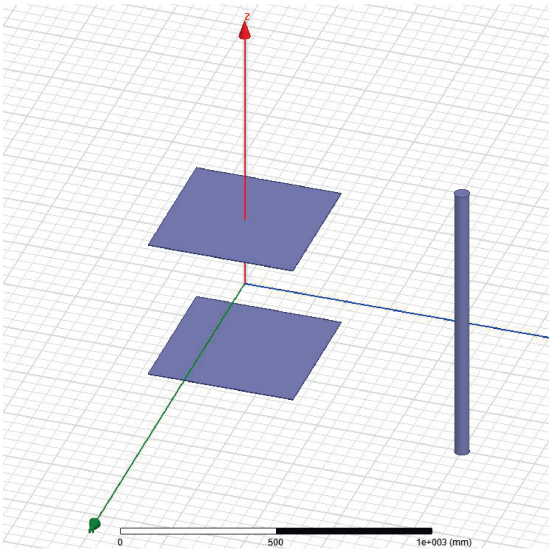

(d) Conductive rod placed near the two plate setup

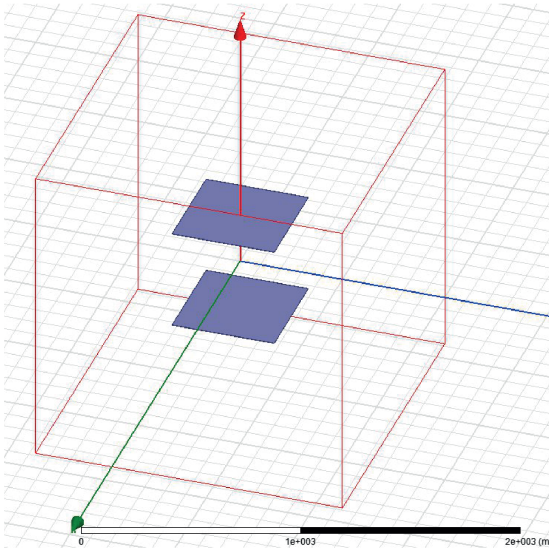

(e) Two Plates in region size of 100% of geometry

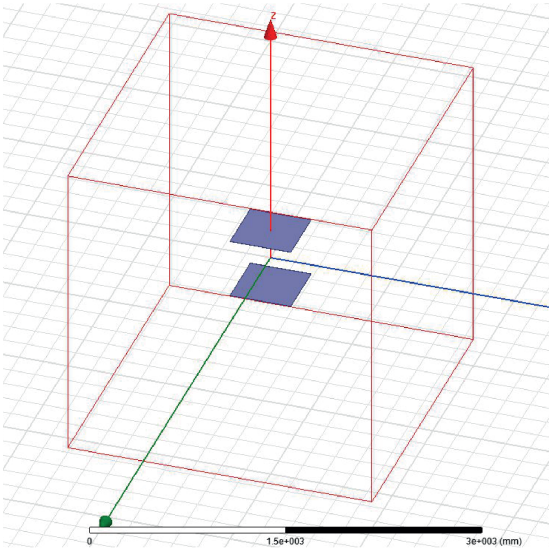

(f) Two Plates in region size of 200% of geometry

Figure 3.2: Various two plate simulations

3.2.2.2 Needle and Plate Model

The previous setups all consisted of alike shaped plates and in some models and in some cases an auxiliary object offset from the primary plates. Assuming the infinitely large two plate capacitor model, these models would result in mostly uniform field lines with no gradient. Upon changing the ratio of sizes between the two plates, a non-uniform gradient in the electric field is produced. This model consists of a single plate at the top situated at the same coordinates as the two plate setup and in place of the bottom plate, a thin cylinder representing a needle is positioned at the bottom inline with the center of the top plate.

3.2.3 Region size

The boundary conditions for the solver are set by an area or volume specified by the user called the region. A geometric cube encapsulating the 3D model is set for each arrangement. A region can be set using two different methods, one being an offset percentage from the geometry in all three axes and the other method is for it to be in a fixed position. The region for the simulations was set by an offset ratio of 100% in all directions from the edges of the geometry of the first two plate setup. Then those positions are acquired and applied as fixed position regions for the rest of the simulations.

A comparison is run comparing the difference in results from a simulation run with a 100% offset from the geometry and 200% offset to compare if results significantly differ. An identical set of geometry to the two plate setup is used but this time with the boundary conditions doubled to what it usually is which is from an offset of 100%, seen in Figure 3.2e, from the edges of the geometry to an offset of 200% from the edges of the geometry as seen in Figure 3.2f.

3.2.4 Material selection

Upon specifying the 3D objects in Maxwell and with the region size set, materials are assigned to each of those objects including the region. Maxwell 3D allows the assignment of materials to all selectable objects. Outlined below are the materials selected for each of the geometries.

Plates The primary plates in all the simulations is set to be pure aluminum. This material is selected for its ease of procurement and its highly conductive properties.

Region The region comprises of all the space around the geometry, which includes the dielectric in between the two plates. The dielectric strength is a material property which is defined as the maximum voltage required to produce a dielectric breakdown through the material and is expressed as Volts per unit thickness. The higher the dielectric strength of a material the better its quality as an insulator. The regions for all the arrangements are set to be vacuum.

High-Impedance Film A simulation was conducted having a highly resistive film placed near the plates to investigate the effects of inducing a gradient field through the material. The material assigned for this film is of custom specifications in Maxwell where the dielectric strength and resistivity can be specified to determine the material's properties. The value of 1 $M\Omega \cdot m$ is assigned for the material to reduce the current flow that could be caused from the high DC voltage induced across the material.

External Conductors Materials are assigned to models where objects are placed near the parallel plates that would represent a structural body of the built environment surrounding the experimental setup. Structural steel is selected as the material for the auxiliary objects which better represents the scenario that is faced during the experimental procedure.

3.2.5 Excitation

An excitation or voltage can be applied to any select-able object in Maxwell. They can be applied to an entire body, a single face, an edge or a point on the drawing. For the plates and auxiliary objects, a voltage is applied to the entire body while the film has two different voltages applied onto the top face and the lower face producing the gradient field along the body of the film. An overview of the voltage values applied to the objects is shown in Table 3.2.

The potential difference between the plates is to be set constant with all the geometric sets. This is to ensure that the evaluation in the end is logical in its correlation to the other geometric sets. A voltage of 5 VDC is set for the upper plate and 0 VDC for the bottom plate. With the set distance of 500 mm between the two plates, it is expected to have a field strength of 10 V/m in parts where the field is uniform.

Table 3.2: Voltages applied to each of the geometries

Geometry	Value [DC Voltage]
Top Plate	5 V
Bottom Plate	0 V
Bottom Needle	0 V
Conductive rod	0 V
Top of Hi-Z film	5 V
Bottom of Hi-Z film	0 V
Region	N/A

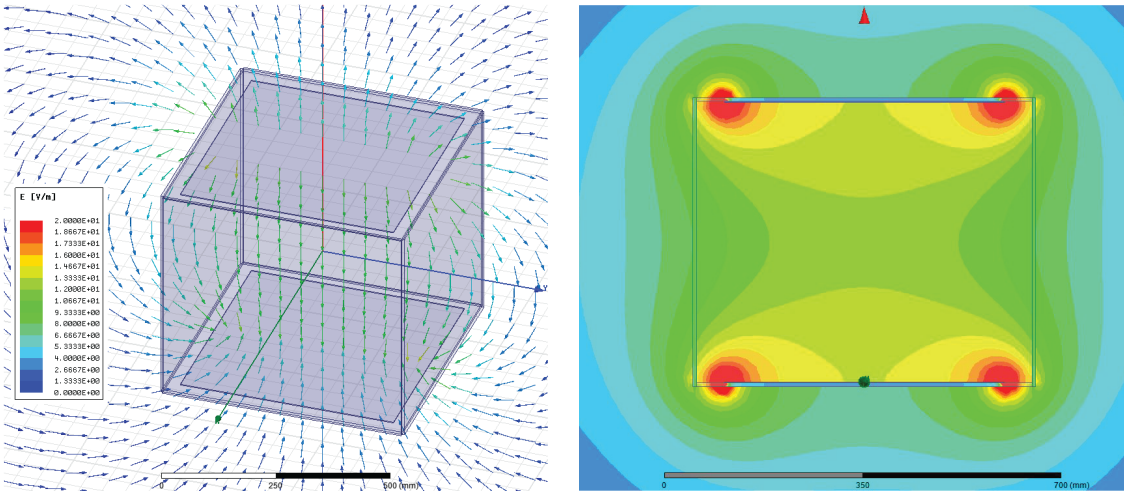

(a) Vector diagram of E-field on YZ plane (b) Magnitude E-field strength on YZ plane

Figure 3.3: Maxwell solution overlays for two boxed plates

3.2.6 Mesh Setup

Maxwell uses its own pre-built mesh generating algorithms to create fine meshes around areas of complex geometry such as edges and corners and coarser meshes around regions with little change in geometry such as a flat surface or open space distant from objects. This reduces computing time significantly and produces results that are reliably consistent within a certain tolerance. However, a fine mesh is not required everywhere in the model for the purposes comparing differences between two fields in particular. This means that coarser meshes in open areas where reading the curvature of the field caused by nearby objects is significant. For this reason, the mesh size was set to be generated so that mesh elements were no larger than 10% of the distance between the two plates. The fundamental unit of the mesh is a tetrahedron.

3.2.7 Solution Interpretation

Selecting how the solution data is represented can be done prior to the solution process. The solution data can be rendered and overlaid on any selectable object, plane and or part of an object like a face. The two relevant overlays for these simulations are the vector field and the magnitude field strength overlays. These overlays are useful to visualize the solution data upon the solver completing its calculations. The Figures in 3.3a and 3.3b show an example the overlays of the vector field and the magnitude field strength on a plane that runs through the center of the arrangement and represents the values of the voltages in each point in the region, the plates and the non-conductive enclosure.

3.2.8 Solution Settings

The electrostatic solver selected goes through all the mesh units and acquires a solution to each one. A single run through solving all the mesh units is called a 'pass'. The solution can be set so that multiple passes are run and then compared with the previous acquired value at that point and the difference between them is evaluated. The solver can be set so that passes continue until the previous value and the current value of each point converges to a certain percentage. In this simulation, the number of passes is set to be 10 and the convergence value is set to be less than 10%. The solver will run until either of the two criteria are met. The settings window with the solver parameters can be seen in Figure 3.4.

Once the solver settings are specified, the drawings and settings are validated by Maxwell to check for any errors. The parameters covered are set to be the same for all arrangements to ensure that the correlations that are made with the data can be valid. The solver is then run once all the parameters are set.

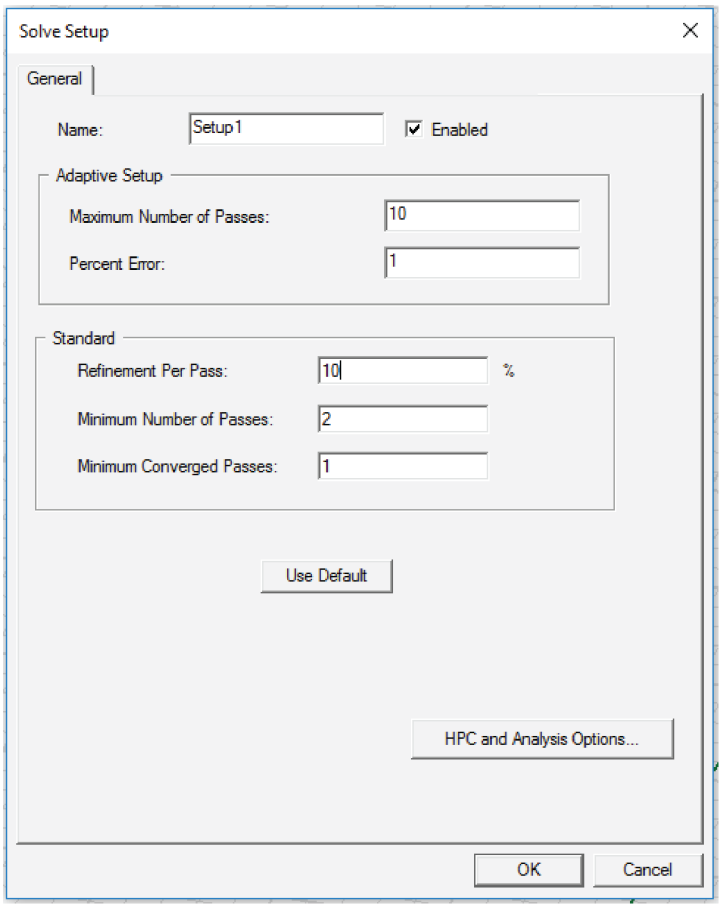

Figure 3.4: Maxwell's solution settings window

3.3 Calculating & Exporting Solution

This section discusses how the data generated by the solver is converted into a data set that can be practically read and analysed using data analysis software such as MATLAB (MathWorks, USA).

3.3.1 Maxwell Calculator

To obtain results from the multiple simulation sets, Maxwell contains a powerful calculator tool that works as a scanner that can be manipulated to obtain data from the simulations and even process the data mathematically directly within Maxwell. A small script is written in the calculator to obtain the electric field vectors from the simulated electric fields around the geometries on a single plane coincident with the z-axis. The calculator is setup to obtain data points on the plane inline with the grid that is set up. The values for the calculator are highlighted in Table 3.3. These include the start points (min), end points (max) and the spacing between each data point that the calculator follows to acquire the data from the model solution as shown in the plane in Figure 3.5.

Prior to the calculator running, Maxwell's plotting tool is used to display results to show any evident discrepancies in the solution. This is to confirm that the results makes sense and that there was not something significantly incorrect such as an excitation not set to the correct level or correct polarity. This is important because beyond this stage the data will be in a text file stored into arrays that are processed and aggregated with other data sets and then displayed as a plotted product of those data sets making it hard to back track the root cause of the discrepancy.

The data is to be represented in three vector components that equate to a 3 dimensional vector that represents the direction and strength of the electric field along the point path setup by the calculator in the grid format shown in the Table 3.3. The values are all in mm and are distances from the origin of the drawing which is set to be located at the mid point between the two plates.

Table 3.3: Start points, end points and spacing of the calculator grid

Axis	Min	Max	Spacing
x	0	0	0
y	0	500 mm	10 mm
z	- 500 mm	500 mm	10 mm

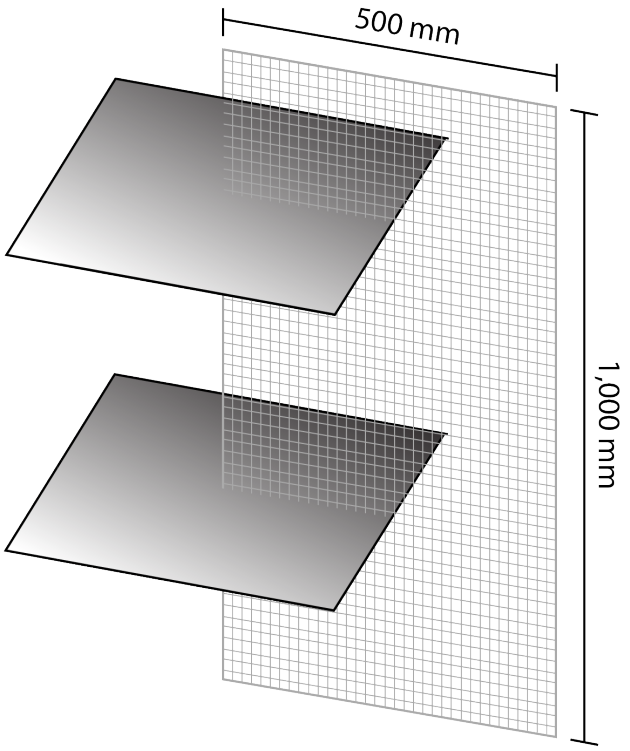

Figure 3.5: Diagram of the two plate setup with the plane that the calculator is setup to follow based on the values in Table 3.3. The gray grid highlights the area of the calculated data points.

The resultant grid is a plane that is 500 mm wide and 1000 mm high. Points were taken from only one side of the plane. This is because symmetry of results is assumed and points are only taken from half of the yz plane. That area or the plane of data acquired is shown in the diagram in Figure 3.5, the x data is not written because of the plane being located on the yz plane.

The data acquired from the plane is set to be put into a delimited text file. The delimited text files contain 6 columns. The first three represent the geometric position of the electric field vector and the last three are the three vector components of that vector at the that geometric point. Table 3.4 shows the structure that the Maxwell calculator data is saved in.

The delimited data file was converted into an excel spreadsheet which was then processed with MATLAB's built in `xlsread`. The implementation of the MATLAB processing and functions used to process the data are discussed in the next section.

Table 3.4: Delimited data structure where '$\cdots$' represents vector components at positions x y z

Coordinates [mm]			**Vector Components**		
x	y	z	i	j	k
-	0	0	$\cdots$	$\cdots$	$\cdots$
-	10	0	$\cdots$	$\cdots$	$\cdots$
		$\vdots$			
-	500	490	$\cdots$	$\cdots$	$\cdots$
-	500	500	$\cdots$	$\cdots$	$\cdots$

3.3.2 MATLAB processing

The data files are processed with MATLAB to investigate the differences between two data sets of electric fields. Using two geometric sets, the approach is to use existing functions from MATLAB to extract the data points and display it in a format that is easily relatable to the geometric models. To achieve this, the three vector components of each vector are summed up into a single magnitude value. Then a mesh is produced using the `meshgrid` function, this generates a grid using a matrix of the same dimensions as the dimension of the point grid from Table 3.3. The grid now exists on the x-y plane and the magnitude data is placed as a grid of the same dimensions on top of the mesh giving a value to each cell on the grid.

Finally the magnitude of the electric field at each point in the grid is super-imposed to show the strength of that field in color. The intensity is represented on a color bar to the right of the plot as shown in the Figures in 3.6. To better understand how the plot is read, such as the one in Figure 3.6b, it is useful to compare it directly to the diagram in Figure 3.5 showing the plane that the calculator grid follows. The plot in Figure 3.6b is the representation of the plane in Figure 3.5.

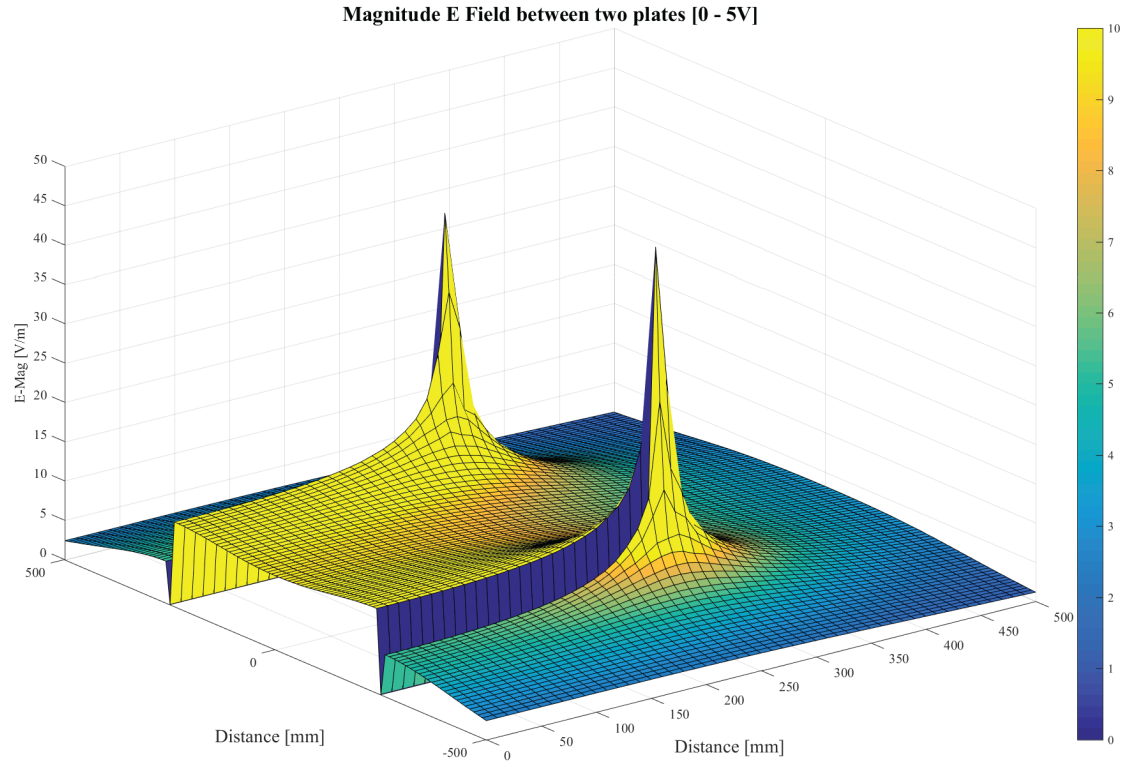

(a) Isometric view of meshgrid plot

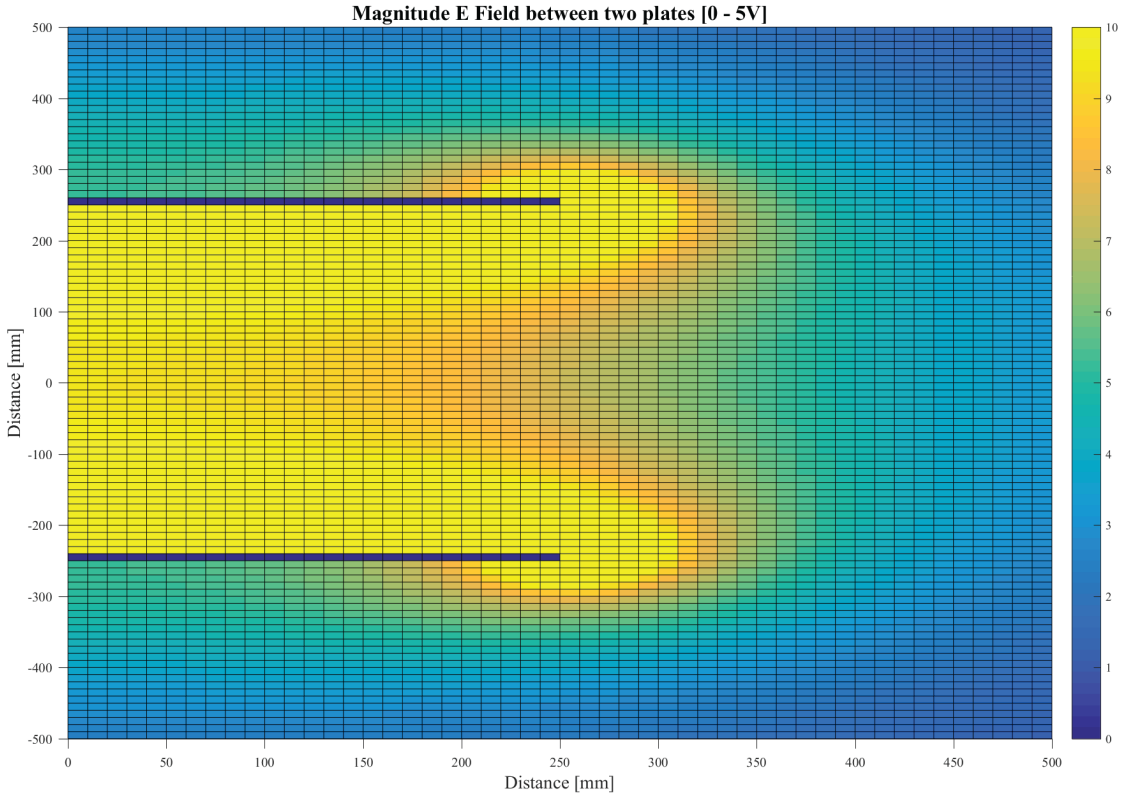

(b) Top view of meshgrid plot in 3.6a

Figure 3.6: MATLAB generated meshgrid plots of the magnitude E-field

3.3.2.1 Data Processing Script

The custom MATLAB script processes the data in the following order, where it starts with the text file outputs from Maxwell:

1. Data files from Maxwell are loaded into equal 5151×6 designated arrays.
2. The first three columns of the array represent the x-y-z position of the unit vectors in the last three columns. They are summed into magnitude values and stored in subset arrays.
3. The difference of two subset arrays are calculated and stored into a single column array.
4. The column vector is then resized into an array sized to the grid layout that the Maxwell calculator acquired the data on using the reshape function
5. The final set of reshaped arrays are now ready to be run on the plotting script All the plotting, meshed grid creation, the unified formatting and color schemes across all plots is done by the custom MATLAB plotting script.

The complete data processing script, code and its comments are appended to Appendix A.

3.3.2.2 Plotting Script

The plotting script runs the following commands for each plot:

1. Start new MATLAB figure environment
2. Create a mesh with the same spacing and dimensions as the calculator path from Maxwell using the MATLAB function `meshgrid`.
3. Use the surface plot function or surf to plot a set of the reshaped magnitude data against the mesh.
4. A set of formatting rules and color scheme is applied to the data plot.
5. The output is also saved as a PDF for scalability of the plot.

The complete plotting and formatting script, and its comments, is given in Appendix A.

3.4 Closure

This chapter outlined the how ANSYS Maxwell 3D was used to simulate and provide the voltage data of the electric fields of various electrode geometries. Highlighted as well is the procedure used to process the data and render it onto a graph that is used to visualize the shape, uniformity and changes in magnitude of the electric field. The plotted results observed in Section 5.3 are subsets of two sets of data used to compare models and evaluate them in relation to the experimental design required. The data collected and the scripts alluded to in this chapter are in Appendix A.

Section 5.3 discusses the results acquired from the FEM simulations and investigates the effects of changing geometry and auxiliary objects on the shape of the field. The following chapter explains how the designed experimental setup addresses field uniformity and the approach to ensuring that it remains consistent throughout the experimental procedure.

Chapter 4

Experimental Investigation

4.1 Introduction

This chapter outlines the experimental setup, experimental procedure, result acquisition methodology and results processing into readable data. The chapter starts with the modeling and design overview of the experimental rig. The experimental procedure follows outlining the requirements for the experiments. That is then followed by the experimental infrastructure of the setup and its components. The pre-experimental regimen is covered as well. This helps validate that the results acquired are true and objective. Other procedural features are covered such as the 3D modeling software used to map out and then construct the rig, the tools, equipment and materials used to construct the experimental rig. The chapter ends with a walk through of the result processing and the evaluation process which results in readable and analyzable data that is discussed in the following chapter.

4.2 Experimental Aim

Experiments were conducted to quantify changes in electrospinning due to

- Changing voltage potential between electrodes (ΔV)
- Voltage polarity of the electrodes
- Electrode positioning

This is followed by analyzing the electrospinning substance in response to those changes.

The experiment is used to test electrospinning in the following configurations

1. Uniform electric field
2. Non-uniform electric fields

In order to explore the effects of the different configurations, the electrospun jet is observed. Once a Taylor cone is formed, the emitted and displaced fluid can be measured in terms of jet diameter using optical imagery. The diameter can be tracked while changing voltage, conductor/electrode geometry and the measured fluid volume placed and displaced in reference to the electrode/conductor. The

diameters are then recorded by means of post processing discussed later in this chapter.

4.3 Experimental Setup

Conventional electrospinning is done by pushing the solution through a charged needle which then spins onto an earthed plate. The charges in the solution accumulate on the surface closer to the earthed plate. Once the forces of surface tension are over come, a Taylor cone forms and a jet of solution is ejected towards the plate. This experimental setup aims to replicate this process and expose the solution to different field shapes and voltage polarities and observe those effects.

This section outlines the components used in the experimental process, followed by a breakdown of the major components and their respective design and composition. The completed diagram of the setup is shown in Figure 4.1 which are discussed in detail in the following sections.

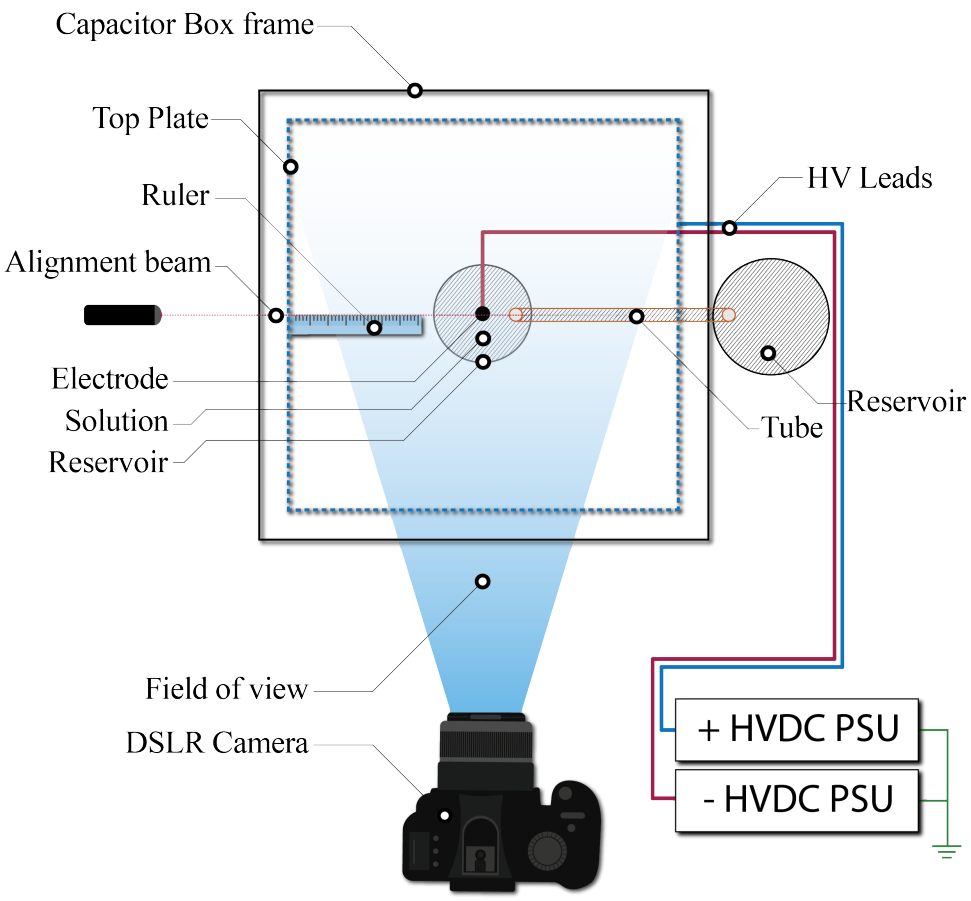

Figure 4.1: Overview of the experimental setup

4.3.1 Setup Design Overview

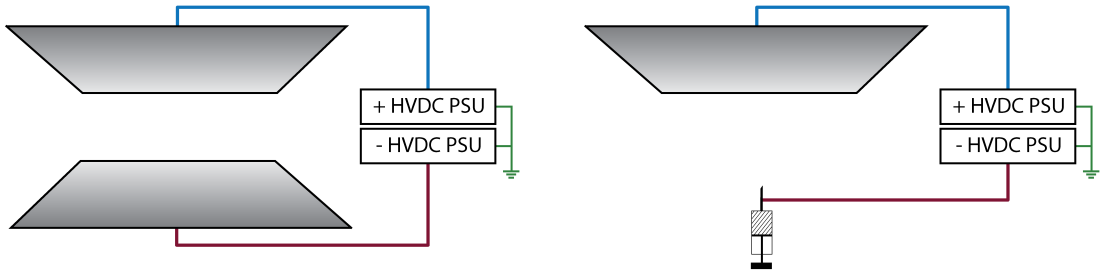

(a) Two plate setup (b) Needle and plate setup

Figure 4.2: Overview of the two experimental setups

Shown in Figure 4.2are the two setups used in the experimentation. There are three main components of the experimental equipment and they are labeled as

1. Capacitor Box
2. Power Supply Racks
3. Camera Setup

Measurements are captured in a setup that replicates the geometric setups covered in the previous chapter. This chapter covers the design of the rig that runs the experiments. Design of the rig is made to allow the integration of existing equipment and apparatus to be able to reconfigure the geometries for the different experiments. For this to be possible, the setup is to have interchangeable parts that also allow movement along a vertical axis, allow for an easy connection from a HVDC supply and hold fluid used to test electrospinning in different locations with various container shapes.

Coupled with the rig that runs the experiments, there is a method of capturing the diameters devised for the setup using DSLR cameras, lighting and means of calibrating distances and alignments using flat beam lasers. Manual work was reduced to only documenting the voltages and changes done to each setup which correlates to the filename of the image saved.

The designed setup is a cube frame with a plate that moves in keeping the top and bottom plates in parallel. This plate is connected with bolts to the walls of the frame and moves along rails allowing its height to be adjusted. A base plate and the adjustable plate allow for fitting different shaped electrodes which shapes the electric field in forms that were evaluated in the previous chapter.

The following sections detail what each of the parts listed consist of and outline the practical purpose and design features of each. Also covered are the materials used to construct, build and run the experiments.

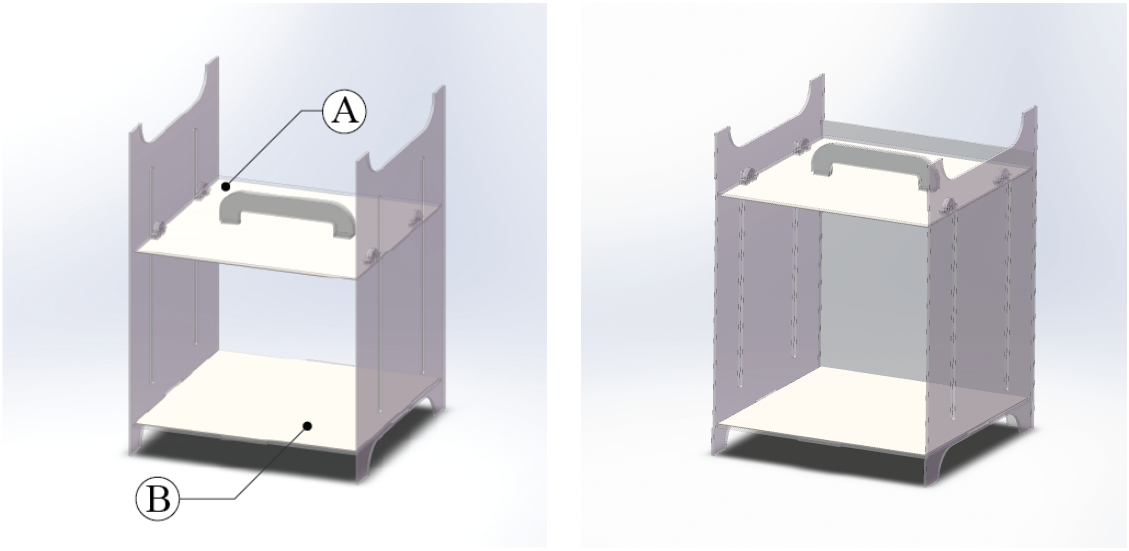

(a) Capacitor box demonstrating movable top plate (A) and fixed bottom plate (B)

(b) Top plate in at highest position

Figure 4.3: 3D render of the designed Capacitor Box done in Solidworks

4.3.2 The Capacitor Box

The core function of the capacitor box is to hold two plates at a set distance in parallel to one another. Achieving uniformity in an electric field is the starting objective of the experimental design. This achieves, in a sense, a parallel plate capacitor.

The enclosure had the following requirements:

- Hold two plates effectively in parallel
- Allow for interchangeable plates
- Allow for an adjustable distance between the two faces of the plates
- Have the capability of holding other apparatus such as needles and syringes when plates are removed

The Capacitor box is designed using only non-conductive components such as nylon nuts and bolts instead of conductive materials such as steel bolts. This is to prevent changes in the electric field that can be potentially caused from those conductive parts.

For the build of the Capacitor Box, the selected material is 6 mm thick sheets of Perspex. These sheets are laser cut to form the parts in the Solidworks diagram shown in the renders in Figure 4.3. The two renders 4.3a & 4.3b demonstrate how the top plate would move along the rails on the frame.

Perspex was selected to be the main construction material of the frame of the Capacitor Box. It is a strong dielectric which helps prevent arcing from occurring to surfaces outside of the capacitor box. It is also a very versatile material, easy to laser cut and is a rigid material for its weight. The plates that were held within the box are to be of 2 mm aluminum sheets, as in the simulations run in ANSYS Maxwell. The aluminum sheets were ordered from a local source and plasma cut to size, giving them a smoother cut around the edges with little to no deformations

or spikes forming from the cutting process. This smoother cut reduces the chances of arcing from a sharper edge to an object at low potentials allowing for a higher potential difference between them. Two different shaped plate pairs were cut up, a pair of square plates and a pair of round plates. The square plates have the same side length as that of the diameter of the circular plates.

4.3.2.1 Construction Process

The construction process of the Capacitor box was simple enough to complete using little to no tools. The process consisted of holding the interlocking parts together and bonding them using strong SCIGRIP Acrylic Cement glue. Figure 4.4 shows the construction stages of the Capacitor Box.

Certain parts on the movable plate such as the top handle and the hooks that hold onto the plate are multiple layers of the same part glued together allowing for improved stability when changing the elevation of the movable plate. Nylon fixings are used instead of steel bolts to mitigate the influence that the fixings would have on the shape of the electric field. Those fixings are pointed out in Figures 4.4b & 4.4c.

Figure 4.4a shows the laser cut outs that were done using a $60W$ laser cutter (Universal Laser System, USA) at the AUT 3D lab. The sheets are covered in a protective sticker that can be peeled off revealing the transparent sheet of perspex. The parts are assembled according to the Solidworks assembly shown in Figure 4.3. The assembly process required that some of the parts be glued together while help up, as seen in Figure 4.4b, and supported to allow the glue to set with the sheets in the correct orientation. The completed frame with all the parts glued and stickers removed is shown in Figure 4.4c.

Plates are then fitted onto the top and bottom plate as shown in Figure 4.5a. The setup is ensure that it is elevated sufficiently above the ground and placed on non-conductive surfaces, such as the platform in Figure 4.5b, to minimize the effects that the earth potential would have on the experiments. The HVDC supplies are in a trolley and have long leads, as seen in Figure 4.5c. This allow the supplies to be moved away from capacitor box.

(a) Laser Cut Perspex (A) shown with protective brown sticker

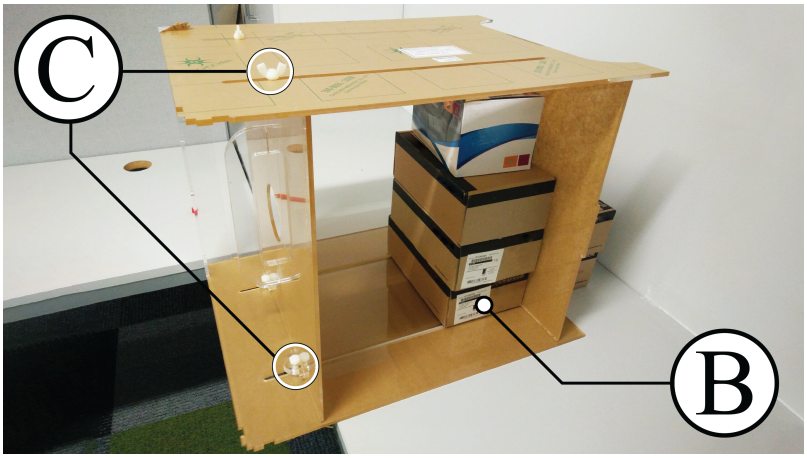

(b) Plates glued to set while supported with boxes (B) and nylon fittings added to hold movable plate (C)

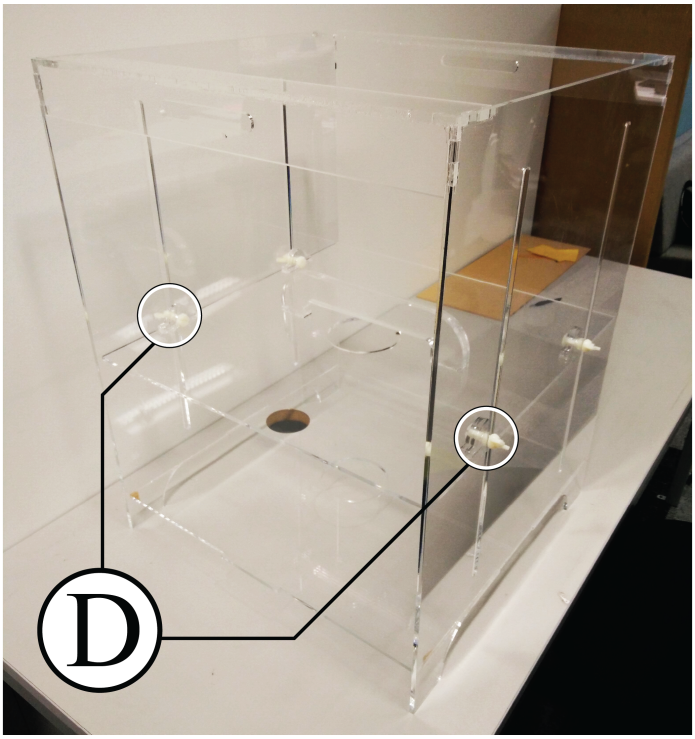

(c) Complete frame without protective sticker. Nylon fittings (D) that allow changing height of top plate within rails

Figure 4.4: Capacitor Box construction process

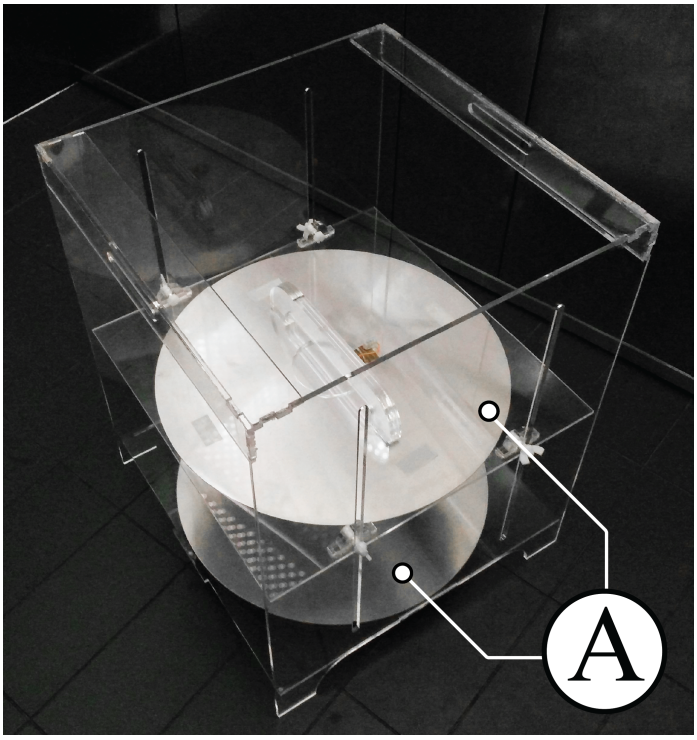

(a) Two round aluminum plates (A) fitted to frame

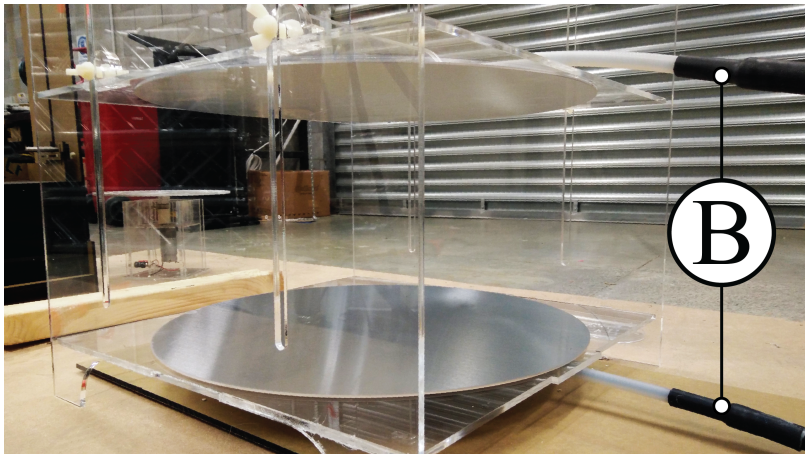

(b) HVDC leads (B) connected to electrode plates.

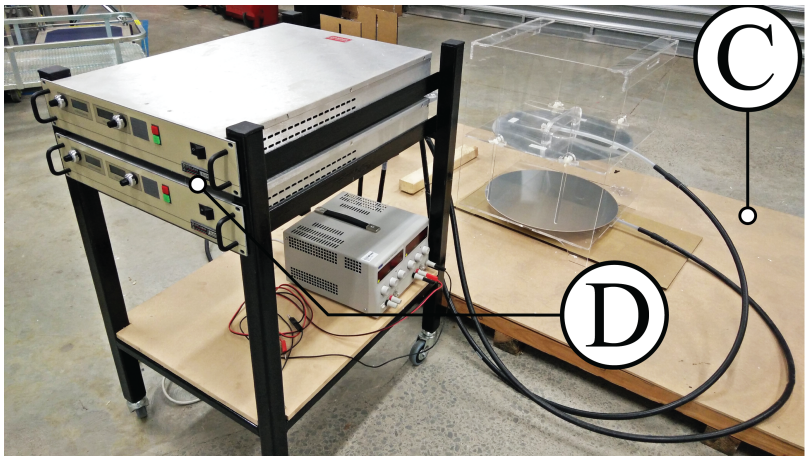

(c) Setup placement on non-conductive wooden platform (C) and HVDC power supplies (D)

Figure 4.5: Capacitor Box complete setup with equipment

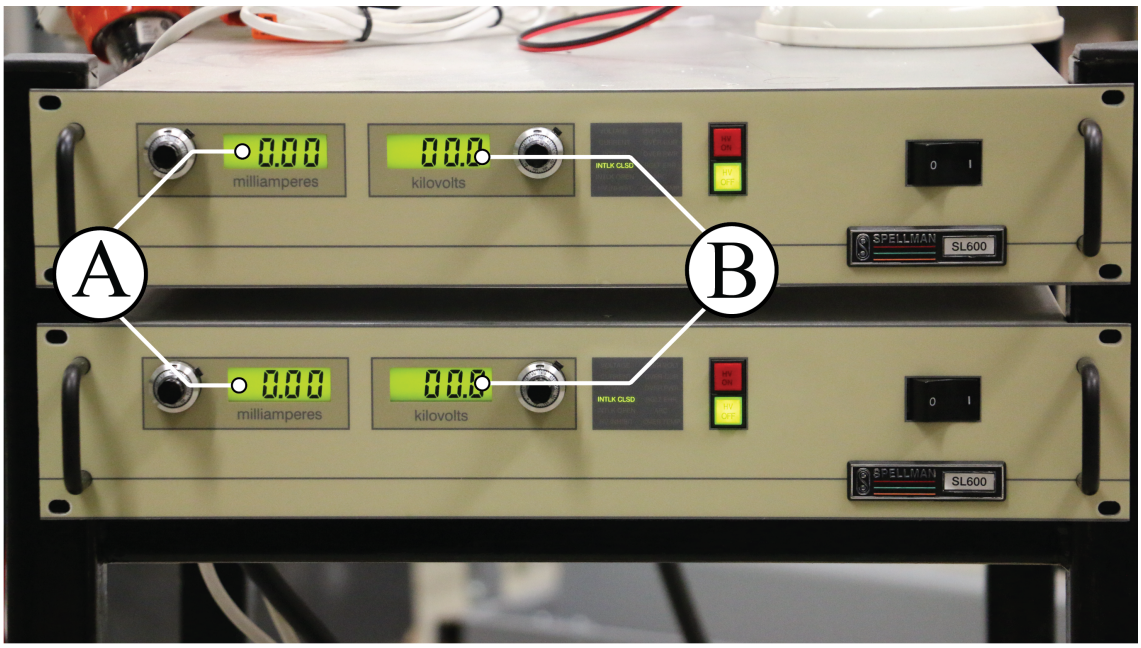

Figure 4.6: Two Spellman SL600 HVDC. Voltage (A) Current draw/limit (B)

4.3.3 Power Supplies

High Voltage Direct Current (HVDC) power supplies are required for electrospinning. For this experiment, the Spellman SL600 (Spellman HV Electronics Corp. USA) supplies are used which are capable of delivering up to 600 W each shown in Figure 4.6. Two supplies that are used, each providing up to 100 kV DC. Up to 200 kV DC potential difference between the plates can therefore be achieved with opposing polarities.

These supplies are provided with built-in current limiting circuits which are fine tunable. This is a safety feature that drops the voltage as soon as limit of the current is exceeded. This mitigates the risk of receiving a high voltage electric shock. The typical limit set throughout the testing is 0.5 mA.

Finally, leads from the two power supplies are tied with terminal blocks connected to thin copper sheets are sandwiched between the aluminum plates and the Perspex as shown in Figure 4.7a. The leads come with a tinned wire end shown in Figure 4.7b which require some form of adapter such as the terminal block in 4.7a. This is validated using a multimeter to show that the resistance was below 0.5 Ω, this includes the internal impedance of the multimeter.

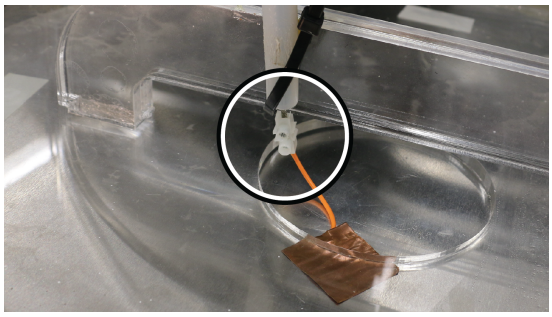

(a) Terminal block connecting lead to plate

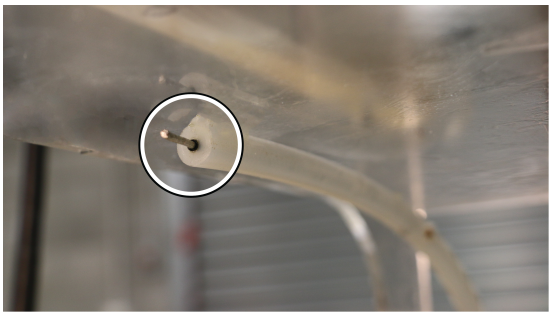

(b) Tinned end of the HVDC lead

Figure 4.7: Leads coming from the Spellman HVDC Supplies

Figure 4.8: Canon 70D DSLR on level tripod stand

4.3.4 Camera Setup

A camera was used to gather visual data about the solutions activity and measure electrospinning performance. The camera in Figure 4.8 is a Canon EOS 70D Single Lens Reflex camera that is used for the experimentation procedure. It is capable of capturing up to 7 frames per second at 20 megapixels per image, this is useful when capturing a series of photos of an electrospun jet and the high resolution allows for more accurate measurements and smaller errors. The lens used is an 18-135mm with the largest f-stop aperture values of 3.5-5.6 depending on the zoom.

The camera is setup to take photos on manual mode, this is to ensure the same photo mode is taken using the same shutter speed, aperture value and sensor sensitivity or ISO. Table 4.1 outlines the numbers dialed into the camera that were appropriate for the lighting and speeds for electrospinning.

Additional lighting is added to the setup pointing at the solution in the reservoir. The position of the lamp is marked and kept consistent throughout the testing procedure.

Table 4.1: Camera photo settings

Parameter	**Value**
Shutter Speed	1/100
Aperture Value	f/5.6
ISO Value	800
Zoom Value	x7.5
Resolution	20.2 MP
File Format	JPEG

4.4 Electrospinning Components & Calibration

The smaller parts and apparatus used to run the experiments and seen in Figure 4.1 are outlined in this section. These components consist of reservoirs that hold electrospinning solution and also with the use of tubing compensate for losses in fluids during the experiment.

The experiments are run using laboratory grade utensils to hold and measure the fluids used for electrospinning. Petri dishes are the main containers used to hold the electrospinning fluids. Petri dishes are versatile, easy to acquire and come in a standard size. Needles are used in the preliminary experiments, by grinding off the pointed end using a diamond cutter, it leaves a very fine flat finish on the needles edge allowing for a more uniform distributed electric field. Syringes and smaller reservoirs are used to help run the experiments with little stoppage.

4.4.1 Electrospinning Fluid

Electrospinning fluid that is used to produce nanofibres is typically made of solvents that are very volatile and dry up very quickly. Sir Geoffrey Taylor's experiments were run with more consistent fluids such as water and oils [2]. Using such fluids mitigates the number of changing variables from one experiment to another and remains consistent over time.

The following fluids were tested for electrospinning

- Mineral Oil
- Silicon Oil
- Sodium Silicate
- Water

The first three fluids were relatively easy to electrospin whereas water seemed to lack cohesion to be able to initiate a jet consistently. This could be attributed to the viscosity of the fluids and their inter-molecular interactions when exposed to a high electric field. Mineral oil is used for all the experiments for its low cost and ease of procurement.

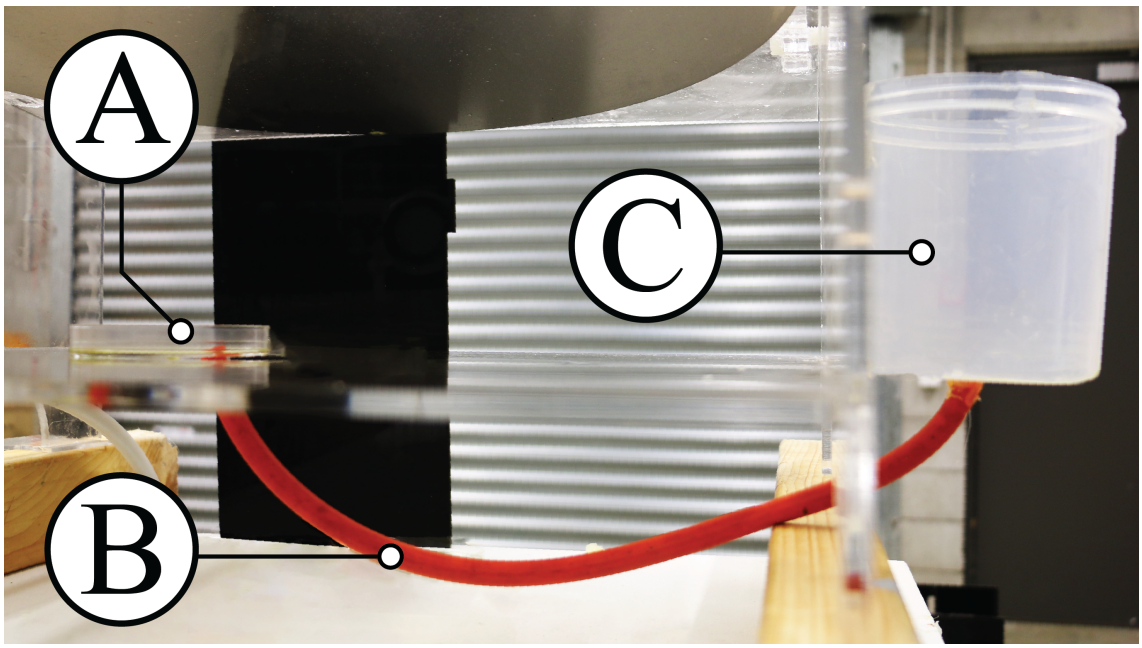

Figure 4.9: The two reservoir setup with Petridish (A) and plastic container (C) connected with rubber tubing (B)

In accordance with the layout set in Figure 4.1 shown earlier in this chapter, it shows a tube link between two solution filled reservoirs. Early testing with the oils shows that the depletion rate of the oil from the reservoir affects the consistency of the jet. This change is not favorable as the changing level of the fluid would not give a clear indication of the spinning quality at a single height of fluid.

To work around this, a second larger reservoir with a larger diameter base is connected using a small tube show in Figure 4.9. This second reservoir replenishes the lost fluid during the experimentation and in turn slowing down the rate of depletion significantly. This allows the experiment to run longer and allowing for more quality data to be captured for that level of fluid.

4.4.2 Measurement tools and Calibration

When recording results using a camera, the means of measuring distances or diameters are complicated to calculate using optics and perspectives. As shown in the full setup overview in Figure 4.1, a finely marked ruler is used as a scale for the diameter measurements of the electrospun jets. This ruler is used as a reference mark for measurement by counting the number of pixels across a few markers in order to calculate the equivalent metric unit of a pixel on screen.

However, for the result to be accurate, the ruler and the measured subject must be on the same plane. This is because if the subject is nearer or farther back from the plane of the ruler, the results would be distorted due to magnification and perspective errors. To work around this issue the use of a flat beam laser, shown in Figure 4.10, is used to align the ruler and the needle or the center of the plate along the beam projected. Safety glasses were used during this process.

The ruler and its markings served as a reference point when focusing the camera lens as well.

Figure 4.10: Laser point source (A) used to calibrate the alignment of the ruler with needle using flat laser projection (B) with the needle and ruler

4.4.3 Experiment Location

As discussed in the previous chapter, the effects of an earthed structure near the experimental setup would pose a significant influence on the shape of the electric field between the two plates. The experiments are to run with little to no interference in the shape of the electric field. A small room would bring up issues and questions around whether the shape of the electric field is shifted towards or affected by a nearby earthed structure. Having the experiments set up in a space distant from any earthed structures or wiring was important. The setting for the experiments was done in a large basement with high ceiling. The experimental setup is placed in the center of the room, shown in Figure 4.11, distant from any walls or civil infrastructure.

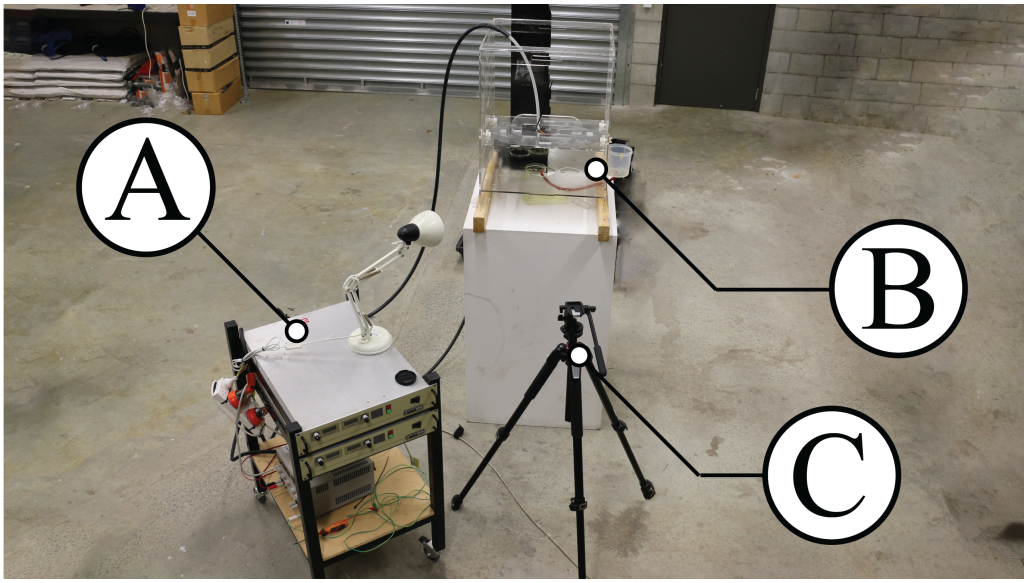

Figure 4.11: The experimental equipment setup in the center of the room with the HVDC supplies (A) and Capacitor box (B) with camera position on tripod (C)

4.5 Experimental Protocol

The purpose of this experimental section is to validate the built setup and determine whether it is suitable for electrospinning. The acquired from the experimentation are discussed in the Experimental Results section (Section 5.4) in Chapter 5.

The experiments are to test electrospinning in two configurations of electric field shapes: uniform and non-uniform electric fields. The capacitor box is set up for two separate experiments, the two plate experiment and the needle plate experiment. This chapter steps through the experimental routine and the validation regimen prior to the result acquisition stage of the experiment. The acquired results are presented at the end of the chapter.

The experimental configurations were:

1. Two plate experiment
    (a) Center position
    (b) Edge position
2. Needle-Plate experiment

4.5.1 Two plate experiment

The first of the two experiments involves testing electrospinning in a uniform field that is generated by two circular plates as seen in Figures 4.12 and 4.13. First test was a petridish filled with mineral oil is placed in the center of the bottom plate where the field is most uniform. In another test, the dish was moved to the edge of the plate where almost half of the reservoir would be on the outside of the plate. The following sections, 4.5.1.1 and 4.5.1.2, expand on the experimental procedure conducted for the both placements of the reservoir.

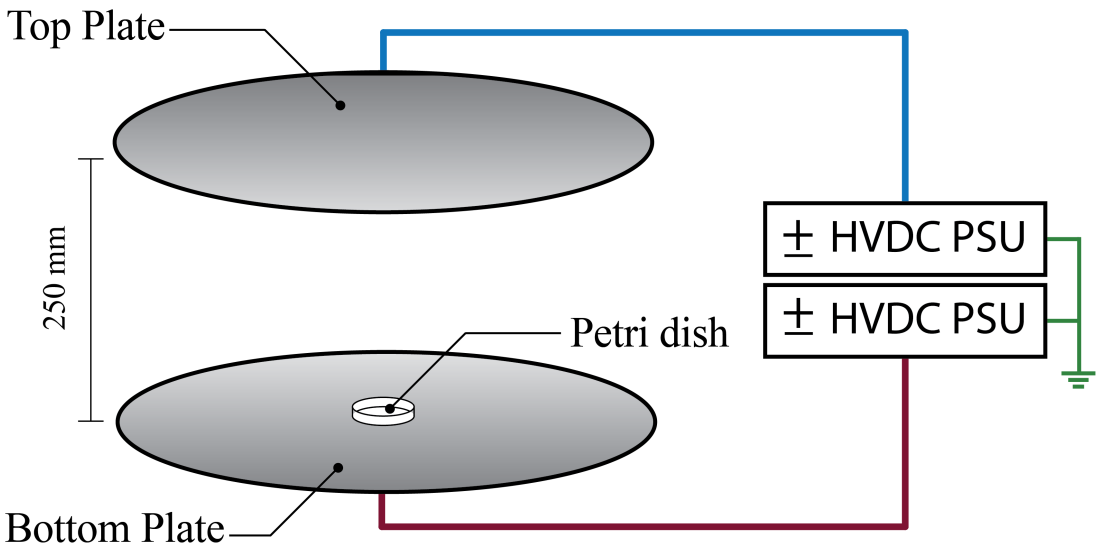

Figure 4.12: Mineral oil in petridish at center Position

4.5.1.1 Center Position

Referring back to the results from Chapter 3, the field is noted to be most uniform in the center of the two plates. Investigating the effects a uniform field would have on the solutions is something that had not been thoroughly investigated in the literature reviewed. The aim of this experiment is to test the condition of spinning in a uniform field and if changing polarity holds any significance to better explain the electrospinning phenomena.

With the plates set apart in parallel at a distance of 250 mm as shown in Figure 4.12, the voltage ramped up from 0 Vdc to the electrospinning threshold or the air breaks down and arcing occurs. Upon the first arc occurring, the experiment is stopped as the voltage cannot be increased further due to arcing that would continuously occur between the two plates.

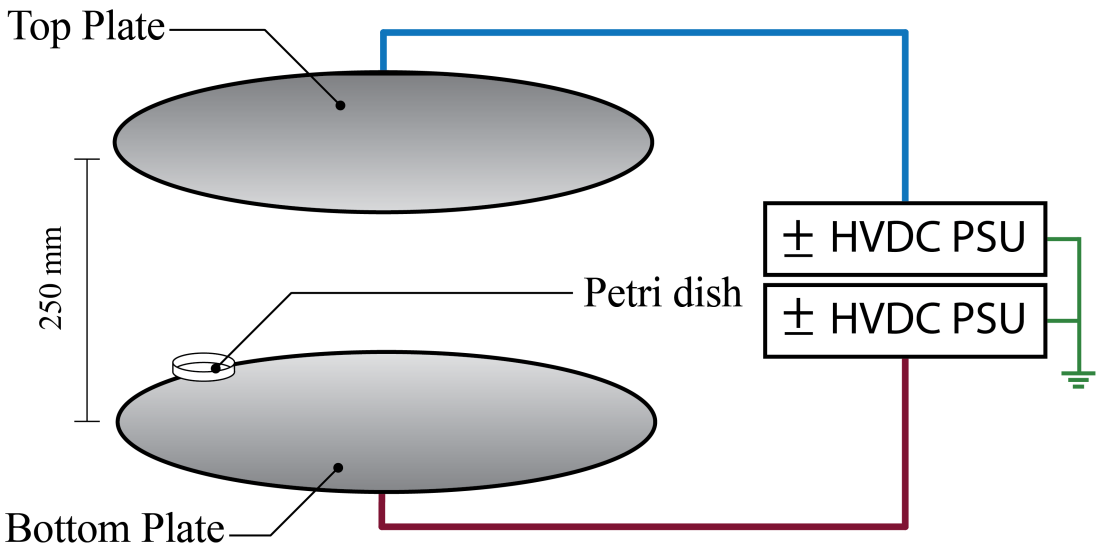

Figure 4.13: Mineral oil in petridish at Edge Position

4.5.1.2 Edge Position

The second position is placing a droplet of mineral oil near and on the edge of the plate and in another case moving the petridish to the edge of the bottom plate as seen in Figure 4.13 where the dish overhangs the edge that runs under the center of the dish. This is to examine the effects of having the same oil placed in a non-uniform electric field would have over a uniform one as run in the previous setup.

The configuration is kept the same with the same distance between the two plates. The voltage ramped up in the same manner from 0 Vdc to the electrospinning threshold or the air breaks down and arcing occurs as well.

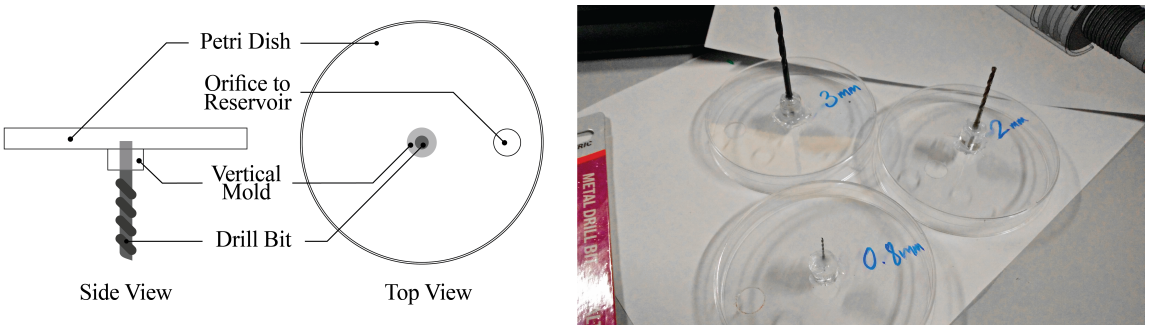

(a) Petridish layout overview (b) Petridish setup with various drill bit diameters

Figure 4.14: Petridish configuration and build

4.5.2 Needle Plate experiment

The second category of experiments is to implement a needle based electrospinning setup. The literature shows that the most common method of electrospinning involves using a conductive hollow needle that is charged and the electrospinning fluid pushed through its center. This thin walled needle adds complications to the model. In this research a simpler model of using a conductive cylinder submerged in the fluid is used. The cylinder used is a precision machined drill bits of various diameters with the flat side used upwards facing the top plate as shown in the image in Figure 4.14.

It can be noted that the petridish has a secondary hole in its base which is to allow a secondary reservoir to be connected. The secondary reservoir allows for more spinning to happen with smaller drops in the level of oil. This reduces the effect that a changing level would have on electrospinning.

A petridish is placed under the center of the top plate. The dish has a drill bit that penetrates 2 mm through the reservoir leaving 8 mm to the surface of the fluid when filled to the brim. Fluid level of the mineral oil in the petridish is a parameter that inherently changes due to the fluid being displaced in the electrospinning process. To mitigate its effect a second reservoir of a larger diameter is placed outside the capacitor box and connected with a tube from underneath the petridish as seen in Figure 4.9. This reduces the change in fluid level where it becomes negligible over a single testing period. The fluid is kept at the same level in all tests and is checked prior to starting the testing.

4.6 Data Processing

Data from the capacitor box is gathered using the camera setup and frames of the different events are analyzed digitally after the testing is complete. The analysis is done separately for the two experiments which have images captured from different angles.

An Excel workbook is used to keep track of the parameters of the experiments. In that workbook, multiple sheets are made with each representing a specific voltage and polarity of the experimental configuration. Each of those sheets holds the references to the images that are captured of that experiment. The workbook contains a summary sheet and individual sheets of acquired data from the images. An outline of the workbook and the different sheets can be seen in Appendix C.

The captured images have the base of the petridish used as a reference for the center of the image and the center axis of the drill bit as the horizontal center. Each image will have a segment of a ruler that is aligned with the same plane as the drill bit. This ruler is used as the reference marker for measuring the diameter of the jet. The electrospun jet is expected to project directly above the drill bit. The placement of the ruler in the field of view of the camera and in reference to the rest of the setup can be seen in Figure 4.1.

4.6.1 Measuring Jet Diameter

The data gathered from each frame is diameter measurements, in mm, of the electrospun jet at 3 different heights. The images captured with the camera contain tools that aid in acquiring those measurements. Figure 4.15a shows the composition of each image captured. The frame would have the base of the petridish at the center of the frame as the reference point. The camera's height is set so that the base of the petridish is in the center of the lens, this ensures that the plane through the center of the drill bit is parallel with the lens. Each frame will show at least 30 mm of ruler markings to be used to calculate the pixel to mm ratio. The pixel to mm ratio is acquired by counting the number of pixels between the etched markers on the ruler in each frame.

The diameter measurements are calculated by counting the number of pixels between the millimeter etchings on the ruler. To reduce the pixel to mm conversion error, a larger sample of pixels of 20 mm is counted and then divided by 20 to calculate the pixels/mm value. This counting process is done using Photoshop CC by using the marquee tool as seen in Figure 4.15b. The number of pixels for 20 mm is then noted down in the sheet that contains the configurations for that frame. The equivalent of 1mm is calculated giving a pixel number. Three diameters are measured at three different heights, the heights are acquired by using the marquee tool to count the number of pixels from the top of the dish to the height in pixels calculated in the sheet. Figure 4.15c shows the marque tool highlighting the number of pixels in the first height at 8 mm which happened to be 232 pixels from the top of the dish. At that height, the number of pixels are counted giving the width of the jet. The pixel count is documented in a spreadsheet. Three diameters are counted at the three heights of $8mm$, $16mm$ and $24mm$ which are clalculated in terms of number of pixels high then converted and recorded as mm values respectively.

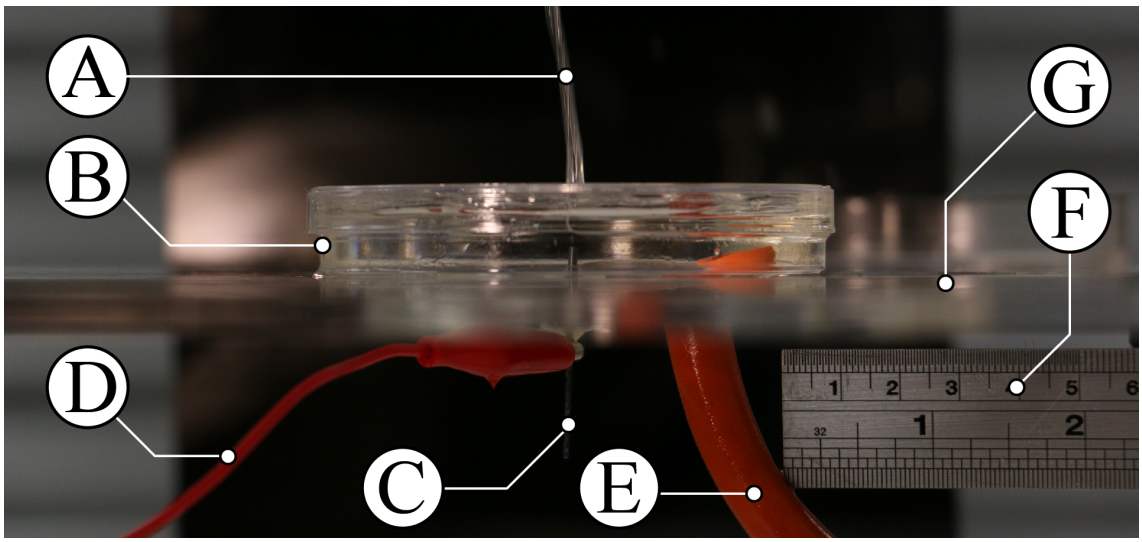

(a) Captured frame of an electrospun jet (A) spinning mineral oil from petridish (B) above the needle electrode (C) that is connected to the HVDC lead (D). Also seen is the oil feeding tube from second reservoir (E) and ruler (F). The base plate (G) is used as reference for center of every frame.

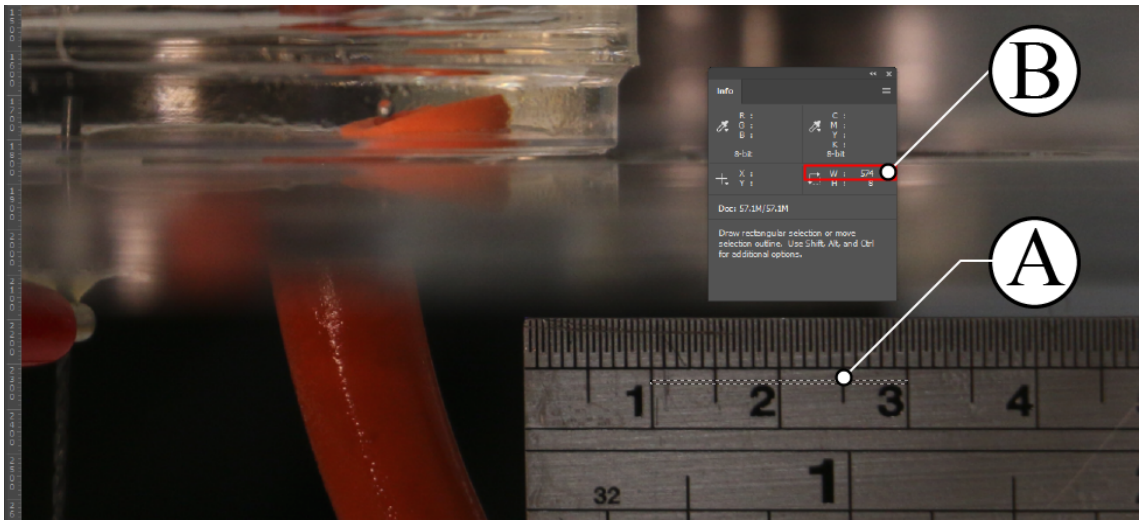

(b) Acquiring pixel count for 20 mm by measuring the number of pixels across the markers (A) and recording count from (B)

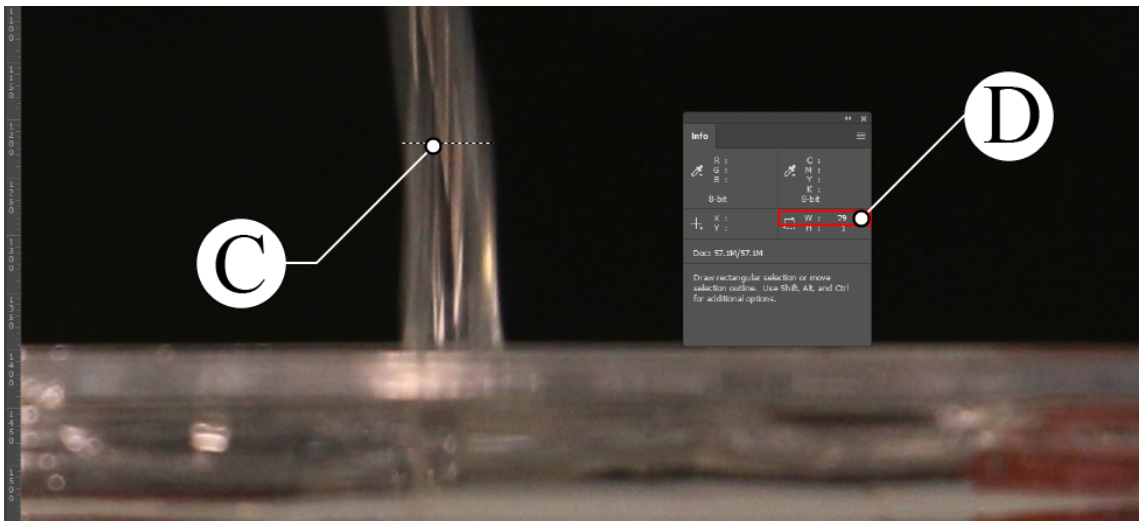

(c) Measuring diameter of jet in pixels (C) and recording count (D)

Figure 4.15: Stages of processing data from a single image for the three diameters of an electrospun jet

4.7 Closure

This completes the experimental setup discussion and all describes the parts in Figure 4.1. This chapter covered the experimental aim and framework and discussed the reasoning behind the design and the experimental protocol followed by a description of the data processing method.

The results obtained from the experiments described in this chapter will be presented and discussed in the following chapter and the feasibility of electrospinning from the aforementioned configurations will be assessed.

Chapter 5

Results and Discussion

5.1 Introduction

This chapter presents and discusses the results acquired in this thesis. Results from the simulations for the various scenarios are discussed and compared. There results were applied to the development of the experimental setup. The two experimental configurations are discussed and interpreted to demonstrate the feasibility of electrospinning with each of them. The results are presented in the same procedural order as in Chapter 4. It starts with the noted effects of a uniform electric field on electrospinning (two plate setup) following by the non-uniform electric field electrospinning (needle-plate setup). The effects the dielectric properties of air has on the process is discussed.

5.2 Assessing Feasibility of Electrospinning

In order to investigate and assess the feasibility of electrospinning, the effects of various design parameters and configurations have on the formation of the electrospinning jet are inferred from the experimental data. Feasibility is assessed by observing the formation of the electrospinning jet from a Taylor cone. Once a cone and jet is initiated, the configuration is deemed feasible for electrospinning.

5.3 FEM Results

This section presents and examines the outcome of the FEM simulations. The plots show a 2D difference plot of distances in *mm* on both axes and a color bar on the right denoting the difference in electric field strength such as in Figure 3.6b from Chapter 3. However, unlike the plots in Figure 3.6b, the following figures will show the difference in voltage magnitude from two datasets. Other figures of all the other arrangements are in Appendix A but not discussed in this section.

The results are represented in a color intensity chart showing areas with high amount of difference in electric field strength in a brighter color. Difference in electric field strength is denoted by $\boldsymbol{\Delta E}$ which is

$$\boldsymbol{\Delta E} = \left| \overrightarrow{E_1} - \overrightarrow{E_2} \right|$$

where $\overrightarrow{E_n}$ is a data set of electric field strength between two plates and n is the number of the data set.

The following figures (Figures 5.1-5.5) show difference in electric field strength plotted on a vertical plane that runs through the center of the two plates. The boundaries and data point spacing of this plane are discussed in detail in Section 3.3.1 in Chapter 3. A total of five result sets of $\boldsymbol{\Delta E}$ are discussed that were acquired from individual result sets of the configurations mentioned in Section 3.2.2.1 of Chapter 3.

The FEM results are discussed showing results in the following order

1. Effects of boundary conditions on $\boldsymbol{\Delta E}$
2. Effect of plate/electrode geometry or shape on $\boldsymbol{\Delta E}$
3. Effects of a non-earthed (floating) conductor placed near the two plate setup on $\boldsymbol{\Delta E}$
4. Effects of an earthed conductor placed near the two plate setup on $\boldsymbol{\Delta E}$
5. Effects of enclosing the two plate setup within a non-conductive enclosure on $\boldsymbol{\Delta E}$

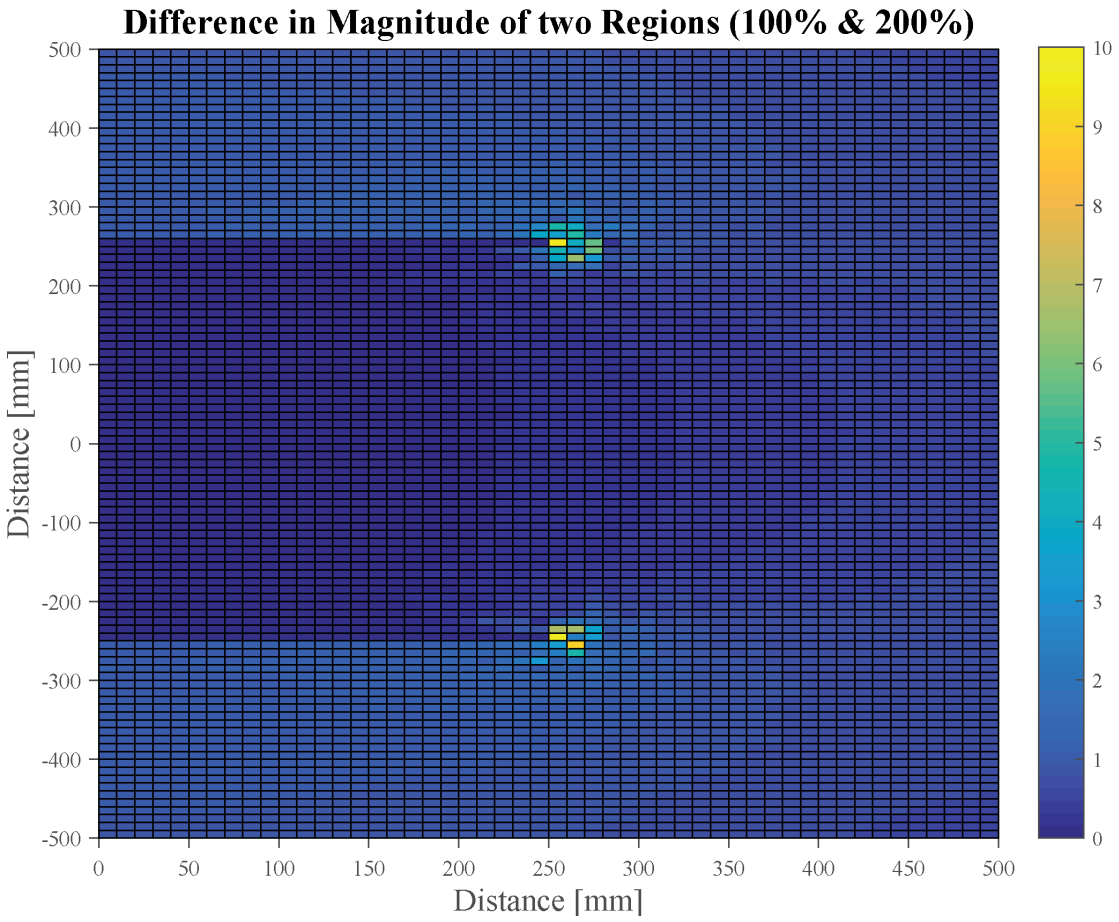

Figure 5.1: ΔE between upper and lower plate for different boundary conditions

5.3.1 Effects of Boundary Conditions

Figure 5.1 illustrates the variance $\boldsymbol{\Delta E}$ when doubling the size of the region around the standard two plate setup. This model tests the effects the change in boundary limits has on the electric field uniformity of the inner region of the two plates. The initial boundary is set to be a distance of 100% from each edge of the geometry and comparing it to 200% would show whether that initial value is sufficient and does not alter the data significantly.

The plotted difference of the two result sets shows that there is a large variance outside of the two plates and more noticeably differences in areas around the edges of the plate. There is little to no change in the inner region of the two plates. Therefore, the assumption can be made that changing the region size does not have a significant impact on the results in terms of field uniformity between the two plates. That is also to say that the middle region is not affected significantly by the initial boundary condition distanced at 100% from the edges of the geometry. The raw data or the vector field diagrams of the 'Two Square Plates with 100% Region Size' setup and the 'Two Square Plates with 200% Region Size' setup can be seen in Figures A.5 and A.7 in Appendix A.

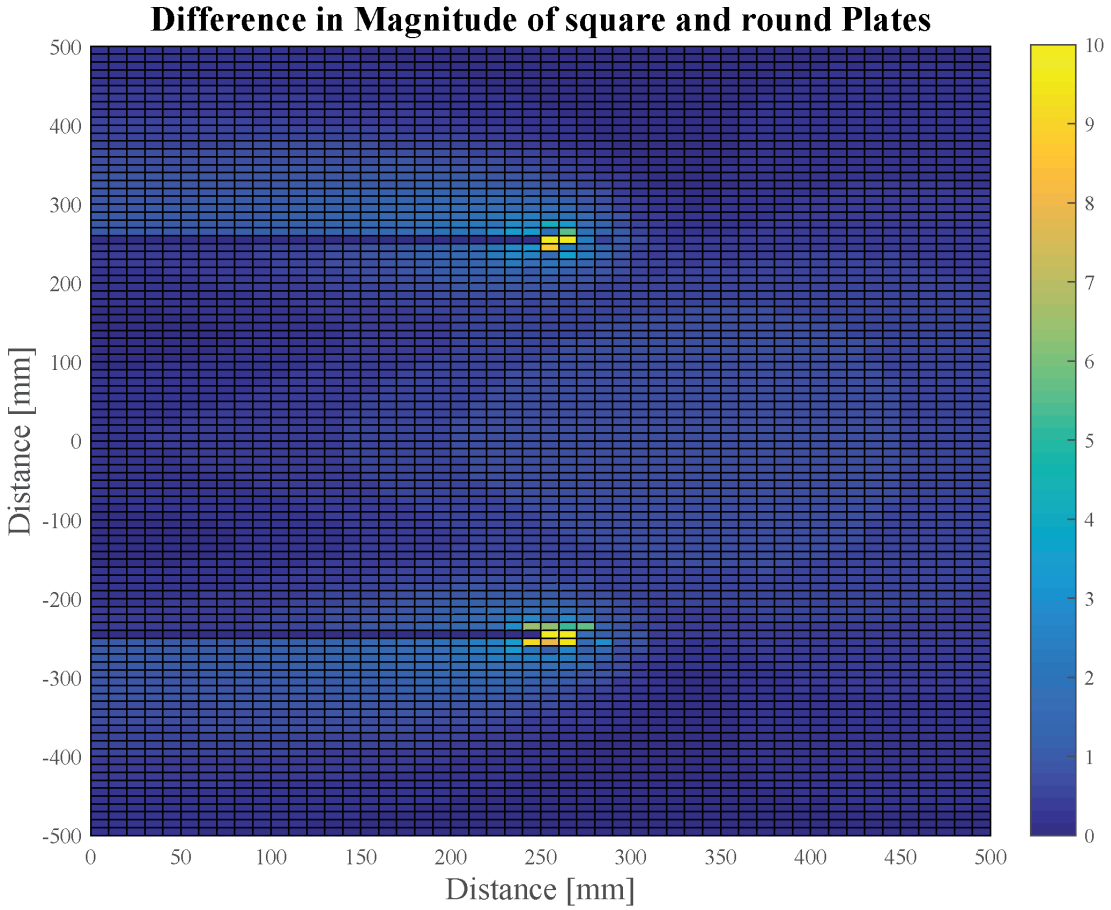

Figure 5.2: ΔE between two square plates and two round plates

5.3.2 Effects of Plate Shape

Two different plate geometries were modeled in Maxwell, two square plates with a 500x500 mm area and two circular plates with a 500 mm diameter. The two geometries have their own consequences on the shape of the electric field. A square plate has its corners which significantly skews the direction of the field nearer to the edges and towards the corners. Whereas a circular plate would be more uniform in its bias all around its edges. However, the circular plate with the same diameter as side length of the square plate has a smaller surface area.

The effect the shape would have on the $\boldsymbol{\Delta E}$ is observed in Figure 5.2. Large voltage differences can be seen at the edges of the plates. The outside regions have had noticeable changes in field magnitude more so on the outside of the top and the lower side of the bottom plates. The center region shows that the midpoint between the two plates has a voltage change that can be associated with the change in surface area between the two shapes. However, that voltage difference is < 1 V which can be considered negligible. Round plates are selected over the square plates reducing the effect that the corners have on the field. The raw data or the vector field diagrams of the 'Two Square Plates' setup and the 'Two Round Plates' setup can be seen in Figures A.5 and A.9 in Appendix A.

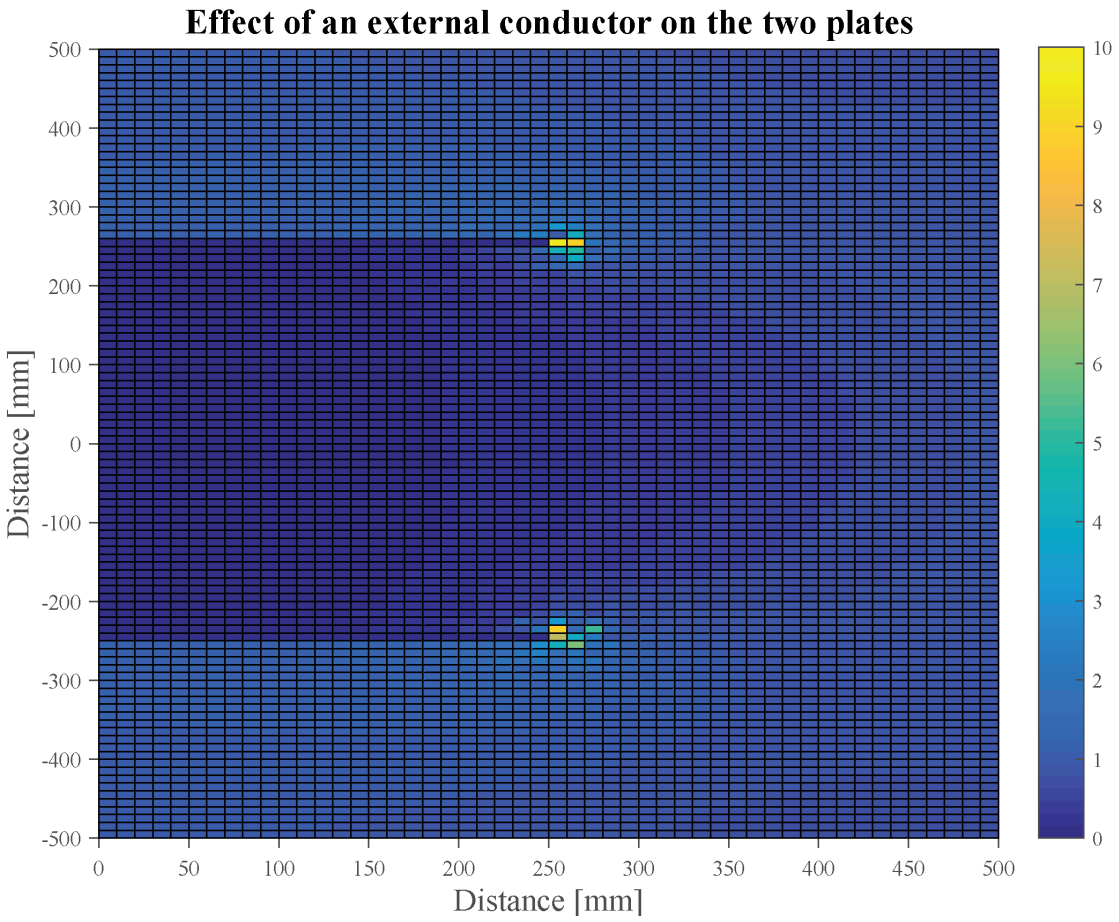

Figure 5.3: ΔE with and without non-earthed conductor

5.3.3 Effect of a non-earthed conductor

Figure 5.3 shows the difference of two sets of electric field strengths. The first is for the square two plate setup and the second is for the same two plates but with a cylindrical conductor placed at a distance of 750 mm from the center of the plates. The cylinder is placed at the center of the same plane that the voltage points are calculated and recorded from Figure 3.5 in Chapter 3. The placement of this conductor is to investigate the effects that a conductive object near the plates would have on the uniformity of the electric field that is not referenced to a voltage, that is, left floating.

Figure 5.3 shows that the effects are only noticeable on the outer regions of the two plates. The inner region shows a creeping change that is noticeable a quarter of the way from the edge of the plate to the center. This can mean that if the conductor is brought closer, the effect would be greater and closer to the center. At the distance of 500 mm from the plate edge, the conductor does not show any significant effect on the uniformity of the electric field. The raw data or the vector field diagrams of the 'Two Square Plates' setup and the 'Floating Non-Earthed Conductor Near Plates' setup can be seen in Figures A.5 and A.8 in Appendix A.

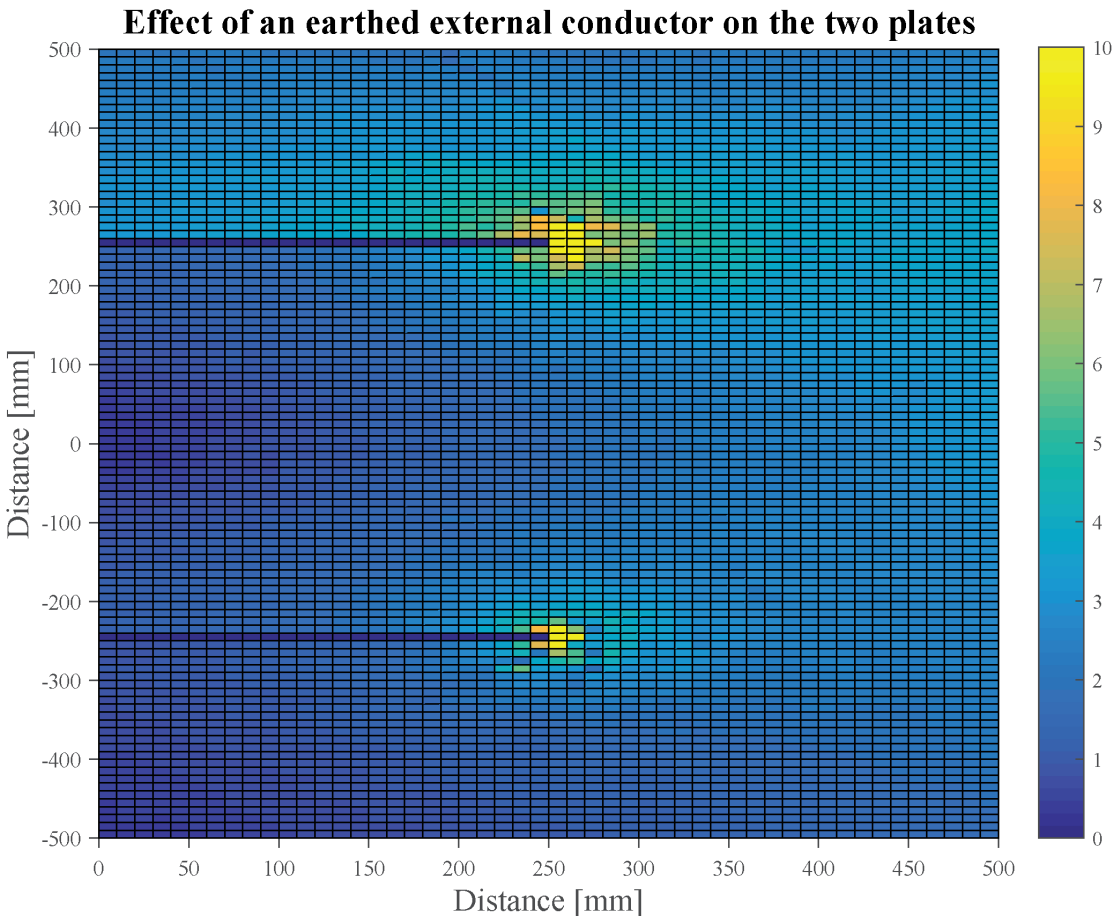

Figure 5.4: ΔE with and with an earthed conductor

5.3.4 Effect of an earthed conductor

As the figure discussed in the previous section, Figure 5.4 shows the $\boldsymbol{\Delta E}$ with and without an earthed conductor. It is the plotted difference between the square two plate setup and square two plate setup with a conductive cylinder where the cylinder is electrically referenced to the bottom plate where both are at the potential of 0 V. This simulates the effects of having earthed infrastructure near the two plate setup.

Figure 5.4 shows a clear and evenly distributed change in voltage throughout the plot. The top edge of the plate shows a larger area of change in comparison to the bottom plate. This can be associated with the fact that both the lower plate and the cylinder are at the same potential.

The inner region nearer to the center shows smaller yet still significant differences. It can be deduced that having an earthed conductor or a conductor referenced to the same voltages of the two plates can have a very significant effect on the uniformity of the electric field and needs to be taken into account when planning the setting of the experiments. The use of two polarities in the experimental setup to have the potential difference set equally apart from 0V is a possible method to mitigate effects that the infrastructure would have.

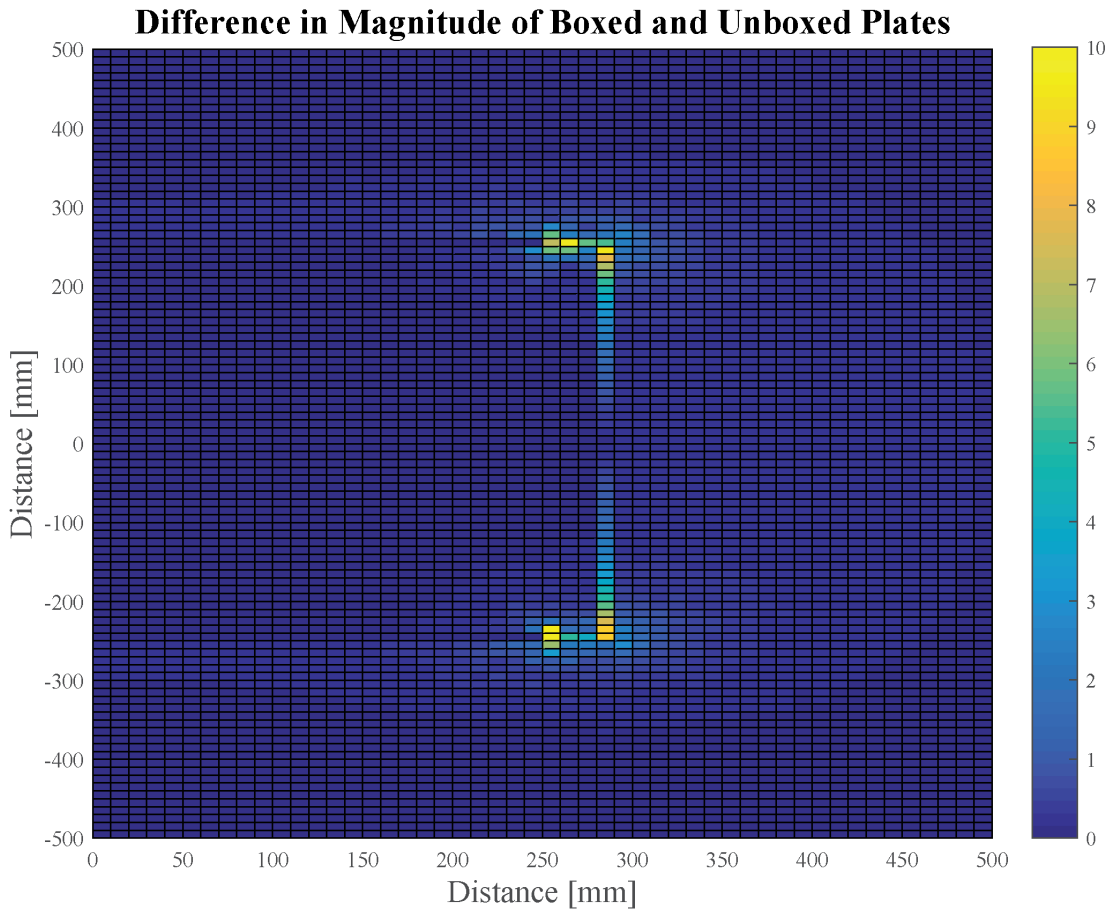

Figure 5.5: ΔE between boxed and unboxed square plates

5.3.5 Effect of enclosing plates

Figure 5.5 illustrates whether the field uniformity is changed upon using a non-conductive enclosure to hold the physical plates apart. It is also useful to use when investigating whether or not the use of auxiliary electrodes as used by Dabirian [10] is required to counter the changes in the field induced by the auxiliary electrode.

The plot in Figure 5.5 shows that the effects of having the dielectric sheets of Perspex as the frame results in a significant voltage drop across where the sheet is on the side of the plates. A voltage gradient is evident on the walls of the enclosure. This is due to the change in electric field polarity induced by the plates. The points closer to the plates show a higher $\boldsymbol{\Delta E}$ due to the higher polarization nearer to the plates.

The center region between the two plates is has little to no change. This result shows that the effects of the boxed setup can be used without having to counter its effects with the use of auxiliary electrodes. The raw data or the vector field diagrams of the 'Two Square Plates' setup and the 'Boxed Plates' setup can be seen in Figures A.5 and A.6 in Appendix A.

5.4 Experimental: Electrospinning in Uniform Field

The first configuration of experiment run is the two plate setup that forms a uniform electric field. There was no observed electrospinning at any voltage prior to any arcing occurring with this configuration. This configuration was tested with both mineral oil in direct contact with the plate conductor and indirect contact with the plate where oil is placed in a petridish and moved to two positions. The following sections present and discuss the observed effects that the uniform field has on mineral oil in the two configurations shown in Figure 5.6 in Chapter 3.

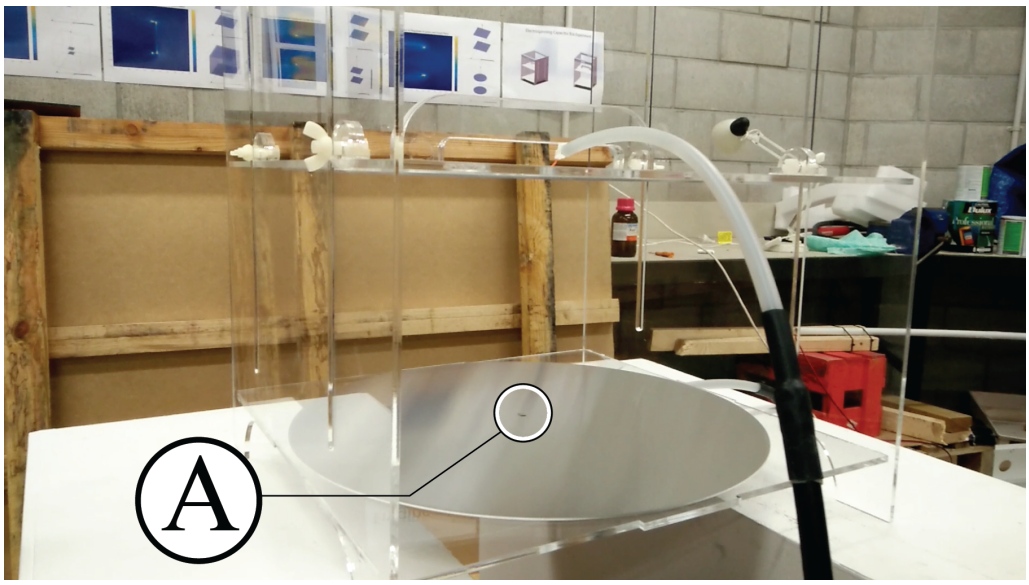

(a) Droplet of mineral oil (A) in direct contact with plate

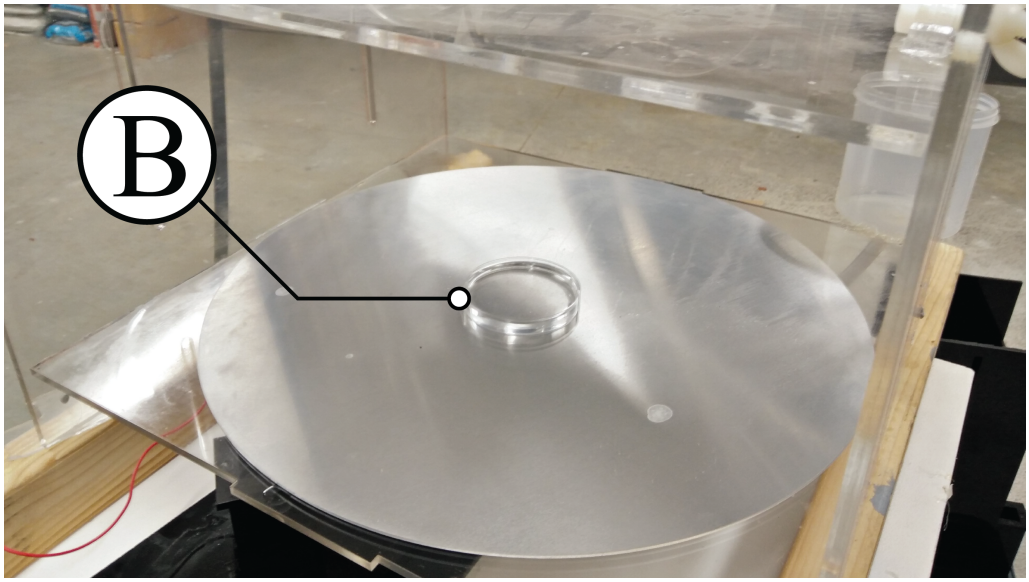

(b) Mineral oil placed in petridish (B) on plate

Figure 5.6: Mineral oil placement in the two plate experiment

5.4.1 Direct Contact

With a small drop of oil placed in the center of the dish, in direct contact with the plate as shown in Figure 5.6a, there was no electrospinning or signs that electrospinning would occur. Signs such as the droplet taking a conical shape on the plate towards the oppositely charged plate were not noted. This may be attributed to the following reasons

- The oil's affinity to the surface of the plate could be the main factor making it harder to break the surface tension of the fluid.
- Charges in the fluid interacting with the uniform electric field where the charge density is evenly distributed across the surface of the droplet.

A potential solution to each of the mentioned is

- An oleophobic coating on the plate, or a surface lacking affinity to oil, can help beading of the oil droplet on the surface of the coated plate reducing the contact angle between the oil and the plate surface. This could present the results that [2] had discussed in his findings that showed the droplet become skewed and bend towards the oppositely charged plate.
- It can be associated that the charges in the fluid interacting with the uniform electric field has an even distribution, where the charge density is evenly distributed across the surface of the droplet. Assuming that the charges in the mineral oil build up on the top of the drop which is the side closest to the plate of the opposite polarity, it would require far more force to displace a layer of the fluid as the charges are evenly distributed along the surface of the fluid.

5.4.2 Indirect Contact (Oil In Petridish)

With the oil placed in a petridish, shown in Figure 5.6b, it was observed that the oil would only start to show signs of fluid convection near and at the edge of the plate. Moving the dish between a center position and an edge position on the bottom plate showed compelling indications that in the presence of a non-uniform electric field the oil visibly interacts with the changing shape of the field.

Two configurations were attempted to investigate the effect of field uniformity.

A) Center Position With the petridish placed in the center of the bottom plate, no movement or surface changes on the oil were evident. Increasing the voltage until arcing occured did not cause any noticeable effects on the oil. The outcome was that there was no evident signs of electrospinning or formation of a Taylor cone on the surface of the fluid in both situations with the oil on the surface of the plate and the oil in the petridish.

B) Edge Position Moving the dish of oil around the base plate resulted in no signs of electrospinning or forming a Taylor cone. However, upon placing the dish closer to the edges of the base plate, the fluid would start to move over as if it was boiling where layers of the oil would start moving. Bringing the dish to the edge of the plate would show signs of fluid flow in different directions similar to that of a boiling fluid. Bringing the dish over the edge of the plate shows that the oil separates within the area where the border of the plate runs under the dish. Figure 5.7 shows the oil dividing into two halves showing where the field gradient is most significant.

Changing the polarity of the field moved the oil in different directions, where when the base plate was positive the oil would split showing a crevice around the edge of the plate and in the case where the plate is negative the oil collects more on top of the edge of the plate.

This can be correlated to the results attained from the Maxwell models portraying the magnitude voltage where the edges of the two plates can be seen to be the highest in field gradient and mostly nonuniform based on the comparisons between two data sets shown in Chapter 3 and in Appendix A.

Having oil placed directly on the edge of the plate showed signs of electrospinning where the oil would spin off the cut edge of the plate, the oil would spread across the surface of the plate and move in different directions. Applying the electric field seemed to evidently speed up or accelerate the oil's movement across the surface of the plate.

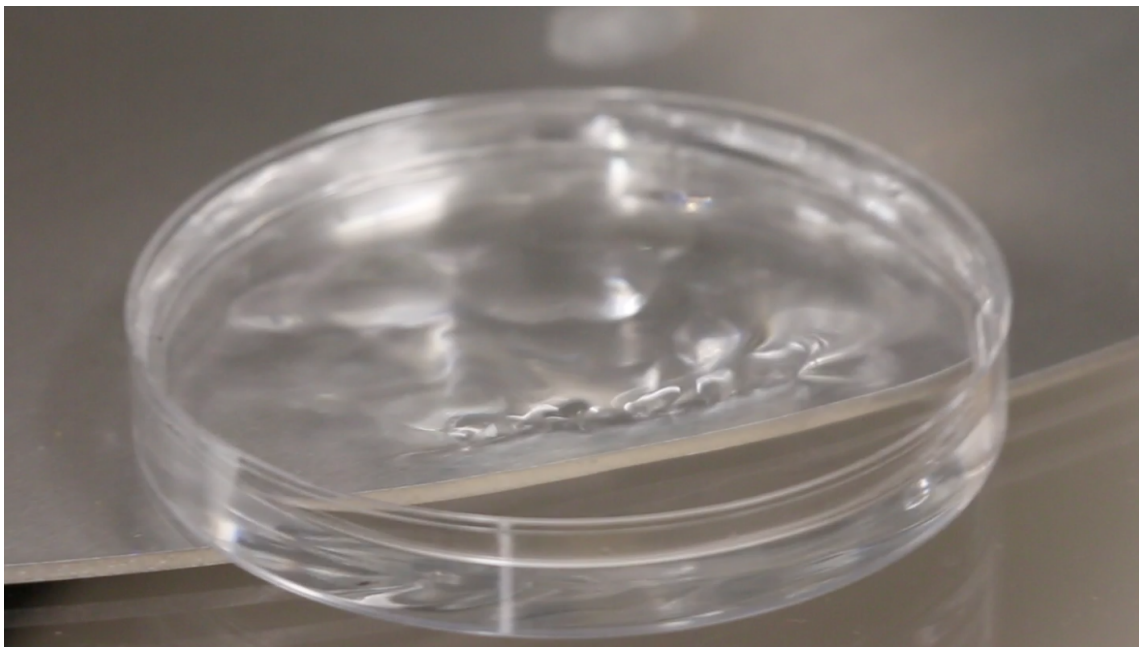

Figure 5.7: Visible convection and separation of oil above the edge of the plate due to non-uniform field

5.5 Experimental: Electrospinning in Non-Uniform Field

The two plate experiment showed that electrospinning was evident in situations where the electrostatic field was less uniform. An example of this was placing the petridish on the edge of the bottom plate as in Section 5.4.2B. Based on the findings from Section 5.4.2, a gradient in the electric field concentrates charges in one part of the fluid that helps initiate the electrospinning Taylor cone at a voltage potential lower than that is required to breakdown air.

The needle-plate experiment presents the effects that non-uniform electric field conditions would have on the mineral oil. The framework setup is outlined in Figure 4.1 in Chapter 4. The interactions of the fluid in a non-uniform field is observed using the petridish-drill bit rig of various drill bit diameters as put forward in Section 4.5.2. The following sections present and discuss the results acquired from the needle plate setup.

5.5.1 Tested Cases

This section highlights and discusses the various configurations tested with the needle-plate setup using the capacitor box. The needle-plate configuration was run with two electrode diameters, specifically electrodes of $0.8\,mm$ and $1.1\,mm$ and a circular plate at the top with a diameter of $500\,mm$. It is noted that the electrospinning threshold, or the ΔV between the two electrodes at which a Taylor cone is formed, is observed at the needle-plate ΔV of ± 70 kV. Spinning was possible up to a needle-plate voltage of ± 85 kV before arcing would occur.

Mineral oil from the petridish is displaced and forms a jet right above the drill bit and flows smoothly towards the oppositely charged plate. This was possible in both polarity configurations with a slight change in electrospinning threshold in one polarity configuration over the other. Table 5.1 highlights the configurations tested for phase one.

Table 5.1: Configurations of experiments run in phase one

Voltages	ΔV	Polarity	Needle Dia.
± 70	140	PN-NP	0.8
± 72	144	PN-NP	0.8
± 75	150	PN-NP	0.8
± 70	140	PN-NP	1.1
± 72	144	PN-NP	1.1
± 75	150	PN-NP	1.1
± 78	156	PN-NP	1.1
± 80	160	PN-NP	1.1
± 85	170	PN-NP	1.1
± 70	140	NN-PP	1.1
± 78	156	NN-PP	1.1
± 80	160	NN-PP	1.1

5.6 Tested Results

As mentioned in Section 5.2 of this chapter and in accordance with the objectives outlined in Section 2.6 of Chapter 2, the developed experimental setup is used to test the feasibility of a novel electrospinning method. This section presents results that were used to assess the feasibility of electrospinning with the different non-uniform configurations highlighted in Table 5.1 using the capacitor box setup. These results are intended to only show the feasibility of testing using the existing setup. The potential applications of the capacitor box and ideas of how these results could help future work are discussed in the next chapter.

5.6.1 The Feasibility of Electrospinning Using a Submerged Needle

As discussed in the introduction, one key thing about electrospinning that was unclear in the literature was effect of polarity of electrodes on electrospinning. Both polarity configurations were shown to electrospin and show very comparable jet diameter when comparing NN-PP and NP-PN configurations at the same ΔV.

The results of the 1.1 *mm* diameter electrode are provided in Figure 5.8. It is observed that polarity does not have a significant role in affecting jet diameter whereas the ΔV seems to have a larger role and generates a larger diameter jet at ± 78 kV in both polarities.

This result set demonstrates that it is feasible to use the capacitor box setup with a submerged needle-plate setup in which a Taylor cone and electrospinning jet emitting from above the needle electrode was observed. A set from the images captured and collected as data in this result set can be seen in Appendix C.

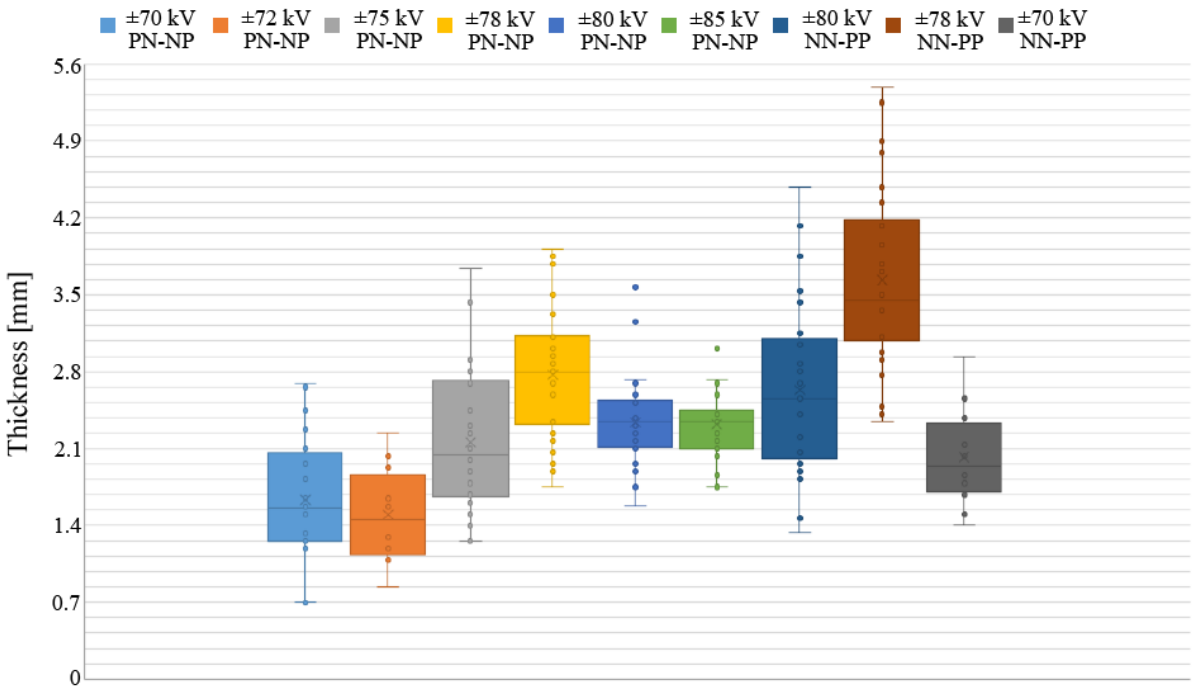

Figure 5.8: Box and Whiskers chart of the results acquired from the different test configurations from Table 5.1

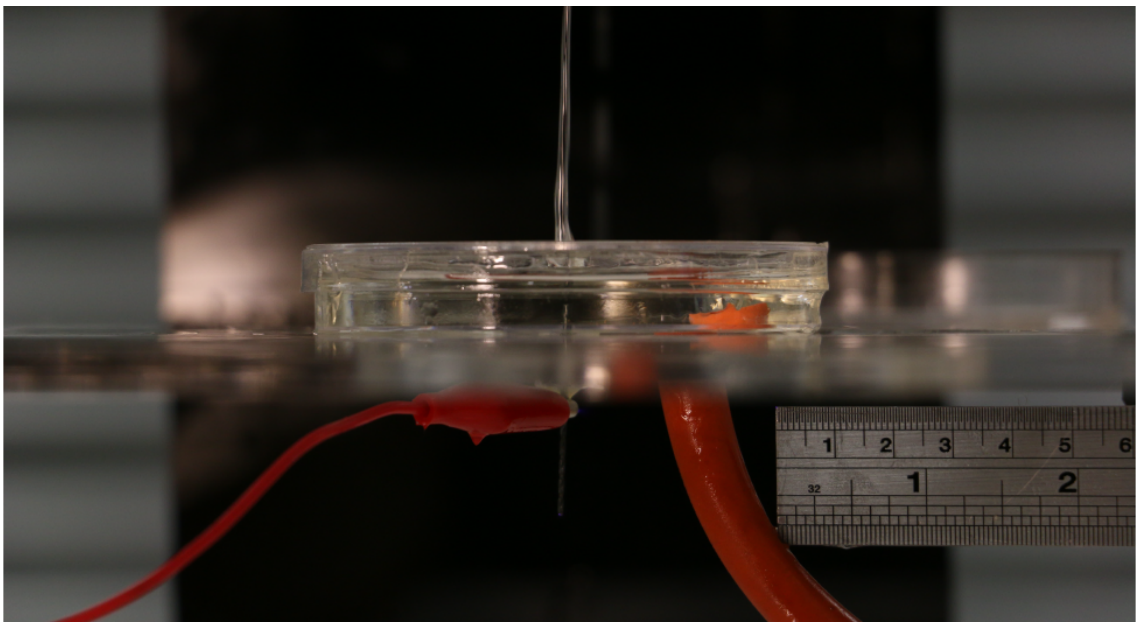

Figure 5.9: Positive result of electrospinning jet above a 0.8 mm submerged needle – Refer to Appendix C for more results.

Figure 5.9 one of the frames used to measure the acquired diameter at different heights. The electrode diameters used in the experiments are highlighted in Table 5.1. The results acquired of the two diameters using the submerged needle configuration show that there is change in the average diameter at a single ΔV between the two needle sizes as seen in the chart in Figure C.11 in Appendix C. Changing polarity at the same ΔV shows that there is substantial change in average diameter as well as seen in Figure 5.10.

These results show that the methodology for testing the effects of changing electrode diameters and polarity was feasible with the capacitor box setup and can be used for optimizing electrospinning parameters for producing nanofibre yarn in terms of controlling the volume of displaced solution.

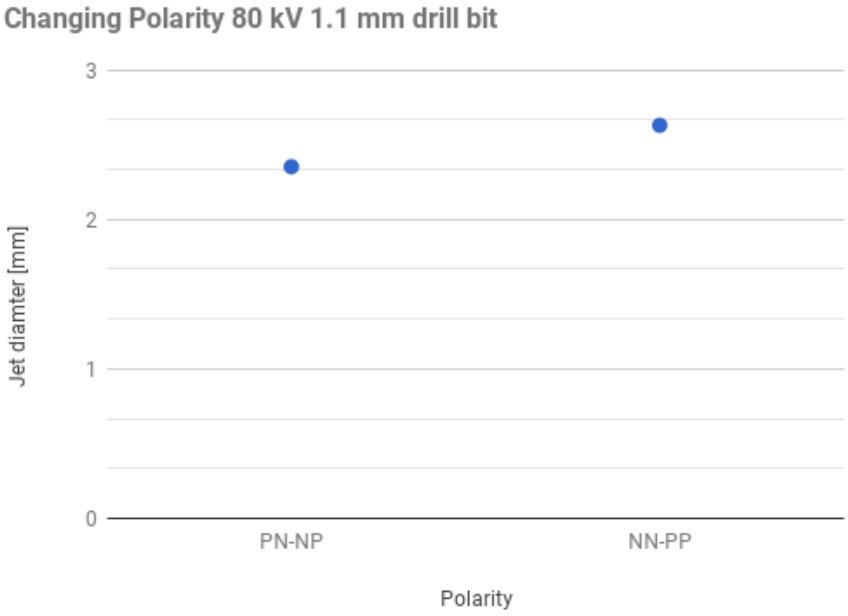

Figure 5.10: Change in average jet diameter accross two electrode polarities

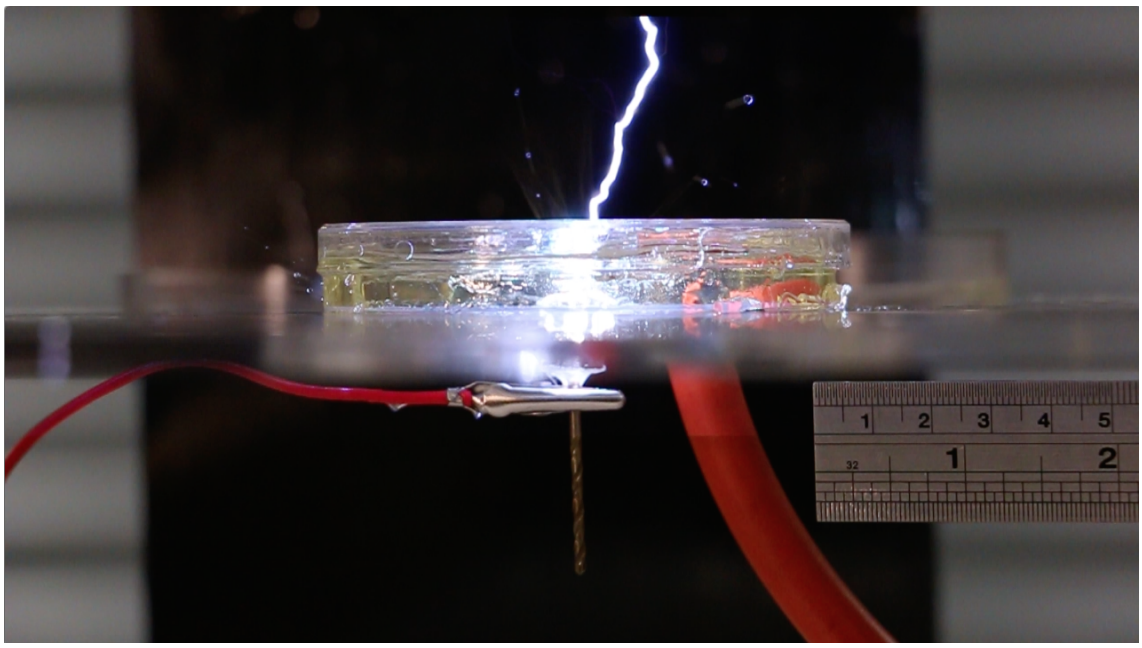

Figure 5.11: Negative result of Streamer signifying dielectric breakdown occurring during experimentation

5.7 Experimental Manifestations

It is observed that the quality of the dielectric can significantly impact whether or not electrospinning can occur in a solution. This is attributed to the changing dielectric strength of air, which is the primary dielectric between the two electrodes. The primary causes of change to the dielectric strength can be attributed to temperature and humidity content of the air. A poorer dielectric strength of air would mean that it would require a lower ΔV value to break down air. This would occur prior to the charge density threshold required in the electrospinning solution to form a Taylor cone.

Figure 5.11 shows the breakdown of air occurring during the experimental phase due to change in weather. The beam of light seen is current traveling through air over a short period of time, this visible light is called a *streamer*. The data relating to successful electrospinning was acquired at a time which coincided with the warm summer time which had successful electrospinning during drier weather and warmer temperatures of less than 40% relative humidity and more than 20° C in ambient temperature respectively.

5.8 Closure

In this chapter the simulation results were detailed and the simulations presented and analyzed and helped form design decisions for the capacitor box.

This chapter also presented and discussed the experimental results acquired from the capacitor box. The setup was capable of running multiple electrospinning configurations successfully. The feasibility of electrospinning was assessed and conclusions were drawn that are outlined and explained in the following chapter.

Chapter 6

Conclusions

As discussed in the Aims and Objectives of this research in Section 1.5 of Chapter 1, the researched covered in this thesis was split into two main components. A computer simulation component which involved acquiring simulation data of various static electric field configurations and an experimental component which involved designing and building a novel electrospinning setup. The conclusions of the two research components are outlined in the following two sections respectively.

6.1 Simulation Conclusions

The work covered in this thesis has been able to produce results that meet the objectives set for the simulations. The analysis in Section 5.3 in Chapter 5 resulted with a series of design stipulations that need to be addressed in the experimental design and experimental procedures. The design must meet the criteria of maintaining uniformity of the electric field by taking into account the following

- Use of circular plates mitigates the fringing effects near the edges of the plates.
- Using a boxed setup made of a Perspex based material does not pose a significant effect on the shape of the electric field between the two plates.
- Conductive parts near the experimental setup do not display a significant effect on the electric field so long they remain unreferenced.
- The setting of the experiments is to be done in an area distant from any earthed infrastructure.

The results of simulating the different configurations was an effective method of improving the design and material selection of the capacitor box.

6.2 Experimental Conclusions

The work covered in this thesis has been able to produce results that meet the objectives set for the experimental setup and build. The developed capacitor box is a modular box that can hold different electrodes and apply a high DC voltage to those electrodes within its walls with little effects on the inner region of the electric field. Mineral oil is used as the electrospinning fluid for its low volatility, consistency and ease of procurement. Lighting and camera is set up to clearly show the events that occur inside the capacitor box. With the use of rulers and a flat laser beam, the electrodes and measurement equipment are aligned in the same field of view for the camera to be able to capture the image with minimal perspective errors.

The presented results and analysis in Sections 5.4 & 5.5 in Chapter 5 established that the following objectives were met:

- A setup that can be configured to test electrospinning with uniform and non-uniform fields
- Materials for this setup were carefully selected according to the results from the simulations and then built to design
- The feasibility of electrospinning with the setup was tested and established based on the methods explained in Section 5.2 of Chapter 5
- Electrospinning in uniform electric fields was not possible before breakdown of air occurred. Sections 5.4 and 5.7 discusses the procedures of the uniform field experiments and the observed breakdown of air respectively
- The submerged needle method of electrospinning was shown to be a feasible way to test electrospinning as discussed in Section 5.6.1 of Chapter 5. It is a viable method of electrospinning that can minimise more of the fringing effects that come with the hollow needle electrospinning methods.

6.3 Further Work

There are a number of areas where improvements could be made to the capacitor box developed in this study. Some have been omitted due to time constraints, while others are possible solutions to problems encountered during the experimental stages.

6.3.1 Controlled Environment Testing

The capacitor box is shown to be a plausible rig to test electrospinning configurations. To further test the parameters that affect electrospinning an enclosed environment that reduces the number of variables that influence the dielectric strength of air is required. Variables such as temperature and humidity affect the system greatly where a decay in the dielectric strength can lead to the breakdown of air at voltages lower than required to initiate electrospinning. This decrease in dielectric strength also leads to charge leakage throughout the system where a lower charge concentration is available in the electrospinning solution. When charge leakage occurs, hissing sounds can be heard arising between the HV conductors used and nearby surfaces.

An investigation into uniform field electrospinning using a controlled environment can be of significance if the dielectric conditions are high enough, allowing for a higher ΔV, which enable a higher charge density on the solution surface that could potentially be sufficient to break the higher surface tension and form a large (or multiple) Taylor cone(s).

Based on the observations highlighted in Section 5.7 of Chapter 5, it is proposed that a setup that encloses the capacitor box is required because the existing open environment diminishes the consistency of electrospinning. Testing electrospinning with the needle-plate setup under different temperature, humidity and atmospheric pressure values to better discern the optimal conditions to electrospin different electrospinning solutions is required.

6.3.2 Data for More Points

The two electrode diameters tested in Section 5.5 of Chapter 5 were used to show that electropsinning was possible with this setup. Acquiring more data points from at least five different diameter electrodes would show the relationship between the jet diameter and the diameter of the electrode using a controlled environment to reduce the effect that external changes such as temperature and humidity would have on the experiment.

6.3.3 Using Other Solvents

The use of mineral oil in this thesis was to remove the issues that come with using conventional electrospinning solutions that are mixtures of volatile solvents such as DMF, DMA and Acetone which evaporate rapidly which in turn changes the concentrations of the mixtures. This thesis aimed at only looking into the nature of the electrospinning process, however solvents are crucial to nanofibre production and an investigation into the right variables required to optimally electrospin with those solvents using the capacitor box is key to predicting the effects that each parameter has on the electrospinning quality and potentially nanofibre morphology. However with a controlled environment setup built for the capacitor box, experimental data

surrounding the most effective electrospinning electrical criteria can be assessed and that can be gauged in terms of fibre morphology.

The rate at which the solvent would evaporate is another important aspect of fibre formation. Controlling the pressure levels inside the enclosed environment can help change the evaporation rate at which the solvents evaporate in turn changing the fibre morphology depending on how quickly the solvents evaporate leaving behind the residue polymer on a collector.

Water can be used as a stable non-volatile solvent coupled with water soluble polymers. Coupled with the use of a controlled environment setup and volatile solvents, the use of water and water-based solvents is commonly used and worthy of further study. This configuration was not investigated in this thesis due to time constraints.

6.3.4 Monitoring Current Draw

Electrospinning is displacing charged fluid. Once a Taylor cone forms, charge is displaced and current is drawn from the power supply to replace those charges. The amount of current drawn can be read from the Spellman SL600 HVDC power supplies as seen on the LCD screen in Figure 4.6 in Chapter 4. The readings can potentially be used as an indicator of how much fluid is being displaced and whether it is being electrospun and whether or not charge is leaking throughout the system. Devising a procedure to monitor the current and depict whether there is charge leakage or not in the system would be a beneficial component to commercialization and troubleshooting issues with electrospinning.

6.3.5 Implementing findings on Yarn Spinning Setup (Aardvark)

Implementing findings from the investigations onto an existing production machine such as the yarn spinner (Aardvark) highlighted in Chapter 1 can potentially directly benefit commercial production of nanofibre in terms of efficiency and servicing. Improvements in the realm of nanofibre yarn production will drive further research in the field and allow for further experimentation with applications for the highly sought after form of material.

6.4 Closure

The methods of electrospinning which have been explored in this thesis can be adapted into existing methods that produce multi-filament electrospun yarn with the use of collection plates. This could help solve issues with existing techniques that deal with fabricating oriented electrospun fibres and fibre collection. This form of material is of significance for tissue engineering of the nervous system, tendons, muscles, or as an artificial extracellular matrix, while the micron diameter yarns are of interest as sutures for medical applications and embedding them into wearable garments for bio-sensing applications.

Appendix A

MATLAB Scripts & Plotted Results

This appendix chapter provides results acquired from Maxwell and processed in MATLAB. Provided as well are the MATLAB scripts used to process the data points acquired from the Maxwell calculator.

```
%% Load data
plates = xlsread('Plates.xlsx','0-500-100-10.fld','A1:F5151');
boxed = xlsread('Boxed.xlsx','0-500-100-10.fld','A1:F5151');
Dregion = xlsread('DoubleRegion.xlsx','0-500-100-10.fld','A1:F5151');
extRod = xlsread('extRod.xlsx','0-500-100-10.fld','A1:F5151');
circular = xlsread('CircularPlates.xlsx','0-500-100-10.fld','A1:F5151');
droplet = xlsread('droplet.xlsx','0-500-100-10.fld','A1:F5151');
earthedRod = xlsread('EarthedRoad.xlsx','0-500-100-10.fld','A1:F5151');

%% Plot ALL datasets 'as is' in vector fields
figure
quiver3(plates(:,1),plates(:,2),plates(:,3),plates(:,4),plates(:,5),plates(:,6)
        ,'r','LineWidth',.1);
title('Two Plates in Vacuum','FontName','Times')

figure
quiver3(boxed(:,1),boxed(:,2),boxed(:,3),boxed(:,4),boxed(:,5),boxed(:,6),'r'
        ,'LineWidth',.1);
title('Two Plates Boxed in Vacuum','FontName','Times')

figure
quiver3(Dregion(:,1),Dregion(:,2),Dregion(:,3),Dregion(:,4)
        ,Dregion(:,5),Dregion(:,6),'r','LineWidth',.1);
title('Two Plates With double the Region Size','FontName','Times')

figure
quiver3(extRod(:,1),extRod(:,2),extRod(:,3),extRod(:,4),extRod(:,5),extRod(:,6),'r','LineWidth',.1);

title('Two Plates With an external conductor to the right','FontName','Times')

figure
quiver3(circular(:,1),circular(:,2),circular(:,3),circular(:,4),circular(:,5),circular(:,6),'r'
        ,'LineWidth',.1);
title('Two round plates in a vacuum','FontName','Times')

figure
quiver3(earthedRod(:,1),earthedRod(:,2),earthedRod(:,3),earthedRod(:,4),earthedRod(:,5),earthedRod(:,6)
        ,'r','LineWidth',.1);
title('Two Plates With an earthed external conductor to the right','FontName','Times')

figure
quiver3(droplet(:,1),droplet(:,2),droplet(:,3),droplet(:,4),droplet(:,5)
        ,droplet(:,6),'r','LineWidth',.1);
title('conductive cone on plate (Represents solution)','FontName','Times')
```

Figure A.1: MATLAB Code – Loading Data from Excel Documents and plotting vector Fields

```
%% Calculations
% Caclulate point by point differences
% Note that the '_' notation in variable names is used to represent the '-' operater
plates_boxed = [plates(:,4)-boxed(:,4),plates(:,5)-boxed(:,5),plates(:,6)-boxed(:,6)];
plates_Dregion = [plates(:,4)-Dregion(:,4),plates(:,5)-Dregion(:,5),plates(:,6)-Dregion(:,6)];
plates_eR = [plates(:,4)-extRod(:,4),plates(:,5)-extRod(:,5),plates(:,6)-extRod(:,6)];
plates_circular = [plates(:,4)-circular(:,4),plates(:,5)-circular(:,5),plates(:,6)-circular(:,6)];
plates_droplet = [plates(:,4)-droplet(:,4),plates(:,5)-droplet(:,5),plates(:,6)-droplet(:,6)];
plates_earthRod = [plates(:,4)-earthedRod(:,4),plates(:,5)-earthedRod(:,5),plates(:,6)-earthedRod(:,6)];

% Magnitude calculations
% Shorthand notations used for variable names:
%   Mag = Magnitude
%   pb  = plates_boxed
%   pD  = plates_Dregion
%   eR  = external rod
%   pc  = Plates_Circular
%   dr  = plates_droplet
%   ee  = Earthed external conductor
for i = 1:length(plates)
    Mag_pb(i) = sqrt(plates_boxed(i,1)^2+plates_boxed(i,2)^2+plates_boxed(i,3)^2);
    Mag_pD(i) = sqrt(plates_Dregion(i,1)^2+plates_Dregion(i,2)^2+plates_Dregion(i,3)^2);
    Mag_eR(i) = sqrt(plates_eR(i,1)^2+plates_eR(i,2)^2+plates_eR(i,3)^2);
    Mag_pc(i) = sqrt(plates_circular(i,1)^2+plates_circular(i,2)^2+plates_circular(i,3)^2);
    Mag_dr(i) = sqrt(plates_droplet(i,1)^2+plates_droplet(i,2)^2+plates_droplet(i,3)^2);
    Mag_ee(i) = sqrt(plates_earthRod(i,1)^2+plates_earthRod(i,2)^2+plates_earthRod(i,3)^2);
    MagPlates(i) = sqrt(plates(i,4)^2+plates(i,5)^2+plates(i,6)^2);
    MagBoxed(i) = sqrt(boxed(i,4)^2+boxed(i,5)^2+boxed(i,6)^2);
    MagExtrod(i) = sqrt(extRod(i,4)^2+extRod(i,5)^2+extRod(i,6)^2);
    MagCircular(i) = sqrt(circular(i,4)^2+circular(i,5)^2+circular(i,6)^2);
end
% Reshape results to work with the meshgrid of 51x101 points

% Reshape magnitudes
MagPlates = reshape(MagPlates,[101,51]);
MagBoxed = reshape(MagBoxed,[101,51]);
MagExtrod = reshape(MagExtrod,[101,51]);
MagCircular = reshape(MagCircular, [101,51]);
% Reshape diff in magnitude
Mag_pb = reshape(Mag_pb,[101,51]);
Mag_pD = reshape(Mag_pD,[101,51]);
Mag_eR = reshape(Mag_eR,[101,51]);
Mag_pc = reshape(Mag_pc,[101,51]);
Mag_dr = reshape(Mag_dr,[101,51]);
Mag_ee = reshape(Mag_ee,[101,51]);
```

Figure A.2: MATLAB Code – Running Vector Calculations

```
%% Surface Plot: mag diff boxed and unboxed plates
% plates - boxed
figure('units','normalised','outerposition',[0 0 1 1])
surf([0:10:500],[-500:10:500],Mag_pb)
set(gca,'FontName','Times')
% shading flat
title('Difference in Magnitude of Boxed and Unboxed Plates','FontName','Times','FontSize',16)
caxis([0 10])
colorbar
view([0 0 90])
% print('-dpdf')

%% Surface plot: mag diff in changing region size
% plates - DoubleRegion
figure('units','normalised','outerposition',[0 0 1 1])
surf([0:10:500],[-500:10:500],Mag_pD)
set(gca,'FontName','Times','TickDir','out','FontSize',10)
title('Difference in Magnitude of two Regions (100% & 200%)','FontName','Times','FontSize',16)
caxis([0 10])
colorbar
view([0 0 90])
% print('-dpdf')

%% Surface plot: effect of external conductor
% plates - extRod
figure('units','normalised','outerposition',[0 0 1 1])
surf([0:10:500],[-500:10:500],Mag_eR)
set(gca,'FontName','Times','TickDir','out','FontSize',10)
title('Effect of an external conductor on the two plates','FontName','Times','FontSize',16)
caxis([0 10])
colorbar
view([0 0 90])
% print('-dpdf')

%% Surface plot: effect of an earthed external conductor
% plates - extRod
figure('units','normalised','outerposition',[0 0 1 1])
surf([0:10:500],[-500:10:500],Mag_ee)
set(gca,'FontName','Times','TickDir','out','FontSize',10)
title('Effect of an earthed external conductor on the two plates','FontName','Times','FontSize',16)
caxis([0 10])
colorbar
view([0 0 90])
% print('-dpdf')

%% Surface Plot: mag diff square and round plates
% plates - boxed
figure('units','normalised','outerposition',[0 0 1 1])
surf([0:10:500],[-500:10:500],Mag_pc)
set(gca,'FontName','Times')
% shading flat
title('Difference in Magnitude of square and round Plates','FontName','Times','FontSize',16)
caxis([0 10])
colorbar
view([0 0 90])
% print('-dpdf')
```

Figure A.3: MATLAB Code – Plotting Results (Part I)

```
%% Surface Plot: mag diff plates and droplet on plate
% plates - boxed
figure('units','normalized','outerposition',[0 0 1 1])
surf([0:10:500],[-500:10:500],Mag_dr)
set(gca,'FontName','Times')
% shading flat
title('Difference in Magnitude of plates and droplet on plate','FontName','Times','FontSize',16)
caxis([0 10])
colorbar
view([0 0 90])
% print('-dpdf')

%% Surface plot: Magnitude field between two plates in vacuum
figure('units','normalized')
surf([0:10:500],[-500:10:500],MagPlates)
set(gca,'FontName','Times','TickDir','out','FontSize',10)
title('Magnitude E Field between two plates [0 - 5V]','FontName','Times','FontSize',16)
caxis([0 10])
ylabel('Distance [mm]','FontSize',14)
xlabel('Distance [mm]','FontSize',14)
zlabel('E-Mag [V/m]')
colorbar
% view([0 0 90])
% print('-dpdf')

%% Surface plot: Magnitude field between two boxed plates in vacuum
figure('units','normalized','outerposition',[0 0 1 1])
surf([0:10:500],[-500:10:500],MagBoxed)
set(gca,'FontName','Times','TickDir','out','FontSize',10)
title('Magnitude E Field between two plates boxed [0 - 5V]','FontName','Times','FontSize',16)
caxis([0 10])
ylabel('Distance [mm]','FontSize',14)
xlabel('Distance [mm]','FontSize',14)
colorbar
view([0 0 90])
print('-dpdf')
%% Surface plot: Magnitude field between two plates with ext. conductor

figure('units','normalized','outerposition',[0 0 1 1])
surf([0:10:500],[-500:10:500],MagExtrod)
set(gca,'FontName','Times','TickDir','out','FontSize',10)
title('Magnitude E Field between two plates [0 - 5V] with external rod conductor [Floating]','FontName'
      ,'Times','FontSize',16)
caxis([0 10])
ylabel('Distance [mm]','FontSize',14)
xlabel('Distance [mm]','FontSize',14)
colorbar
view([0 0 90])
% print('-dpdf')
%% Surface plot: Magnitude field between two round plates

figure('units','normalized','outerposition',[0 0 1 1])
surf([0:10:500],[-500:10:500],MagCircular)
set(gca,'FontName','Times','TickDir','out','FontSize',10)
title('Magnitude E Field between two round plates [0 - 5V]','FontName','Times','FontSize',16)
caxis([0 10])
ylabel('Distance [mm]','FontSize',14)
xlabel('Distance [mm]','FontSize',14)
colorbar
view([0 0 90])
% print('-dpdf')
```

Figure A.4: MATLAB Code – Plotting Results (Part II)

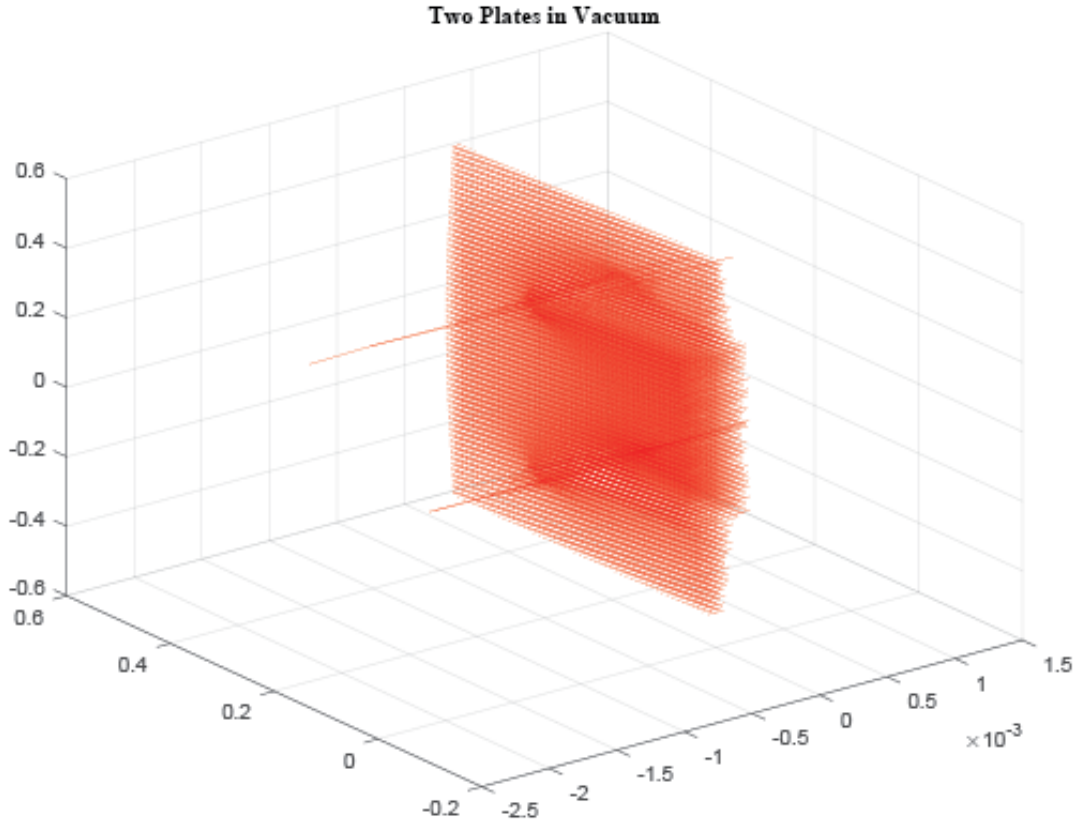

Figure A.5: ANSYS Maxwell Results – Raw Vector Field Data of Two Square Plates in Vacuum

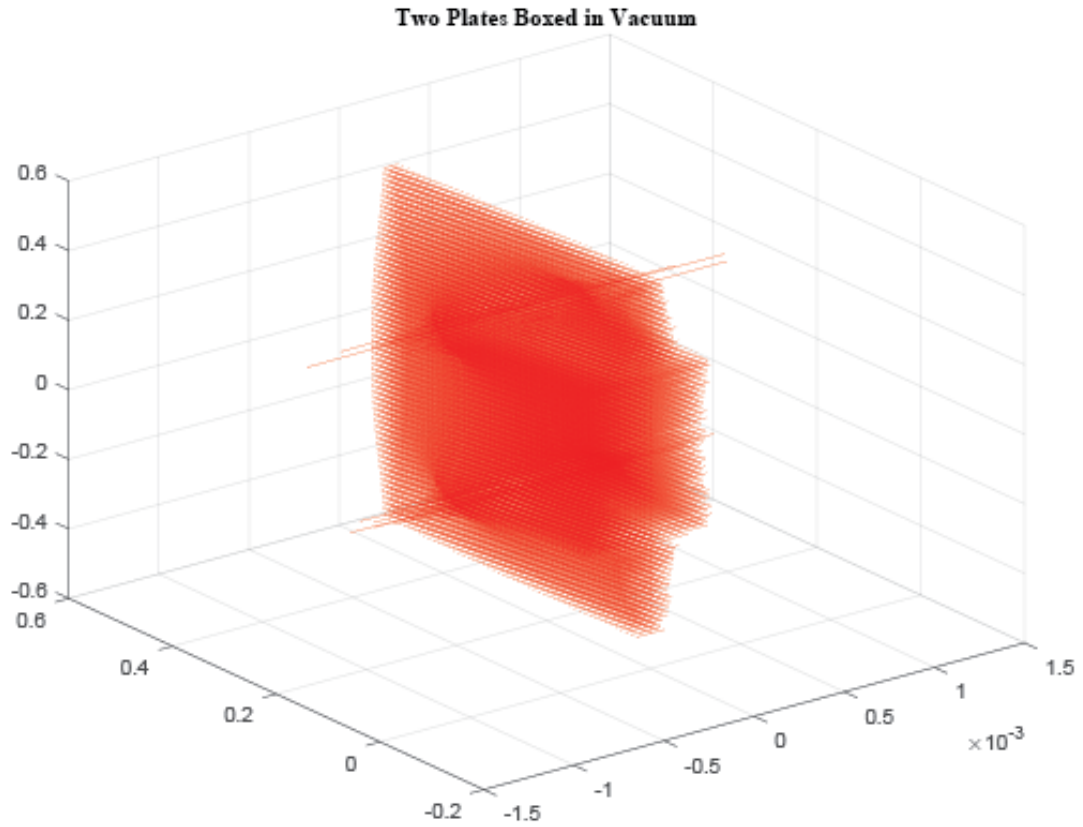

Figure A.6: ANSYS Maxwell Results – Raw Vector Field Data of Two Boxed Plates

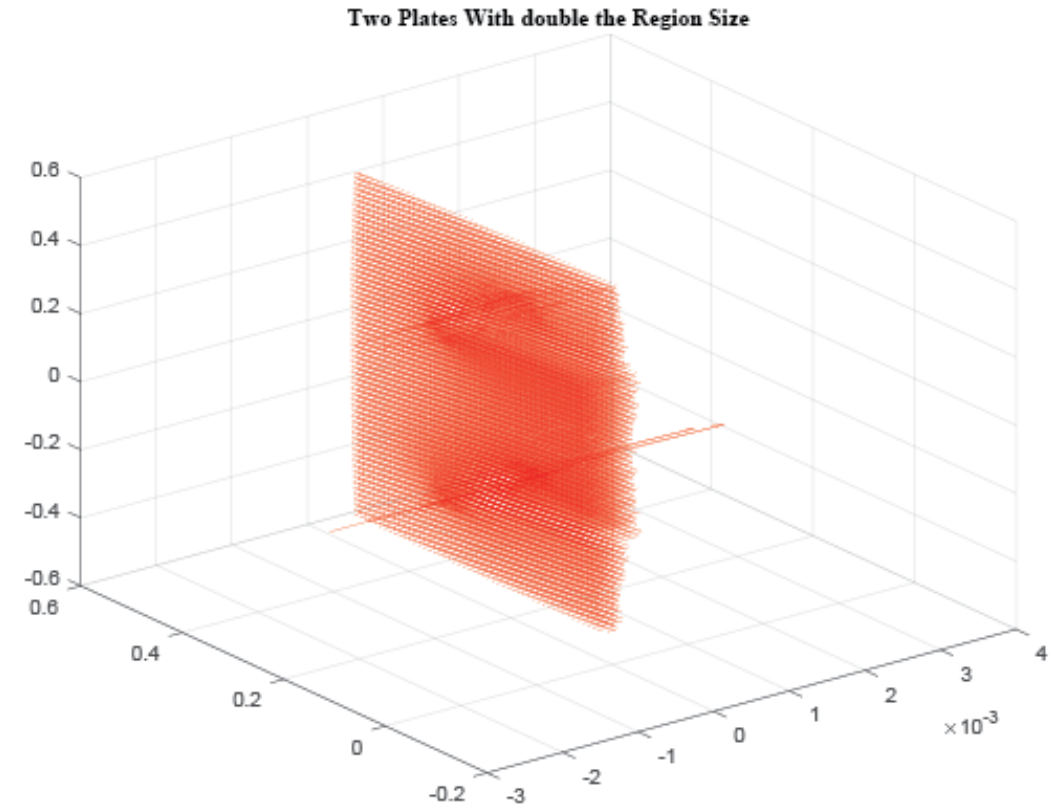

Figure A.7: ANSYS Maxwell Results – Raw Vector Field Data of Two Plates with Region Size Doubled

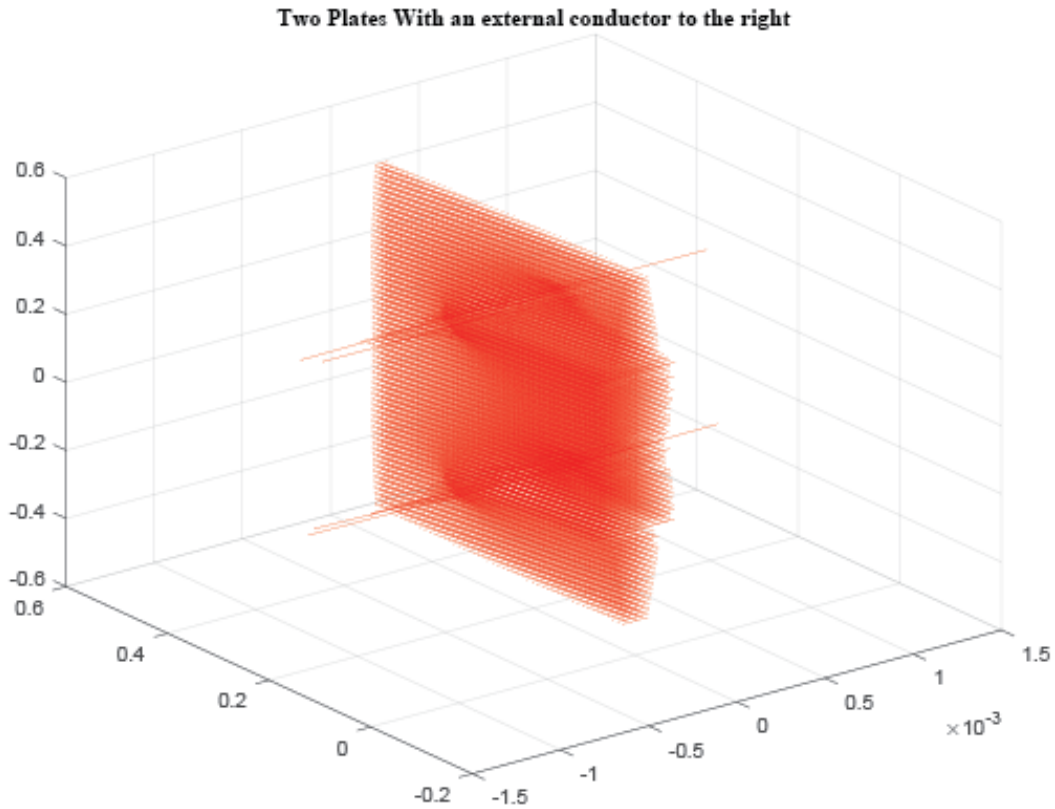

Figure A.8: ANSYS Maxwell Results – Raw Vector Field Data of Floating Conductor near Two Plates

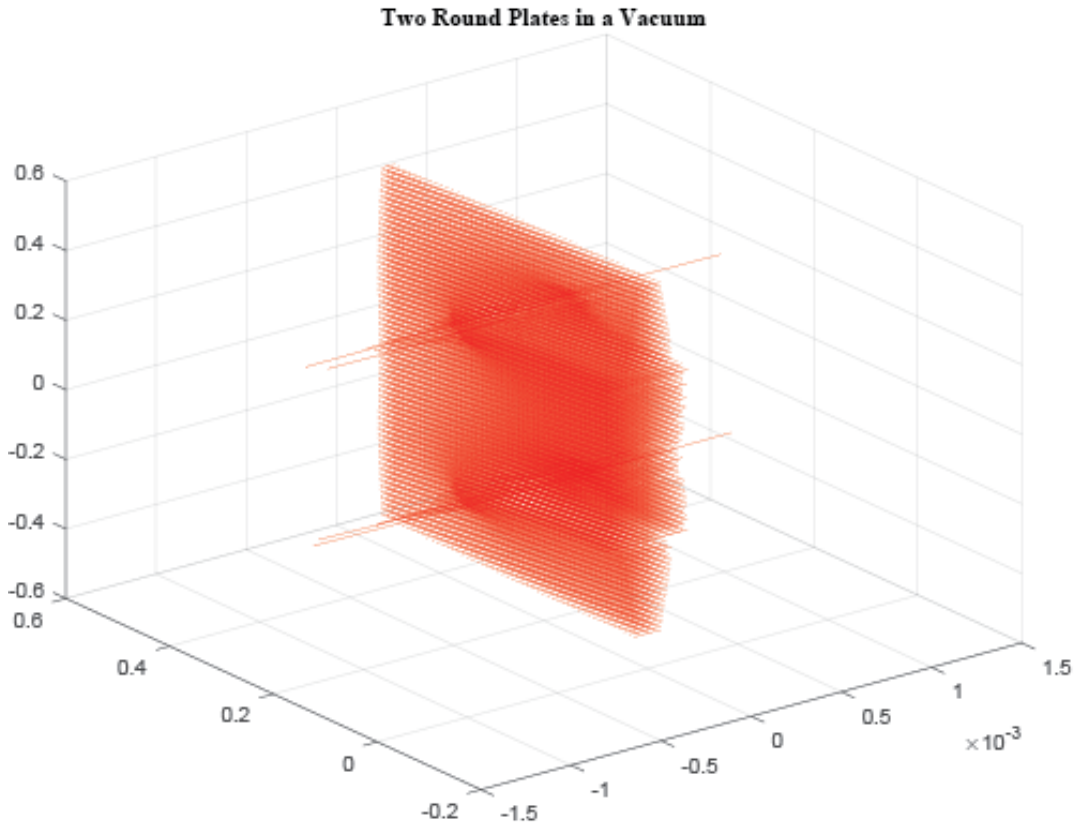

Figure A.9: ANSYS Maxwell Results – Raw Vector Field Data of Two Round Plates

Appendix B

Capacitor Box Drawings

This appendix chapter provides the CAD diagrams that were used to fabricate the Capacitor box. The diagrams were designed and rendered in Solidworks (Dassault Systèmes, France).

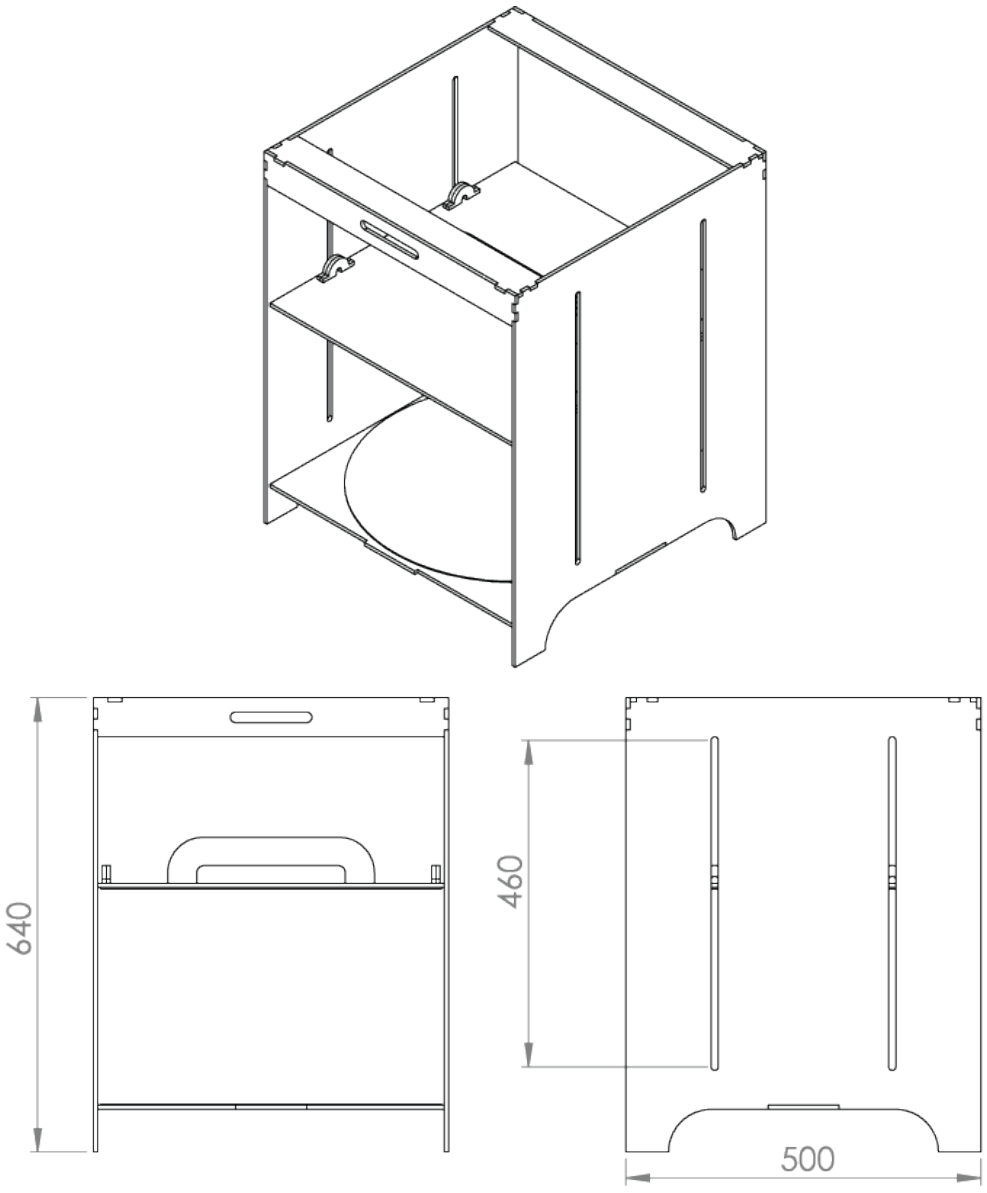

Figure B.1: Capacitor Box – Schematics & Dimensions

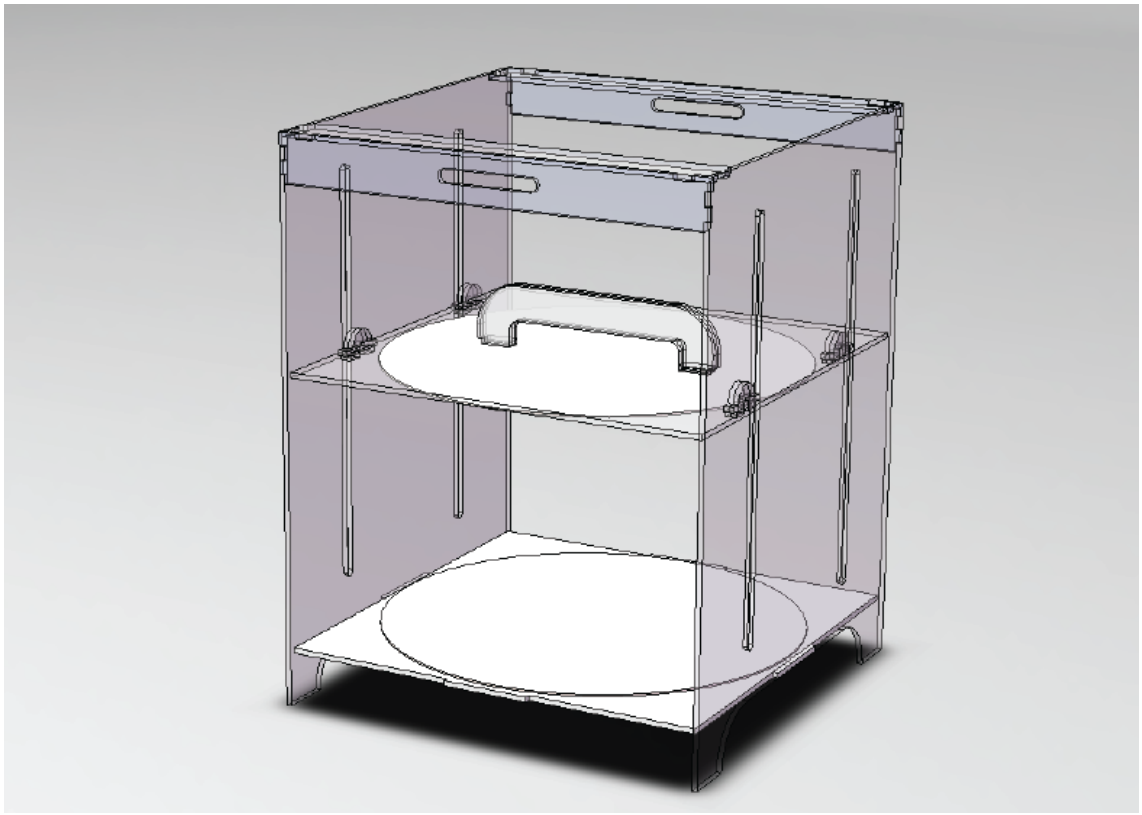

(a) Normal View

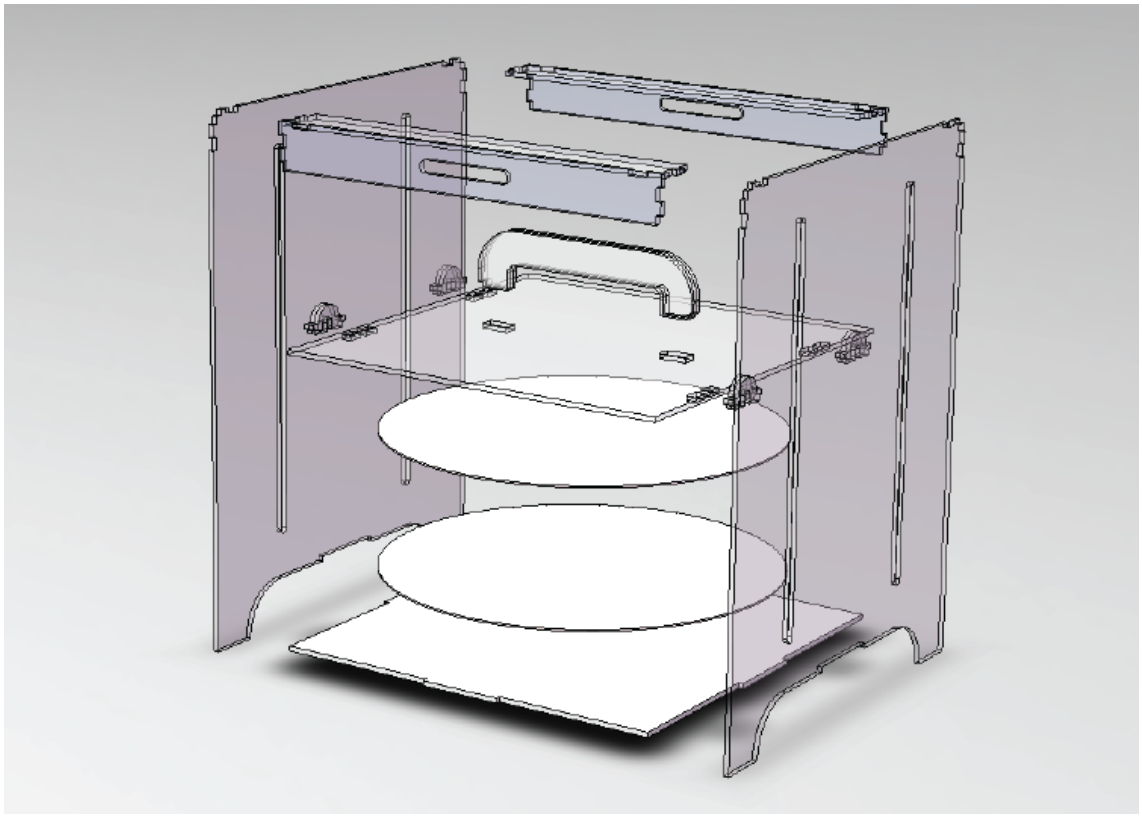

(b) Exploded View

Figure B.2: Capacitor Box Assembly

Appendix C

Experimental Setup & Results

This appendix chapter provides experimental results captured and processed from the non-uniform electric field configuration using the submerged needle setup.

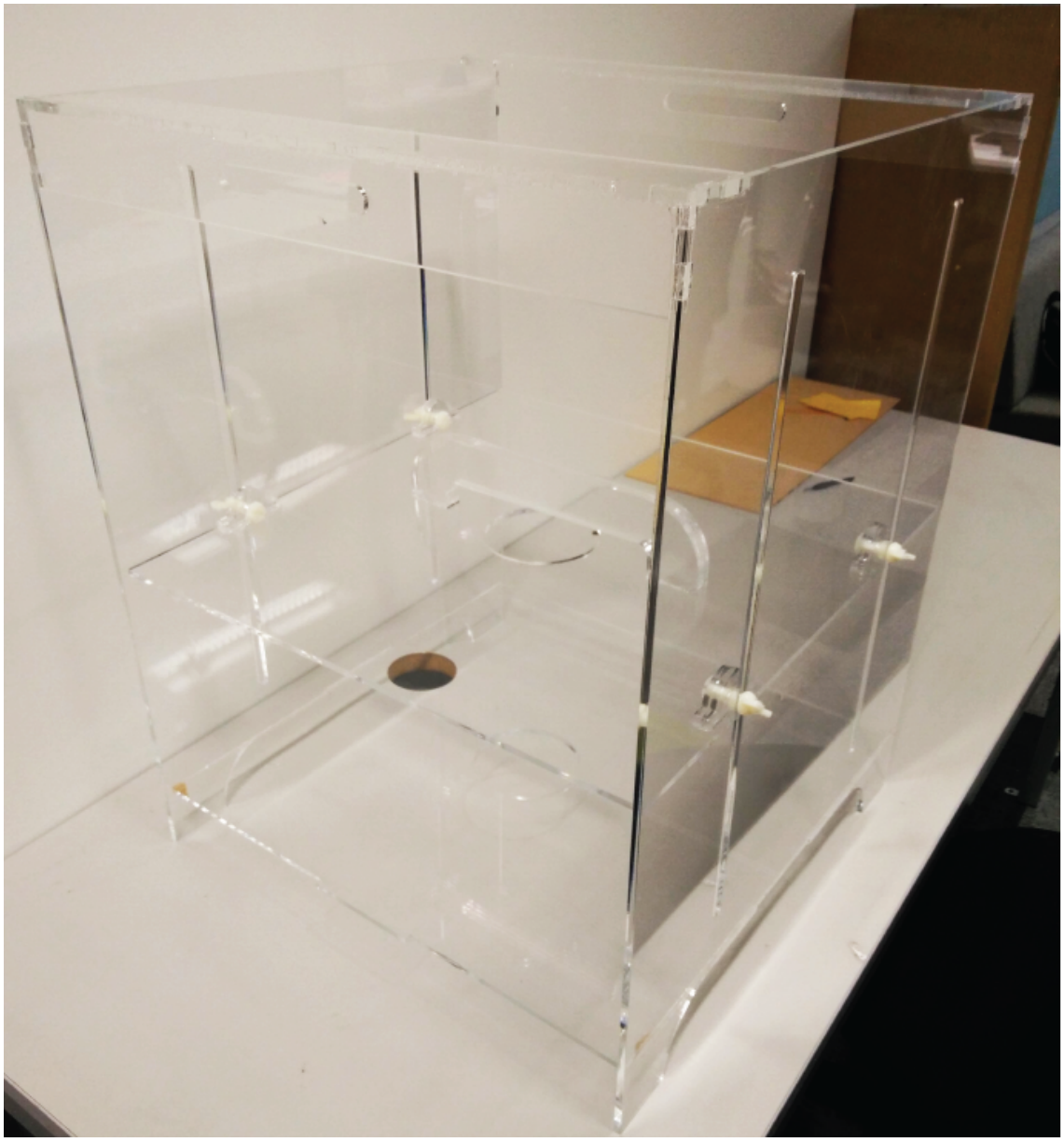

Figure C.1: Capacitor Box Setup – Complete Build without Electrodes

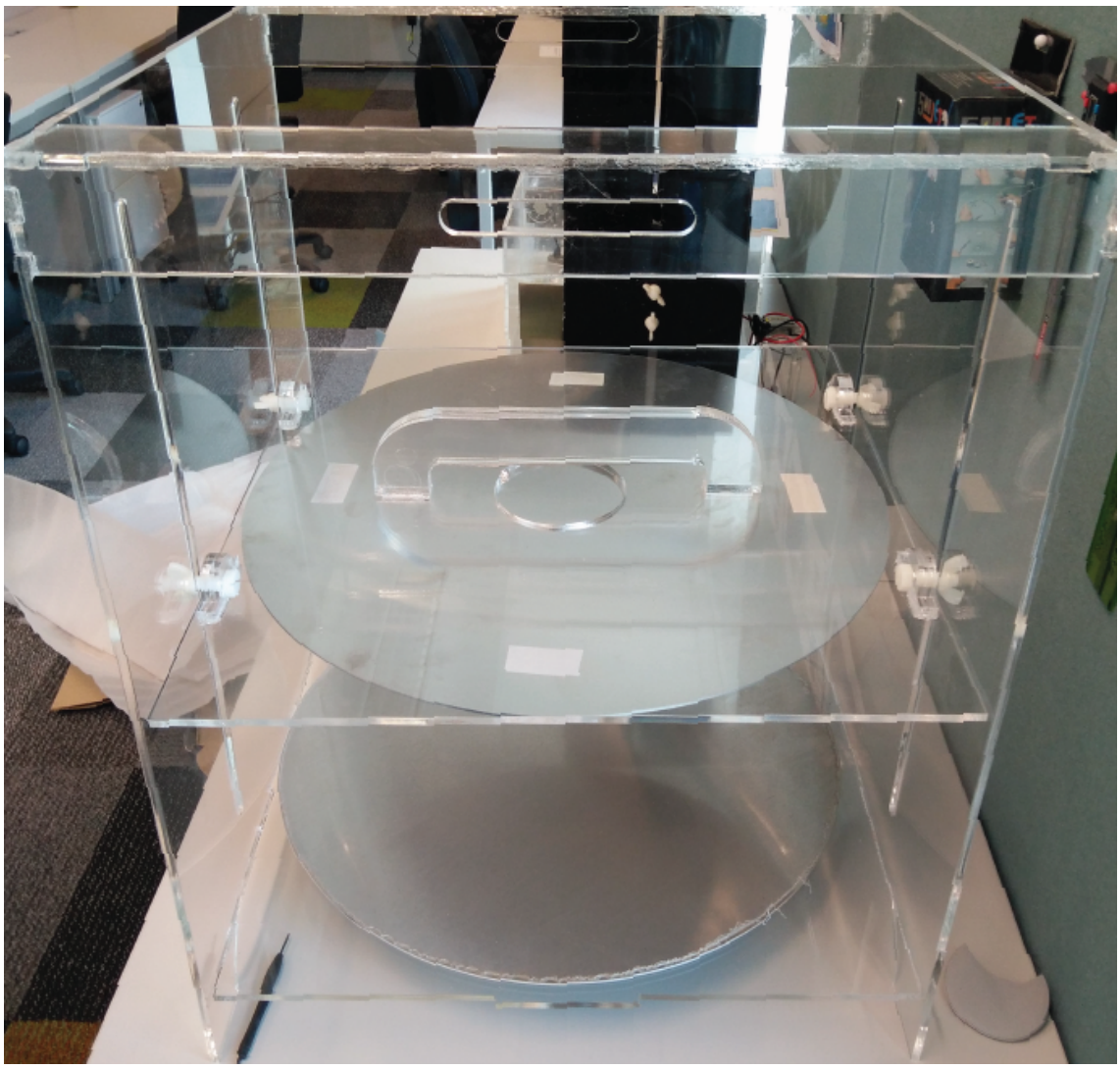

Figure C.2: Capacitor Box Setup – Complete Build with Two Round Plate Electrodes

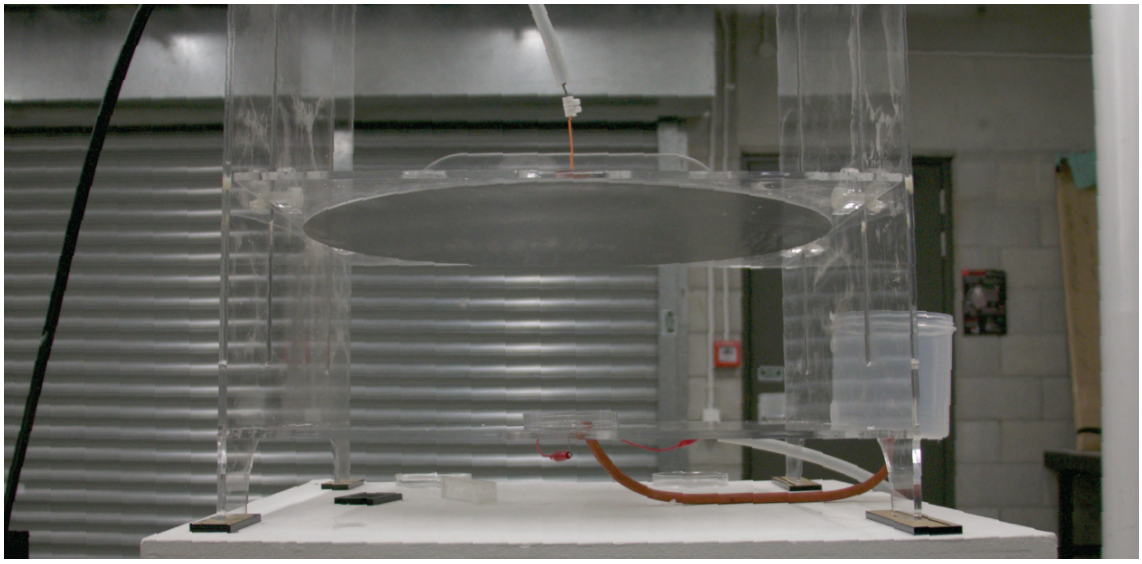

Figure C.3: Capacitor Box Setup – Under the Bottom Plate with Mounted Ruler, Tube to Second Reservoir & HVDC Lead

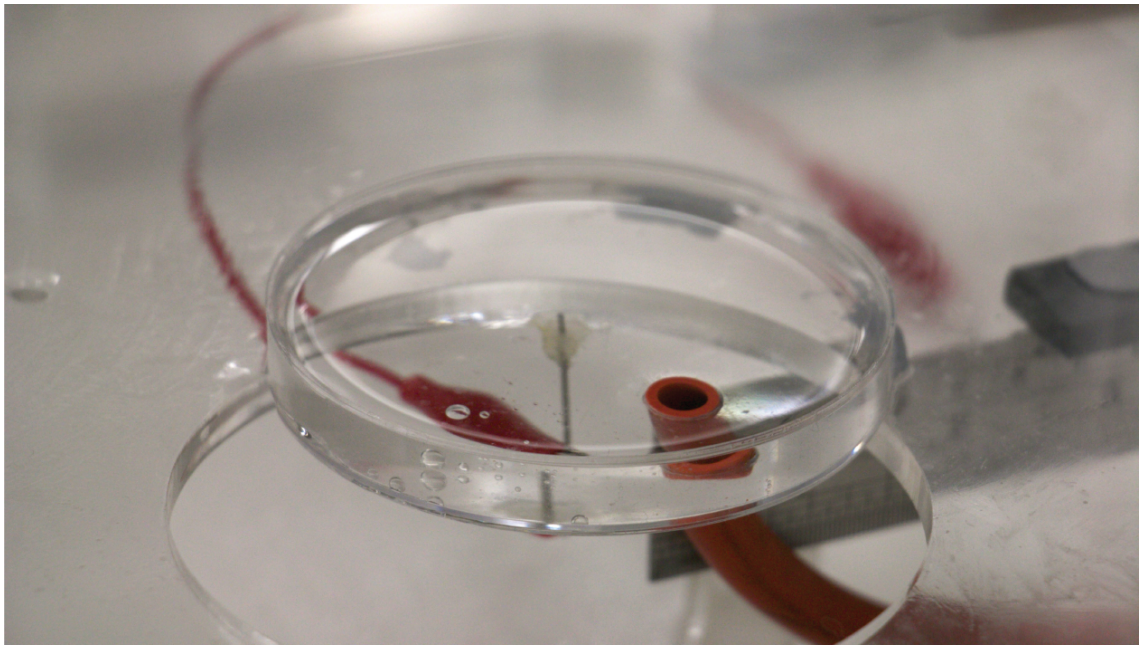

(a) Capacitor Box Setup – Submerged Needle Configuration with Water Filled Petridish with HVDC Lead Connecting to Needle

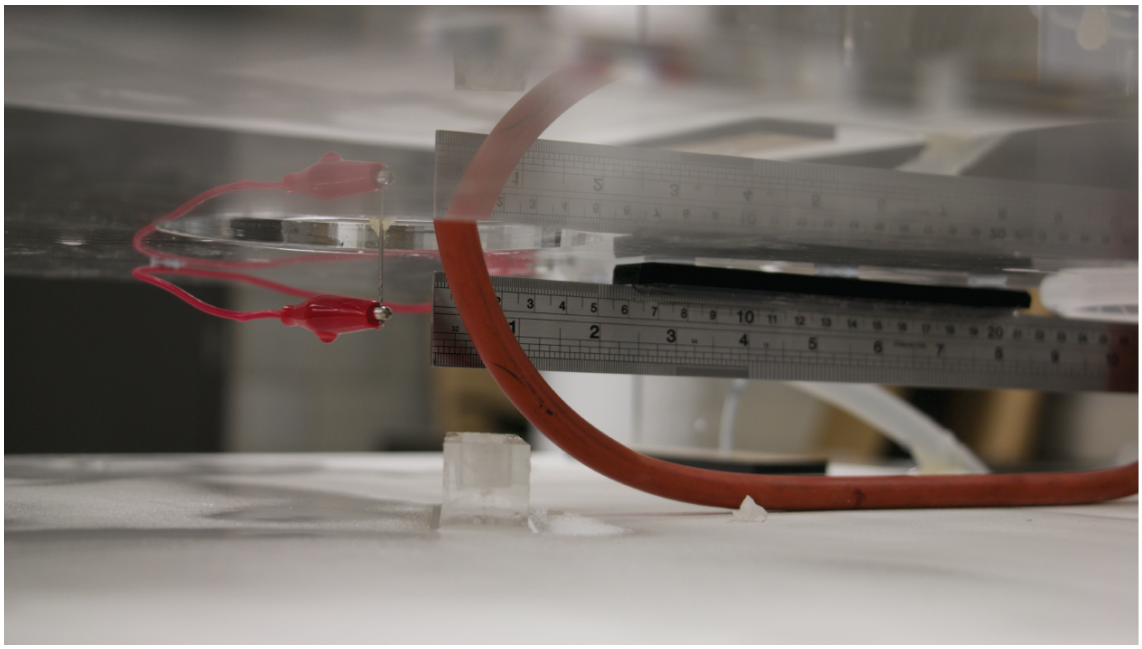

(b) Capacitor Box Setup – Under the Bottom Plate with Mounted Ruler, Tube to Second Reservoir & HVDC Lead

Figure C.4: Capacitor Box Setup – Submerged Needle Components

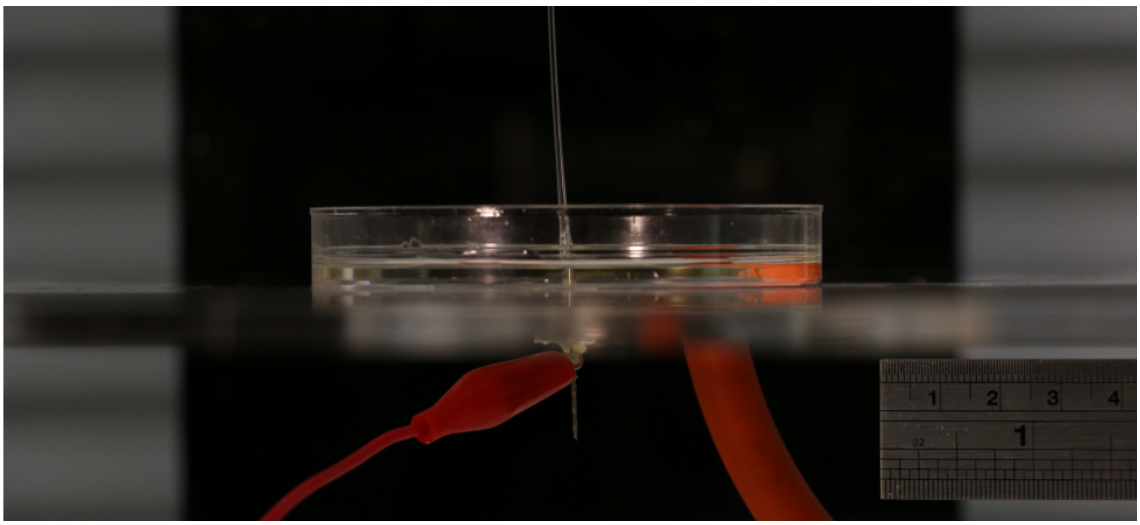

Figure C.5: Needle Plate Experiment – Preliminary Testing without Petridish Cover

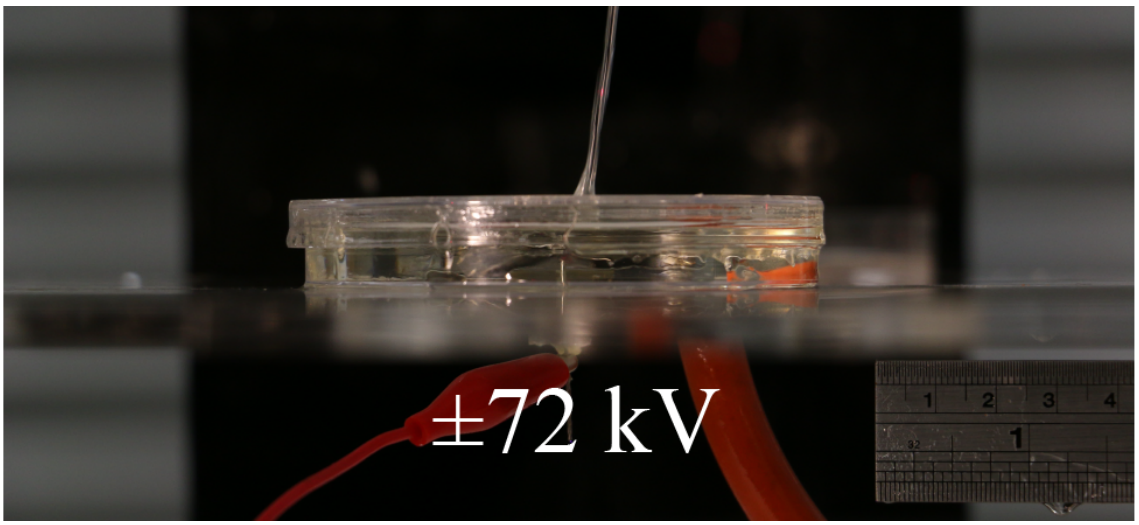

Figure C.6: Needle Plate Experiment – Documented Result for ΔV of 144 kV

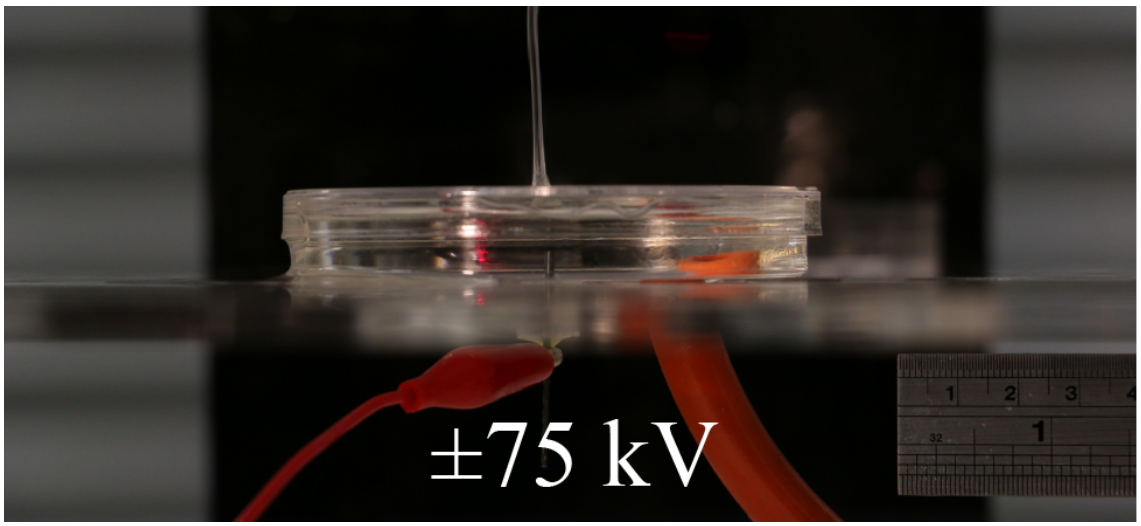

Figure C.7: Needle Plate Experiment – Documented Result for ΔV of 150 kV

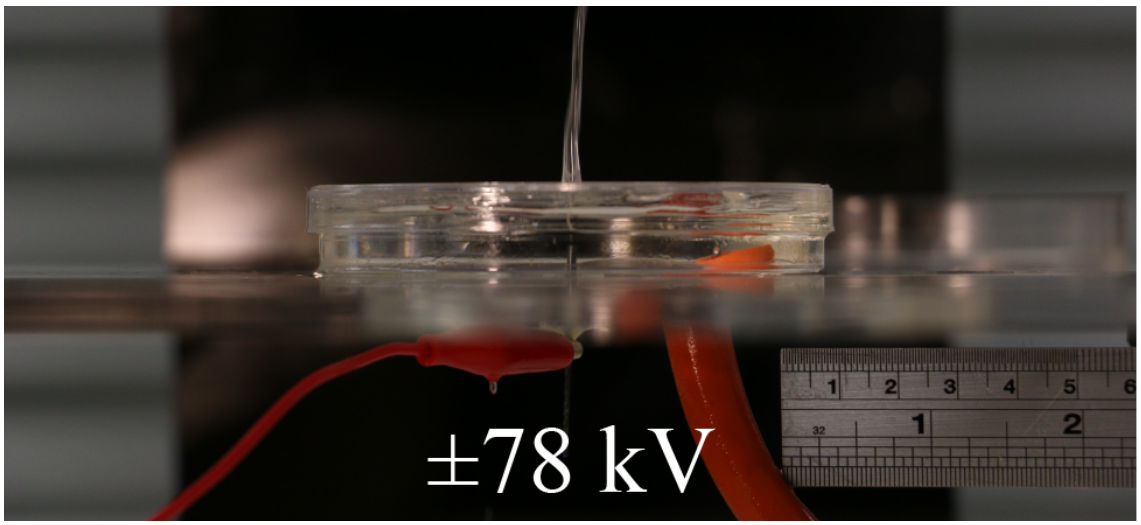

Figure C.8: Needle Plate Experiment – Documented Result for ΔV of 156 kV

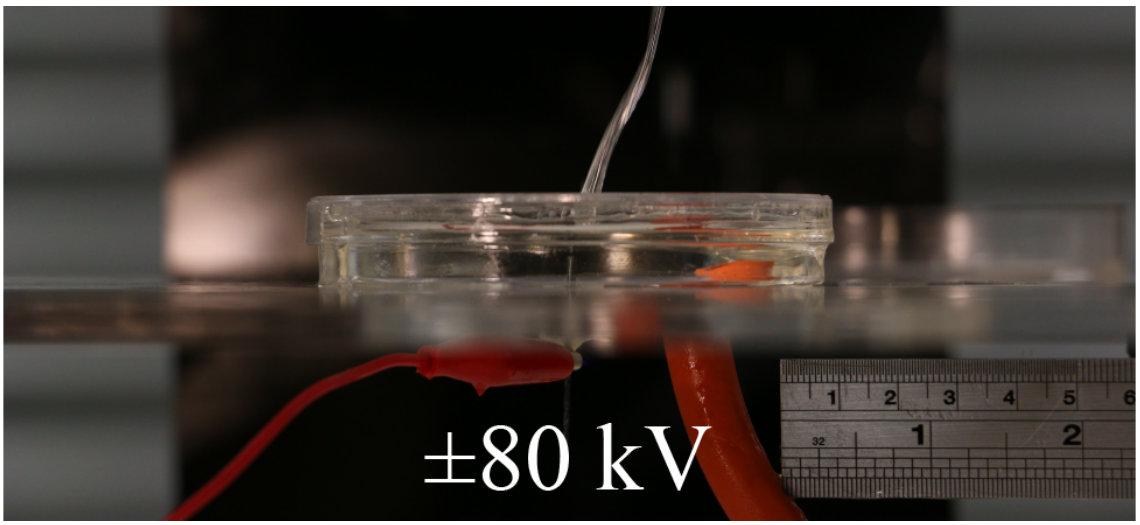

Figure C.9: Needle Plate Experiment – Documented Result for ΔV of 160V

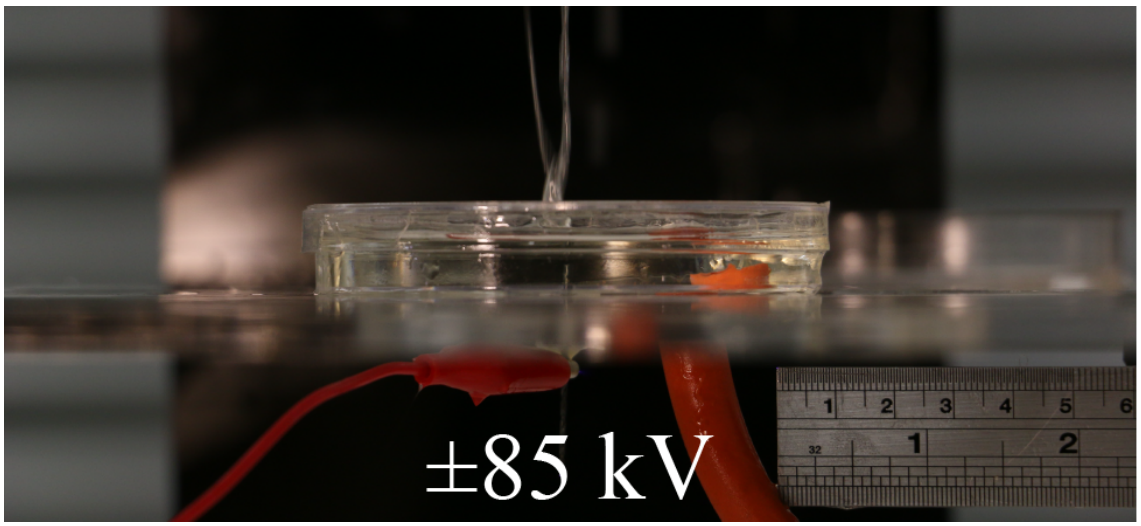

Figure C.10: Needle Plate Experiment – Documented Result for ΔV of 170 kV

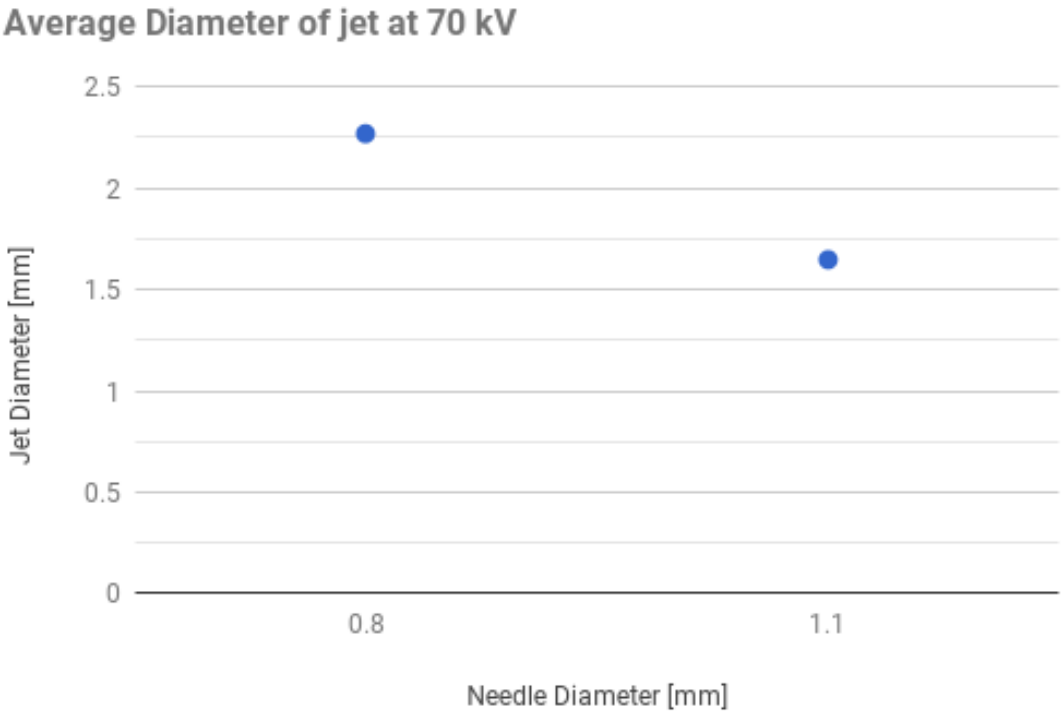

Figure C.11: Change in average jet diameter accross two electrode diameters

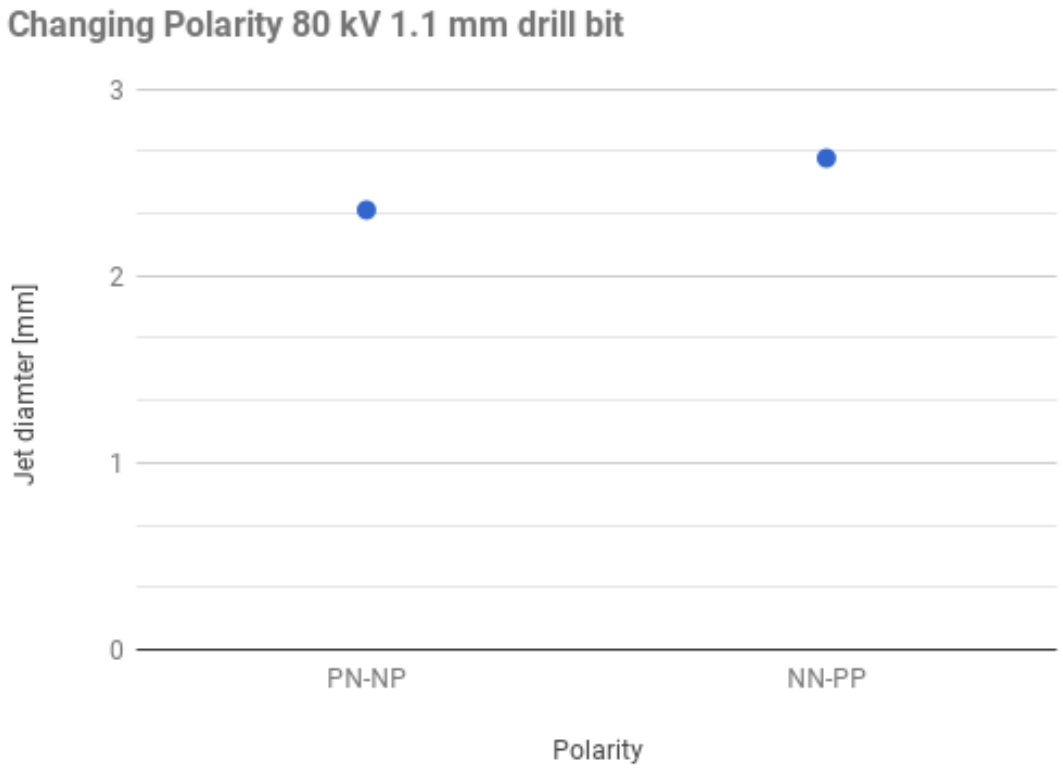

Figure C.12: Change in average jet diameter accross two electrode polarities

Frame Number	Voltage	Polarity	Needle Dia.[mm]	Needle Type	height [mm]	Comments	Sheet Number	Avg. Diameter
8	0	PN-NP	0.8	Drill Bit	2	Reference frame		
9-18	±70	PN-NP	0.8	Drill Bit	2	two tests of rapid fire		
19-24	±70	PN-NP	0.8	Drill Bit	2	took a while to start	1	2.268199234
25-36	±72	PN-NP	0.8	Drill Bit	2	Got a bit more consistency	2	1.708812261
37-45	±75	PN-NP	0.8	Drill Bit	2	Achieved consistent jet	3	1.449917898
47	0	PN-NP	1.1	Drill Bit	2	Empty dish		
48	0	PN-NP	1.1	Drill Bit	2	Full dish		
49-59	±75	PN-NP	1.1	Drill Bit	2	Perfect	4	2.153256705
61-68	±72	PN-NP	1.1	Drill Bit	2	done	5	1.478927203
69-76	±70	PN-NP	1.1	Drill Bit	2	done	6	1.646962233
78-92	±78	PN-NP	1.1	Drill Bit	2	done	7	2.798212005
93-113	±80	PN-NP	1.1	Drill Bit	2	done	8	2.352490421
117-126	±85	PN-NP	1.1	Drill Bit	2	done	9	2.30316092
129- 132	±85	NN-PP	1.1	Drill Bit	2	Arcs without much jet		
135-154	±80	NN-PP	1.1	Drill Bit	2	Done	10	2.62962963
155-172	±78	NN-PP	1.1	Drill Bit	2	arcing problem	11	3.403940887
174-183	±72	NN-PP	1.1	Drill Bit	2			
184-197	±70	NN-PP	1.1	Drill Bit	2		13	2.049808429

Figure C.13: Results Database – Reference Sheet

Frame Number	Ruler Measurement of 20 mm [Px]	Equivalent 1mm [Px]	Height Position from top lid [Px]	Measurement [Px]	Average Measurer
36	586	29	232	54	2.011494253
			464	69	
			696	52	
9	588	29	232	59	2.149425287
			464	81	
			696	47	
10	587	29	232	104	2.114942529
			464	40	
			696	40	
15	588	29	232	82	2.540229885
			464	84	
			696	55	
				Average Total:	2.268199234

Figure C.14: Results Database – Sheet I

Frame Number	Ruler Measurement of 20 mm [Px]	Equivalent 1mm [Px]	Height Position from top lid [Px]	Measurement [Px]	Average Measu
26	588	29	232	43	1.149425287
			464	23	
			696	34	
32	586	29	232	38	1.195402299
			464	25	
			696	41	
35	586	29	232	76	2.091954023
			464	51	
			696	55	
36	587	29	232	47	1.83908046
			464	65	
			696	48	
				Average Total:	1.708812261

Figure C.15: Results Database – Sheet II

Frame Number	Ruler Measurement of 20 mm [Px]	Equivalent 1mm [Px]	Height Position from top lid [Px]	Measurement [Px]	Average Measur
49	587	29	232	64	1.862068966
			464	41	
			696	57	
50	588	29	232	51	1.75862069
			464	48	
			696	54	
52	589	29	232	40	1.344827586
			464	36	
			696	41	
53	588	29	232	70	1.850574713
			464	55	
			696	36	
54	588	29	232	66	2.011494253
			464	52	
			696	57	
55	588	29	232	61	1.793103448
			464	43	
			696	52	
56	588	29	0	46	2.413793103
			0	66	
			0	98	
57	588	29	0	81	2.735632184
			0	80	
			0	77	
58	587	29	0	107	2.896551724
			0	65	
			0	80	
59	588	29	0	81	2.574712644
			0	83	
			0	60	
				Average Total:	2.153256705

Figure C.16: Results Database – Sheet III

Frame Number	Ruler Measurement of 20 mm [Px]	Equivalent 1mm [Px]	Height Position from top lid [Px]	Measurement [Px]	Average Measur
62	588	29	232	31	1.459770115
			464	38	
			696	58	
63	589	29	232	34	1.183908046
			464	32	
			696	37	
64	587	29	232	48	1.804597701
			464	45	
			696	64	
67	587	29	232	24	1.448275862
			464	55	
			696	47	
				Average Total:	1.478927203

Figure C.17: Results Database – Sheet IV

Frame Number	Ruler Measurement of 20 mm [Px]	Equivalent 1mm [Px]	Height Position from top lid [Px]	Measurement [Px]	Average Measur
69	588	29	232	36	1.333333333
			464	60	
			696	20	
70	588	29	232	38	1.747126437
			464	44	
			696	70	
71	588	29	232	36	1.448275862
			464	45	
			696	45	
72	586	29	232	37	1.689655172
			464	34	
			696	76	
73	588	29	232	39	1.344827586
			464	43	
			696	35	
74	589	29	232	45	1.908045977
			464	56	
			696	65	
75	588	29	0	52	1.873563218
			0	34	
			0	77	
76	589	29	0	47	1.517241379
			0	20	
			0	65	
				Average Total:	1.646962233

Figure C.18: Results Database – Sheet V

Frame Number	Ruler Measurement of 20 mm [Px]	Equivalent 1mm [Px]	Height Position from top lid [Px]	Measurement [Px]	Average Measur
87	573	29	232	77	2.149425287
			464	54	
			696	56	
88	573	29	232	80	2.712643678
			464	74	
			696	82	
87	572	29	232	67	2.287356322
			464	64	
			696	68	
88	572	29	232	96	3.126436782
			464	87	
			696	89	
89	571	29	232	78	2.356321839
			464	68	
			696	59	
92	573	29	232	84	3.517241379
			464	110	
			696	112	
87	573	29	232	75	3.022988506
			464	80	
			696	108	
88	573	29	232	90	2.32183908
			464	62	
			696	50	
89	573	29	232	82	2.885057471
			464	83	
			696	86	
92	573	29	232	62	2.954022989
			464	95	
			696	100	
				Average Total:	2.798212005

Figure C.19: Results Database – Sheet VI

Frame Number	Ruler Measurement of 20 mm [Px]	Equivalent 1mm [Px]	Height Position from top lid [Px]	Measurement [Px]	Average Measur
93	571	29	232	78	2.275862069
			464	51	
			696	69	
94	571	29	232	63	2.011494253
			464	62	
			696	50	
95	571	29	232	78	2.459770115
			464	69	
			696	67	
96	571	29	232	68	2.218390805
			464	61	
			696	64	
99	571	29	232	72	2.057471264
			464	51	
			696	56	
101	571	29	232	78	2.494252874
			464	72	
			696	67	
102	571	29	232	73	2.482758621
			464	66	
			696	77	
103	571	29	232	72	2.459770115
			464	74	
			696	68	
105	571	29	232	102	2.505747126
			464	66	
			696	50	
106	575	29	232	63	2.482758621
			464	60	
			696	93	
108	575	29	232	65	1.885057471
			464	54	
			696	45	
				Average Total:	2.352490421

Figure C.20: Results Database – Sheet VII

Frame Number	Ruler Measurement of 20 mm [Px]	Equivalent 1mm [Px]	Height Position from top lid [Px]	Measurement [Px]	Average Measur
117	572	29	232	68	2.16091954
			464	67	
			696	53	
118	572	29	232	64	2.609195402
			464	77	
			696	86	
119	572	29	232	70	2.379310345
			464	68	
			696	69	
120	572	29	232	77	2.643678161
			464	75	
			696	78	
121	572	29	232	62	2.206896552
			464	65	
			696	65	
122	572	29	232	70	2.183908046
			464	60	
			696	60	
123	572	29	232	61	2.195402299
			464	60	
			696	70	
124	572	29	232	70	2.045977011
			464	58	
			696	50	
125	572	29	232	64	2.16091954
			464	50	
			696	74	
				Average Total:	2.30316092

Figure C.21: Results Database – Sheet VIII

Frame Number	Ruler Measurement of 20 mm [Px]	Equivalent 1mm [Px]	Height Position from top lid [Px]	Measurement [Px]	Average Measur
135	575	29	232	38	1.597701149
			464	42	
			696	59	
136	571	29	232	56	1.896551724
			464	55	
			696	54	
137	574	29	232	43	1.770114943
			464	52	
			696	59	
142	571	29	232	80	2.67816092
			464	80	
			696	73	
143	571	29	232	69	2.827586207
			464	78	
			696	99	
144	571	29	232	70	3.425287356
			464	110	
			696	118	
145	571	29	232	77	3.482758621
			464	98	
			696	128	
148	571	29	232	90	2.379310345
			464	63	
			696	54	
149	571	29	232	73	2.67816092
			464	87	
			696	73	
153	576	29	232	64	2.528735632
			464	82	
			696	74	
154	571	29	232	80	3.252873563
			464	101	
			696	102	
				Average Total:	2.62962963

Figure C.22: Results Database – Sheet IX

Frame Number	Ruler Measurement of 20 mm [Px]	Equivalent 1mm [Px]	Height Position from top lid [Px]	Measurement [Px]	Average Measur
156	575	29	232	128	4.816091954
			464	154	
			696	137	
158	571	29	232	113	3.425287356
			464	67	
			696	118	
160	571	29	232	140	3.747126437
			464	90	
			696	96	
166	571	29	232	97	3.149425287
			464	108	
			696	69	
167	571	29	232	79	3.586206897
			464	83	
			696	150	
168	571	29	232	89	2.988505747
			464	100	
			696	71	
169	571	29	232	106	3.287356322
			464	90	
			696	90	
172	571	29	232	124	3.643678161
			464	108	
			696	85	
				Average Total:	3.403940887

Figure C.23: Results Database – Sheet X

Frame Number	Ruler Measurement of 20 mm [Px]	Equivalent 1mm [Px]	Height Position from top lid [Px]	Measurement [Px]	Average Measur
186	575	29	232	51	1.827586207
			464	40	
			696	68	
187	575	29	232	84	2.471264368
			464	73	
			696	58	
188	575	29	232	53	1.804597701
			464	61	
			696	43	
191	571	29	232	48	1.873563218
			464	62	
			696	53	
				Average Total:	2.049808429

Figure C.24: Results Database – Sheet XI

Appendix D

Aardvark Setup

This appendix chapter provides images of the existing nanofibre yarn electrospinning setup called the Aardvark at AUT.

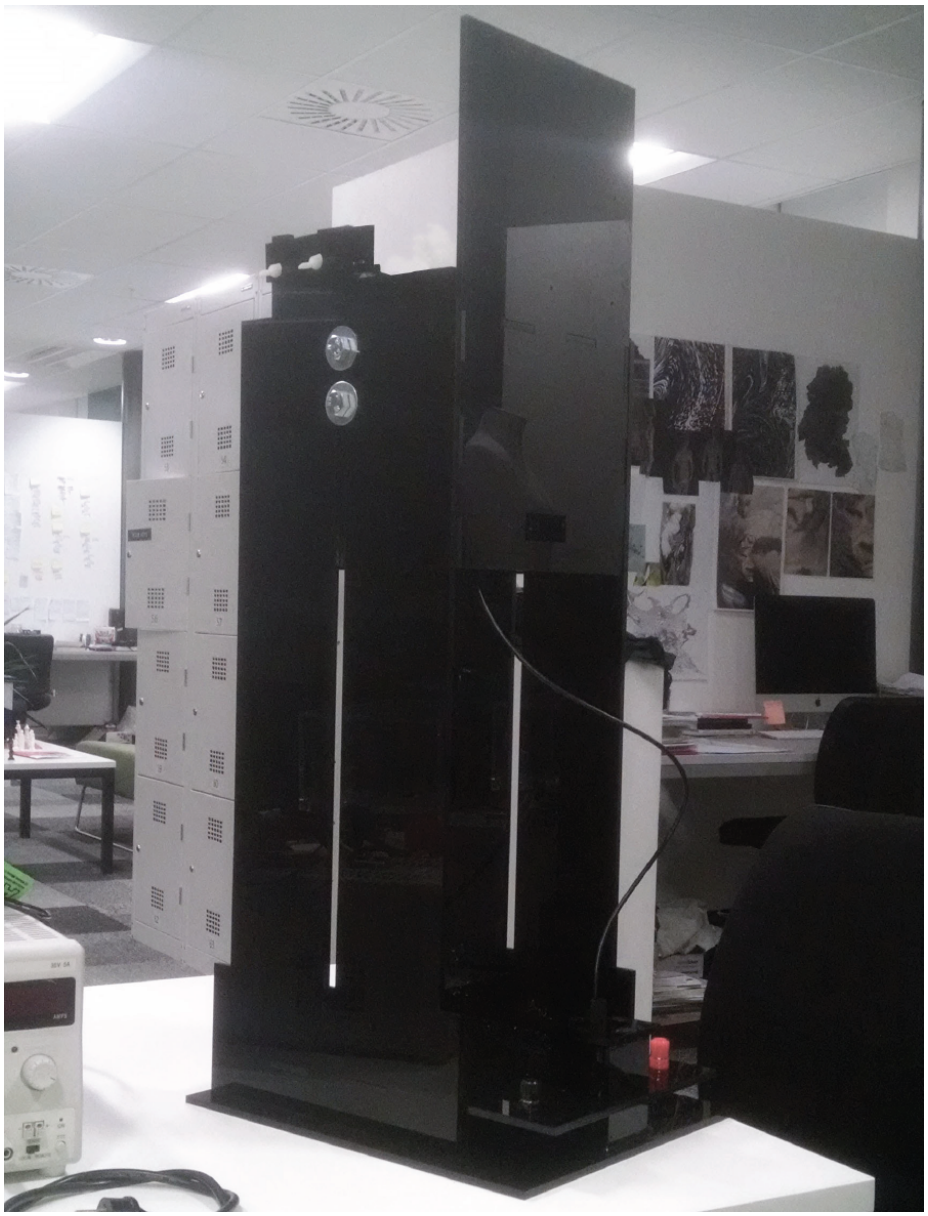

Figure D.1: Aardvark – Spinner Tower

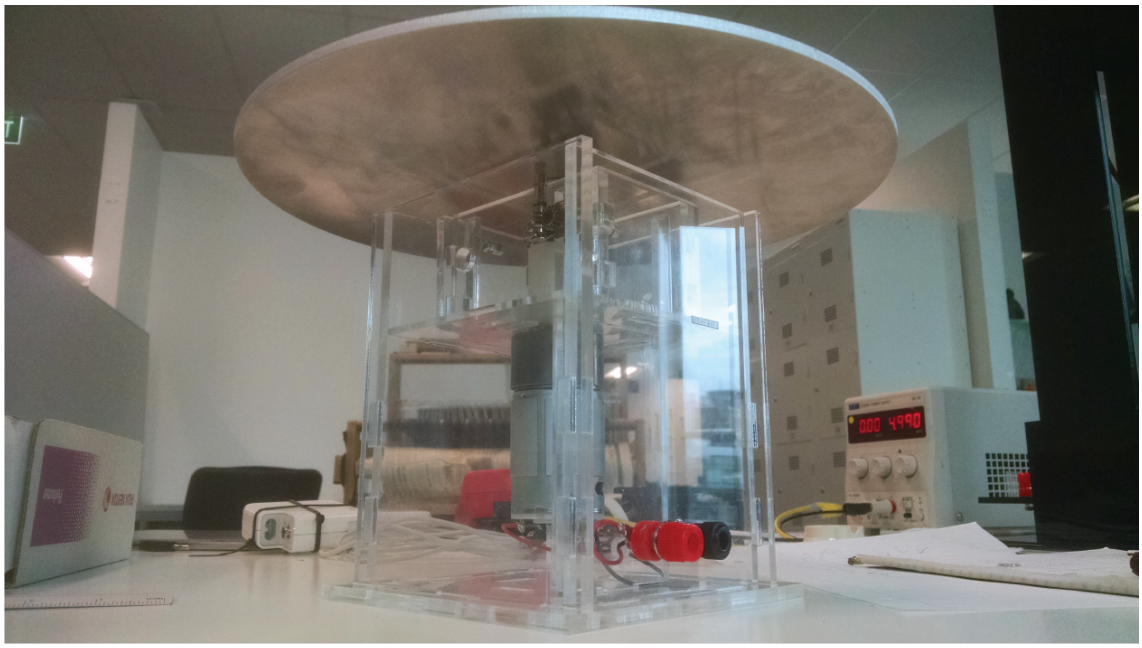

Figure D.2: Aardvark – The Collector with HVDC Connectivity

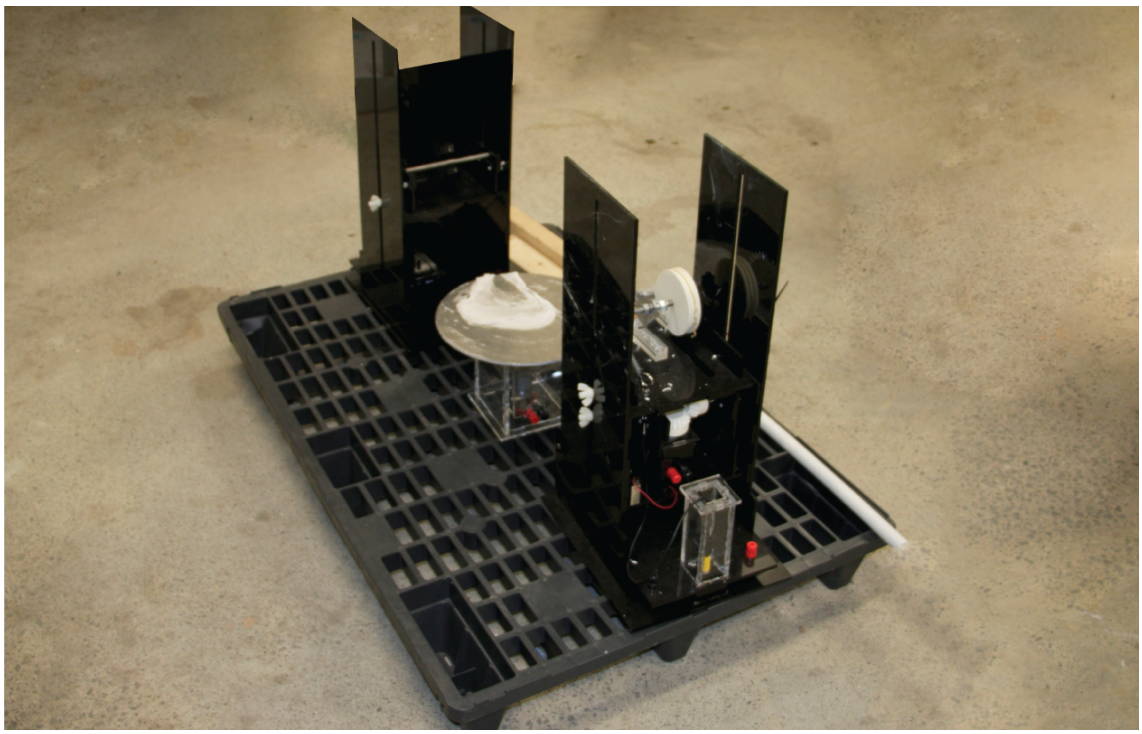

Figure D.3: Aardvark – Two Tower Setup with Rotating Disc Collector

Bibliography

[1] Volker Strobel. Pold87/academic-keyword-occurrence.

[2] Geoffrey Taylor. Electrically driven jets. In *Proceedings of the Royal Society of London A: Mathematical, Physical and Engineering Sciences*, volume 313, pages 453–475. The Royal Society, 1969.

[3] Peter K Baumgarten. Electrostatic spinning of acrylic microfibers. *Journal of colloid and interface science*, 36(1):71–79, 1971.

[4] Darrell H Reneker, Alexander L Yarin, Hao Fong, and Sureeporn Koombhongse. Bending instability of electrically charged liquid jets of polymer solutions in electrospinning. *Journal of Applied physics*, 87(9):4531–4547, 2000.

[5] JM Deitzel, JD Kleinmeyer, JK Hirvonen, and NC Beck Tan. Controlled deposition of electrospun poly (ethylene oxide) fibers. *Polymer*, 42(19):8163–8170, 2001.

[6] Paul D Dalton, Doris Klee, and Martin Möller. Electrospinning with dual collection rings. *Polymer*, 46(3):611–614, 2005.

[7] F Dabirian and SA Hosseini. Novel method for nanofibre yarn production using two differently charged nozzles. *Fibres & Textiles in Eastern Europe*, 17(3):74, 2009.

[8] Lu-Qi Liu, Michaela Eder, Ingo Burgert, Dimitrios Tasis, Maurizio Prato, and H Daniel Wagner. One-step electrospun nanofiber-based composite ropes. *Applied physics letters*, 90(8):083108, 2007.

[9] PV Mayuri and P Ramesh. Fabrication and characterization of silver nanoparticle impregnated uniaxially aligned fibre yarns by one-step electrospinning process. *Journal of Materials Science*, pages 1–8, 2015.

[10] F Dabirian, SA Hosseini Ravandi, R Hashemi Sanatgar, and JP Hinestroza. Manufacturing of twisted continuous PAN nanofiber yarn by electrospinning process. *Fibers and Polymers*, 12(5):610–615, 2011.

[11] F Hajiani, Ali AA Jeddi, and AA Gharehaghaji. An investigation on the effects of twist on geometry of the electrospinning triangle and polyamide 66 nanofiber yarn strength. *Fibers and Polymers*, 13(2):244–252, 2012.

[12] Jianxin He, Kun Qi, Yuman Zhou, and Shizhong Cui. Multiple conjugate electrospinning method for the preparation of continuous polyacrylonitrile nanofiber yarn. *Journal of Applied Polymer Science*, 131(8), 2014.

[13] F Dabirian, Y Hosseini, and SA Hosseini Ravandi. Manipulation of the electric field of electrospinning system to produce polyacrylonitrile nanofiber yarn. *Journal of the Textile Institute*, 98(3):237–241, 2007.

[14] Fuqian Sun, Chen Yao, Tangying Song, and Xinsong Li. Fabrication of poly (vinylidenefluoride-co-hexafluoropropylene) nanofiber yarns by conjugate electrospinning. *The Journal of The Textile Institute*, 102(7):633–638, 2011.

[15] Nadeem Shuakat and Tong Lin. Highly-twisted, Continuous Nanofibre Yarns Prepared by a Hybrid Needle-Needleless Electrospinning. *RSC Advances*, 2015.

[16] Jianxin He, Yuman Zhou, Kun Qi, Lidan Wang, Pingping Li, and Shizhong Cui. Continuous twisted nanofiber yarns fabricated by double conjugate electrospinning. *Fibers and Polymers*, 14(11):1857–1863, 2013.

[17] Liang Wei and Xiaohong Qin. Nanofiber bundles and nanofiber yarn device and their mechanical properties: A review. *Textile Research Journal*, page 0040517515617422, 2016.

[18] Fatemeh Bateni, Seyed Abdolkarim Hosseini Ravandi, and Afsaneh Valipouri. Structural characterization and investigation of selected properties of hybrid yarn coated with carbon nanotube composite nanofibers. *Journal of Applied Polymer Science*, 128(2):1143–1151, 2013.

[19] Victor A Agubra, Luis Zuniga, David Flores, Jahaziel Villareal, and Mataz Alcoutlabi. Composite Nanofibers as Advanced Materials for Li-ion, Li-O 2 and Li-S Batteries. *Electrochimica Acta*, 2016.

[20] Darrell H Reneker and Iksoo Chun. Nanometre diameter fibres of polymer, produced by electrospinning. *Nanotechnology*, 7(3):216, 1996.

[21] Razieh Hashemi Sanatgar, Sedigheh Borhani, Seyed Abdolkarim Hosseini Ravandi, and Ali Akbar Gharehaghaji. The influence of solvent type and polymer concentration on the physical properties of solid state polymerized PA66 nanofiber yarn. *Journal of Applied Polymer Science*, 126(3):1112–1120, 2012.

[22] M Coyle. The lifeshirt system: Bringing high-tech patient monitoring from hospital to home. In *Proc. Avantex*.

[23] Baicheng Weng, Fenghua Xu, Alfonso Salinas, and Karen Lozano. Mass production of carbon nanotube reinforced poly (methyl methacrylate) nonwoven nanofiber mats. *Carbon*, 75:217–226, 2014.

[24] Atta Akbari, Omid Moini Jazani, Mohammad Reza Saeb, Kobra Pourabdollah, and Fariba Soltanolkottabi. Towards Well-aligned electrospun PAN/MWCNTs composite nanofibers: Design, fabrication, and development. *Fibers and Polymers*, 15(6):1230–1235, 2014.

[25] Kaili Jiang, Qunqing Li, and Shoushan Fan. Nanotechnology: Spinning continuous carbon nanotube yarns. *Nature*, 419(6909):801–801, 2002.

[26] Kyungho Hwang, Byeongmin Kwon, and Hongsik Byun. Preparation of PVDF nanofiber membranes by electrospinning and their use as secondary battery separators. *Journal of Membrane Science*, 378(1):111–116, 2011.

[27] Jing Ning, Xin Zhang, Hu Yang, Zhen-Liang Xu, and Yong-Ming Wei. Preparation of porous PVDF nanofiber coated with Ag NPs for photocatalysis application. *Fibers and Polymers*, 17(1):21–29, 2016.

[28] Phil Brown and Kathryn Stevens. *Nanofibers and nanotechnology in textiles*. Elsevier, 2007.

[29] Zheng-Ming Huang, Y-Z Zhang, M Kotaki, and S Ramakrishna. A review on polymer nanofibers by electrospinning and their applications in nanocomposites. *Composites science and technology*, 63(15):2223–2253, 2003.

[30] SungCheal Moon and Richard J Farris. How is it possible to produce highly oriented yarns of electrospun fibers? *Polymer Engineering & Science*, 47(10):1530–1535, 2007.

[31] Cheng-Kun Liu, Run-Jun Sun, Kan Lai, Chui-Qing Sun, and Yao-Wu Wang. Preparation of short submicron-fiber yarn by an annular collector through electrospinning. *Materials letters*, 62(29):4467–4469, 2008.

[32] Bin Ding, Moran Wang, Xianfeng Wang, Jianyong Yu, and Gang Sun. Electrospun nanomaterials for ultrasensitive sensors. *Materials Today*, 13(11):16–27, 2010.

[33] Jayesh Doshi and Darrell H Reneker. Electrospinning process and applications of electrospun fibers. In *Industry Applications Society Annual Meeting, 1993., Conference Record of the 1993 IEEE*, pages 1698–1703. IEEE, 1995.

[34] Armstrong Xie, Haitao Niu, and Tong Lin. Continuous Polyacrylonitrile Nanofiber Yarns: Preparation and Dry-drawing Treatment for Carbon Nanofiber Production. *RSC Advances*, 2015.

[35] Anton Formhals. Production of artificial fibers. April 1937.

[36] Ernest K Gladding. Apparatus for the production of filaments, threads, and the like. August 1939.

[37] Elaheh Daneshvar, Mohammad Amani Tehran, Saeideh Gorji Kandi, and Fatemeh Zeighami. Investigating the characteristics of two different methods in nanofiber yarn coloration. *The Journal of The Textile Institute*, (ahead-of-print):1–9, 2015.

[38] Steven B Warner, A Buer, SC Ugbolue, GC Rutledge, and MY Shin. A fundamental investigation of the formation and properties of electrospun fibers. *National textile center annual report*, pages 83–90, 1998.

[39] Hao Yan, Luqi Liu, and Zhong Zhang. Continually fabricating staple yarns with aligned electrospun polyacrylonitrile nanofibers. *Materials Letters*, 65(15):2419–2421, 2011.

[40] Maryam Yousefzadeh, Masoud Latifi, Wee-Eong Teo, Mohammad Amani-Tehran, and Seeram Ramakrishna. Producing continuous twisted yarn from well-aligned nanofibers by water vortex. *Polymer Engineering & Science*, 51(2):323–329, 2011.

[41] Matthias ML Arras, Christian Grasl, Helga Bergmeister, and Heinrich Schima. Electrospinning of aligned fibers with adjustable orientation using auxiliary electrodes. *Science and Technology of Advanced Materials*, 13(3):035008, 2012.

[42] Lu-Qi Liu, Michaela Eder, Ingo Burgert, Dimitrios Tasis, Maurizio Prato, and H Daniel Wagner. One-step electrospun nanofiber-based composite ropes. *Applied physics letters*, 90(8):083108, 2007.

[43] Muhammad Nadeem Shuakat and Tong Lin. Direct electrospinning of nanofibre yarns using a rotating ring collector. *The Journal of The Textile Institute*, (ahead-of-print):1–9, 2015.

[44] SA Hosseini Ravandi, R Bayat Tork, F Dabirian, AA Gharehaghaji, and A Sajjadi. Characteristics of Yarn and Fabric Made out of Nanofibers. *Materials Sciences and Applications*, 6(01):103, 2015.

[45] Amalina M Afifi, Shigeyuki Nakano, Hideki Yamane, and Yoshiharu Kimura. Electrospinning of Continuous Aligning Yarns with a 'Funnel'Target. *Macromolecular Materials and Engineering*, 295(7):660–665, 2010.

[46] Usman Ali, Yaqiong Zhou, Xungai Wang, and Tong Lin. Direct electrospinning of highly twisted, continuous nanofiber yarns. *Journal of the Textile Institute*, 103(1):80–88, 2012.

[47] Ni Li, Quan Hui, Hua Xue, and Jie Xiong. Electrospun Polyacrylonitrile nanofiber yarn prepared by funnel-shape collector. *Materials Letters*, 79:245–247, 2012.

[48] Yuman Zhou, Jianxin He, Hongbo Wang, Kun Qi, Bin Ding, and Shizhong Cui. Carbon nanofiber yarns fabricated from co-electrospun nanofibers. *Materials & Design*, 95:591–598, 2016.

Acknowledgments

This section is devoted to those whom had supported and contributed to making the journey through my masters degree a joyful and an unforgetful one.

Samuel Aickin his the ability to analyze a given task, ask the relevant questions, identify gaps in understanding and then, in a programmatic manner, lay out a plan of attack that would address those holes that would help direct research towards a productive goal. Sam's strong understanding of physics helped identify what at face value seemed to to be "well established" knowledge. This lead us to forming the experimental setup that this masters and more importantly a unique and true friendship.

Jinan Hadi can do attitude, a bright spot within the struggles of organizing and conducting the experiments which involved apparatus from the medical laboratories in the school of science. I thank her for her support and her unreserved generosity in supporting the research.

Ahmed AlJumaily his veteran experience and insights into the realm of academic research was an eye opening experience. I thank him for his guidance and direction through my degree and in articulating and conveying complex engineering concepts. His presence in this project was invaluable

Frances Joseph besides being my secondary supervisor, I thank her for her vision and drive that I find inspiring. Her efforts to make my work apart of her vision was a big reason for me being able to study for this degree and for that I am thankful for her support and energetic spirit.

Peter Heslop along with Frances, Peter helped initiate the discussion with Callaghan Innovation. Peter helped deliver upon any requests I had to help the progress the research, whether it be ordering materials or managing a working space, he was the one that made things happen.

Nathan Stantial this opportunity came up from a discussion with Nathan from Callaghan Innovation how the organization felt that a conjoint project with Revolution Fibres and AUT is something they would like to back.

The Postgraduates their work did not stop them from giving a helping hand *Anubha Kalra - Guatam Anand - Andres Mentes - Hanon Lim - Hanin Rajeh*

Finally I would like to thank my parents (*Zaid & Zainab*) and siblings (*Yasmin, Alaa & Mohammad*) for supporting me throughout my studies and for being patient enough for me to complete them, without them I would not have been in this position I am in today.